Reactions at surfaces. Plasma Reactivity and Nanoparticles. Insights using Molecular Dynamics simulations

Pascal Brault

Reactions at surfaces
Plasma Reactivity and Nanoparticles
Insights using Molecular Dynamics simulations

Pascal Brault
GREMI, UMR7344 CNRS Université d'Orléans,
Orléans, France
pascal.brault@univ-orleans.fr
http://www.univ-orleans.fr/gremi/pascal-brault

GREMI cnrs UNIVERSITE D'ORLEANS

Reactions at surfaces

⇓

Which reaction pathways ?
How to identify them ?

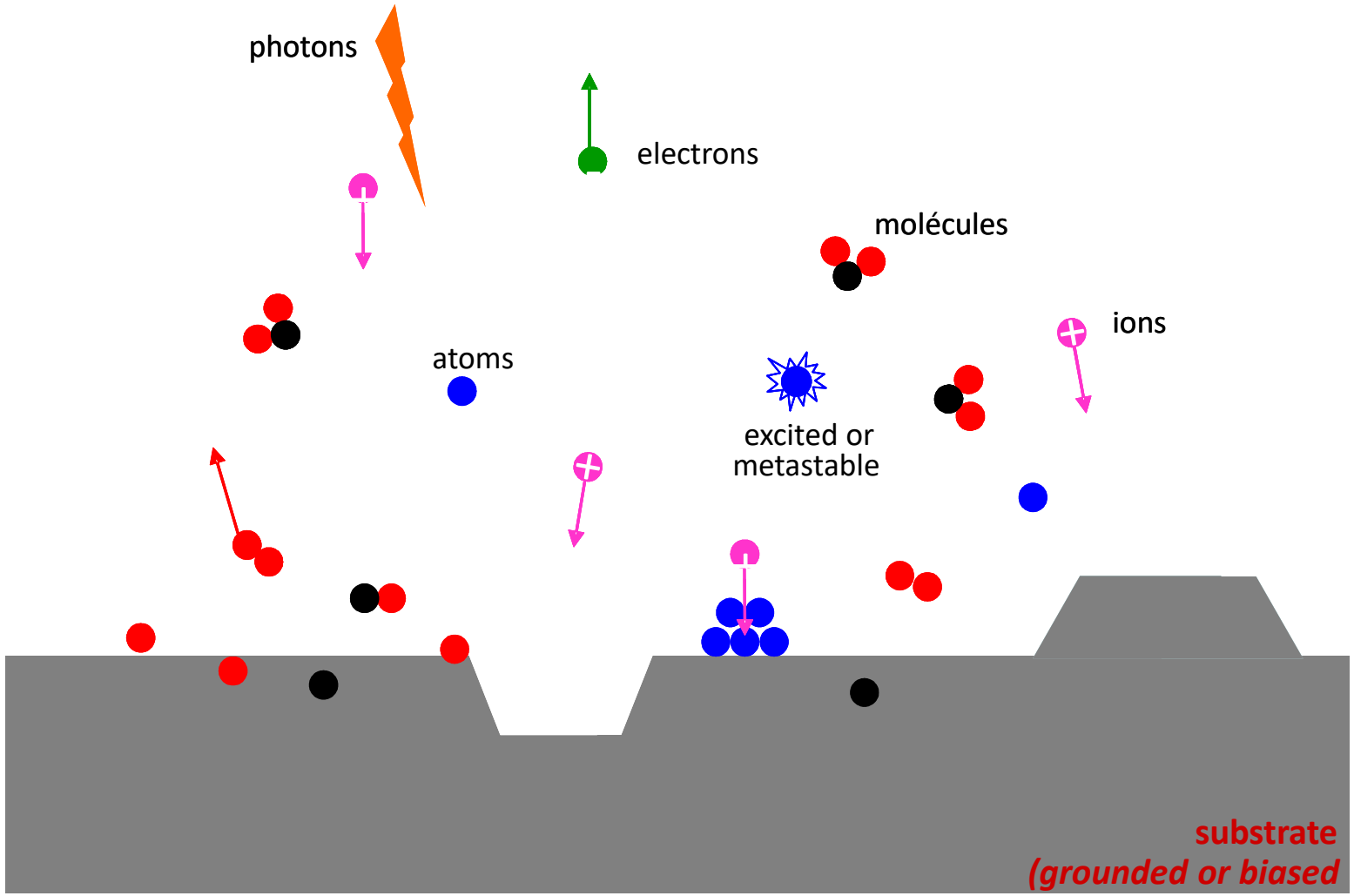

Which species?

Electrons : E = 1 eV – 6 eV → keV → MeV → GeV
plasmas materials → e- beams → Tokamaks → CERN
treatments

Photons : plasmas – photochemistry – laser treatments

Atoms : 1 – 20 eV : déeposition – etching – surface treatments
(fondamental or metastable states)

Molecules & clusters : 1 – 20 eV : réactivité - dépôts – gravure – traitements de surface
(fondamental ou electronicv – vibra^{l} – rota^{l} excit ed states)

Ions : 1 eV – 1 keV → 10 keV – 10 MeV
plasmas & ion beams implantations
materials Tokamaks (fusion devices)

Which Surfaces ?

Ordered

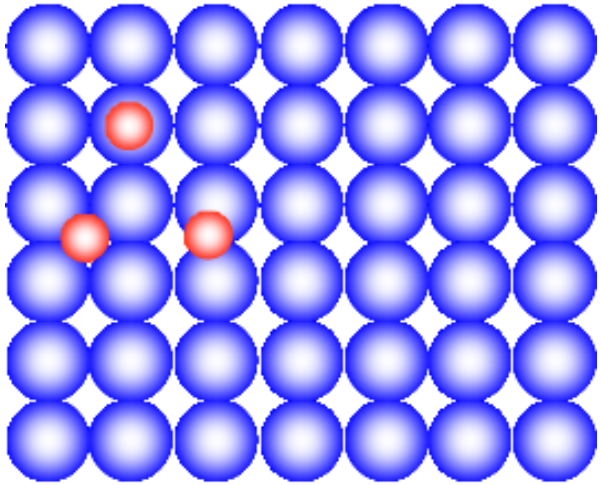

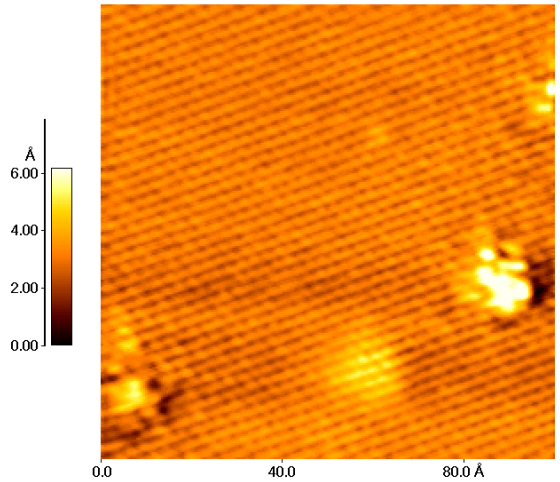

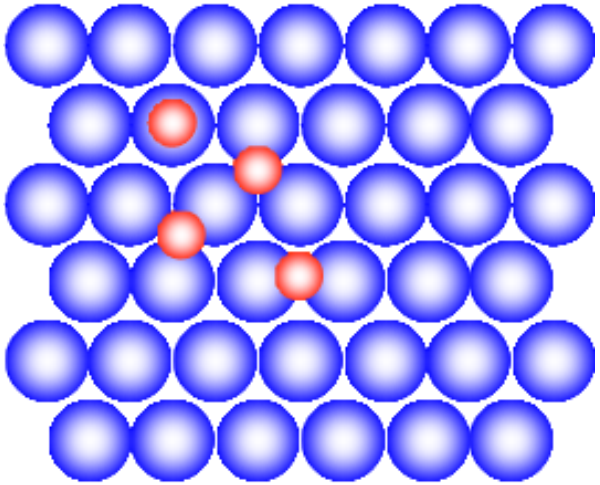

fcc (100) C(0001) fcc (111)

Surface structure ⇒ reaction sites ⇒ Reactivity

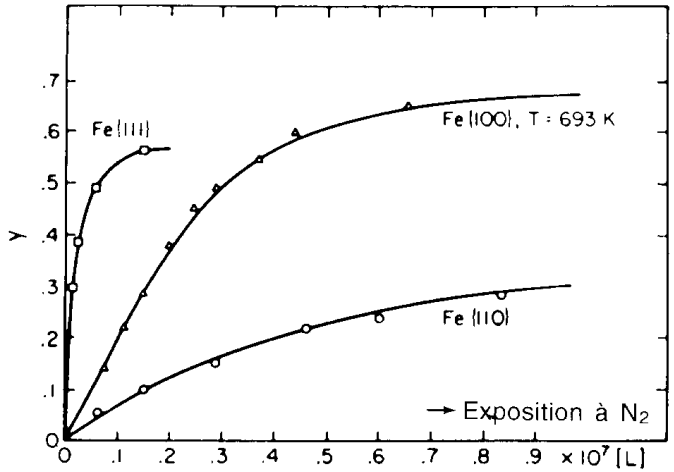

Figure 7.16. Variations de la concentration superficielle relative, y, en azote atomique en fonction de l'exposition à N_2 [33]. 1 L (Langmuir) = $1{,}333 \cdot 10^{-4}$ Pa · s (10^{-6} torr · s).

Which surfaces ?

Complex ordered
Disordered

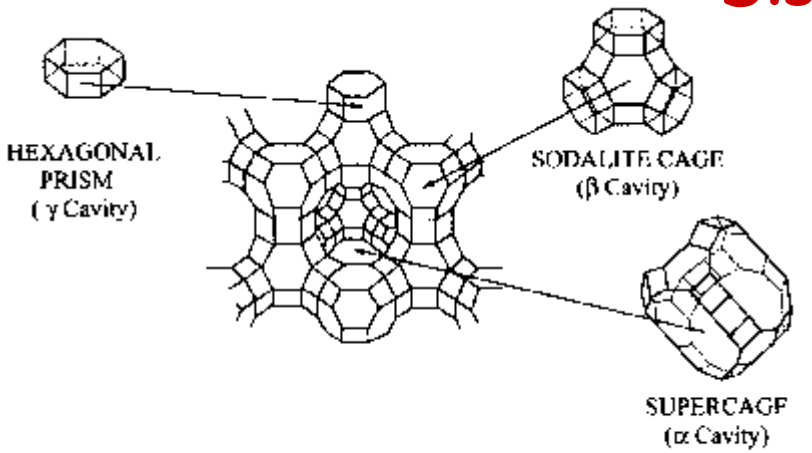

Zeolite NaY

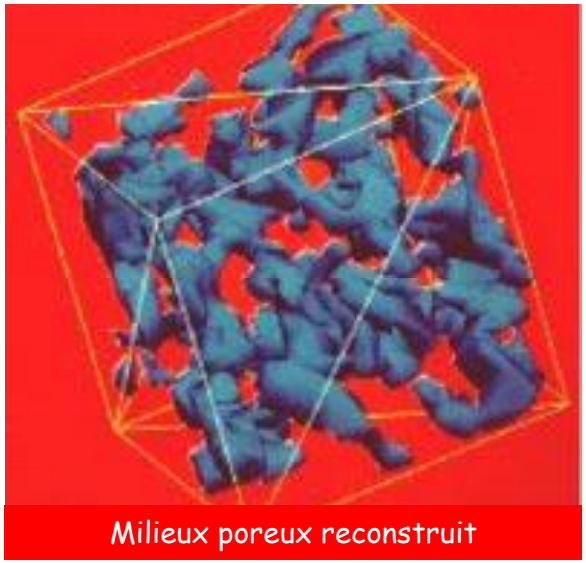

Milieux poreux reconstruit

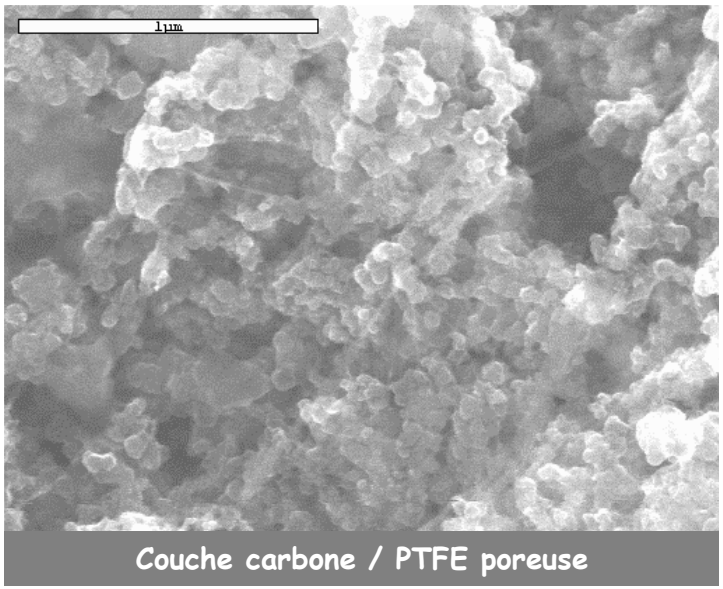

Cliché D. Cot, ENSCM

Couche carbone / PTFE poreuse

Adsorption

Surface mechanism quick picture

- ✓ Transport to surface (Boundary layer at high pressure)
- ✓ Sticking
- ✓ Reactants diffusion at surface
- ✓ Adsorption of one or many reactants at surface
- ✓ Reactions at surface
- ✓ Product desorption from surface
- ✓ Transport outwards surface (Boundary layer at HP)

About Sticking

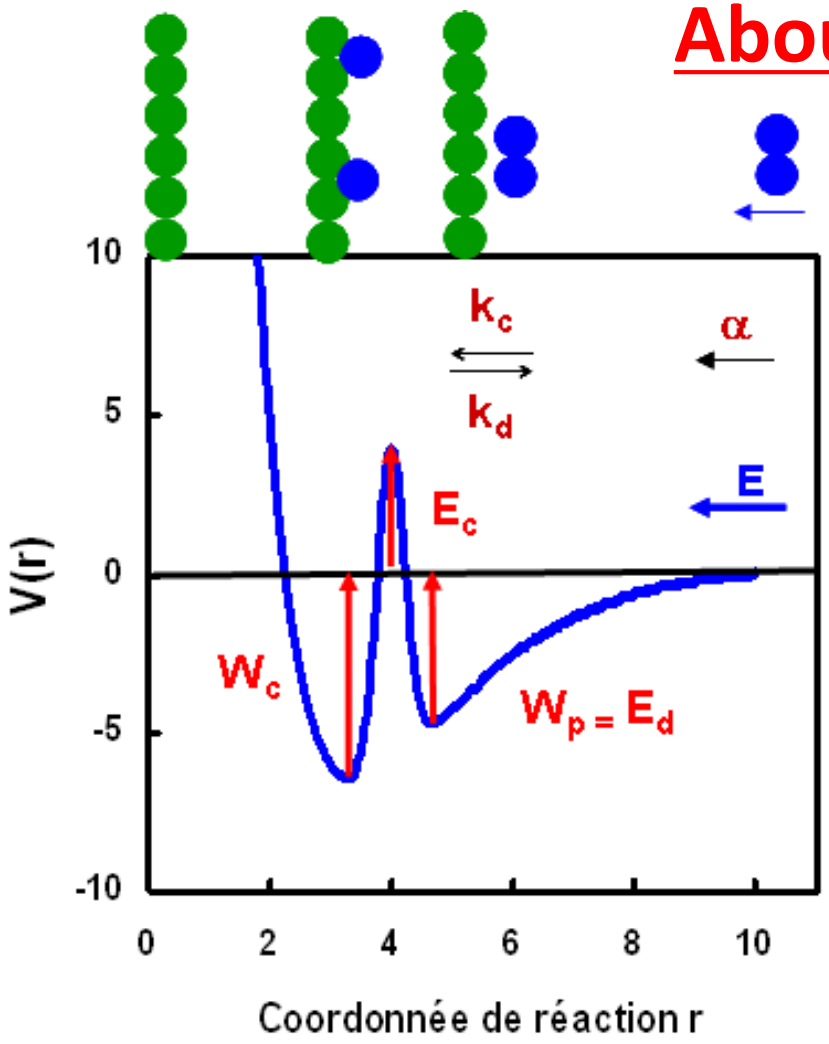

Sticking coefficient S_{0p} (physisorption)

$E < 1.5 - 2\ E_c$

$$S_0 = \alpha \frac{k_c}{k_c + k_d}$$

$$k_d = \nu_d \exp\left(-\frac{E_d}{kT_s}\right)$$

$$k_c = \nu_c \exp\left(-\frac{E_c + E_d}{kT_s}\right)$$

$$S_0 = \frac{\alpha}{1 + \left(\frac{\nu_d}{\nu_c}\right)\exp\left(\frac{E_c}{kT_s}\right)}$$

W_c : Chemisorption well

W_p : Physisorption well

E_c : Barrier to chemisorption

E_d : Desorption energy

k_c : Chemisorption rate

k_d : Desorption rate

α : Physisorption probability

T_s : Surface temperature

About sticking (more complicated)

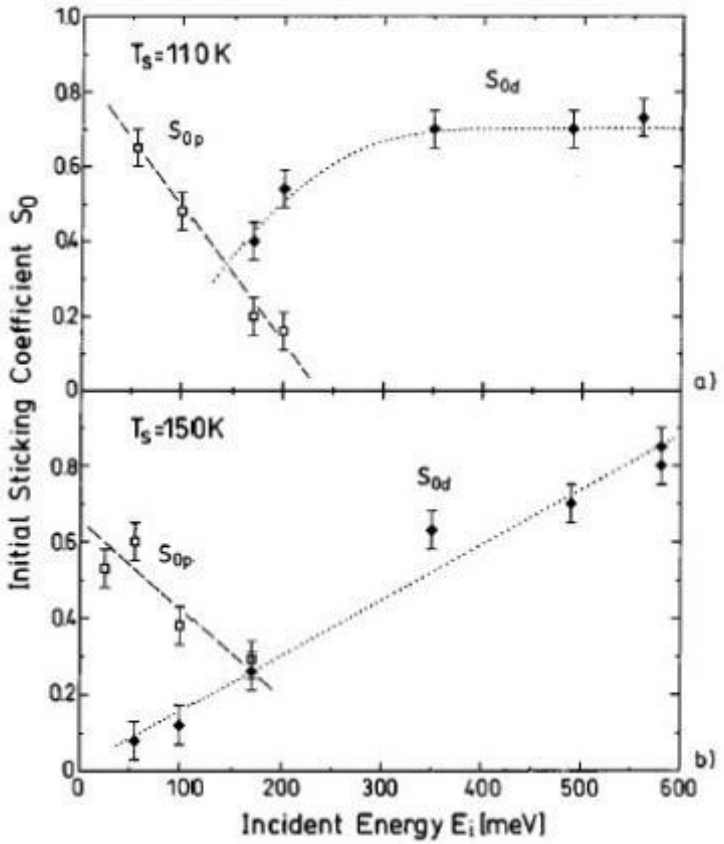

FIG. 6. The initial sticking coefficient S_0 of O_2 on Rh(111) as a function of the incident beam energy E_i for an angle of incidence of $\theta_i = 0°$ and two surface temperatures (a) $T_S = 110$ K and (b) $T_S = 150$ K. The filled symbols (◆) indicate S_{0d} and the open symbols (□) indicate S_{0p}. The error bars have been estimated from the $S(t)$ curves similar to those in Fig. 4. The curves are shown to guide the eye.

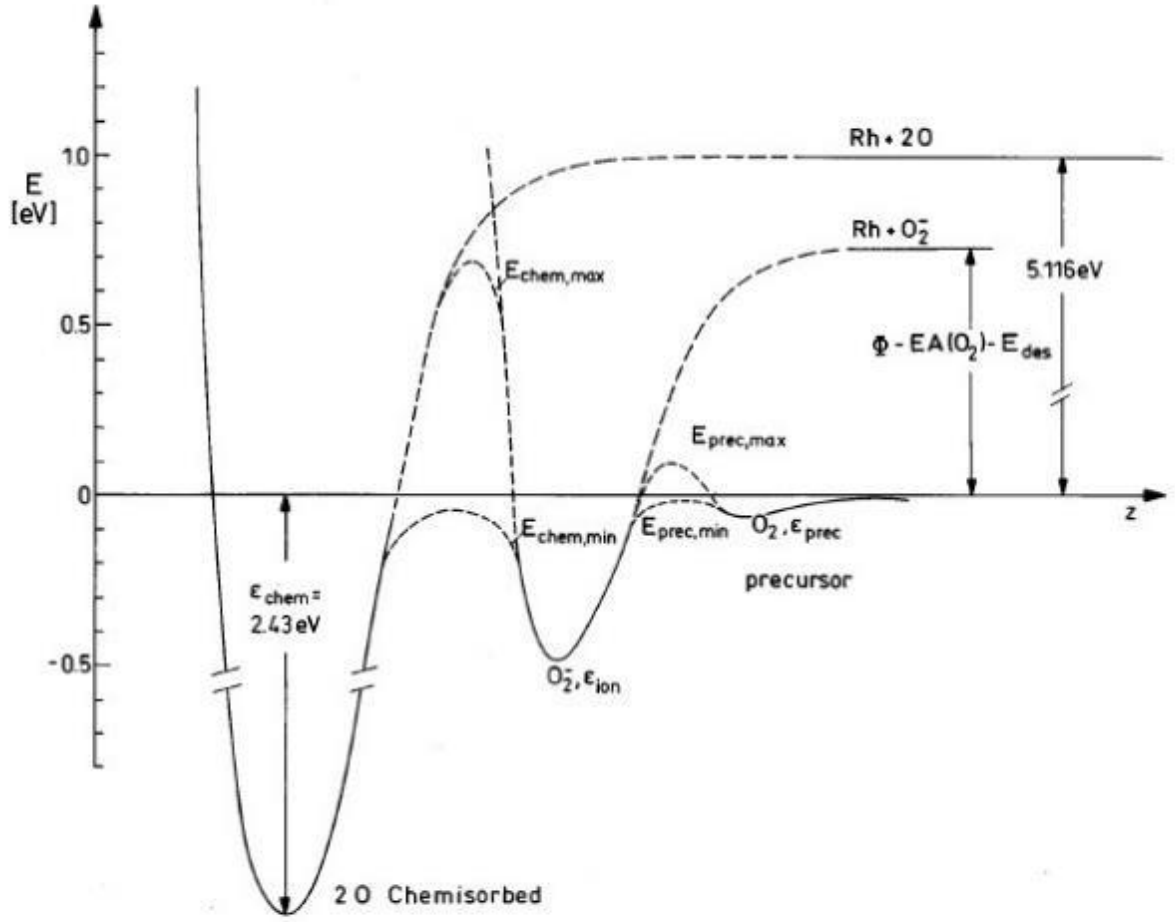

G. 1. Schematic diagram of a one-dimensional potential energy surface for the oxygen adsorption on Rh(111) based on the model proposed for O_2 on (111) Ref. 16. E_{prec} and E_{chem} represent the barrier heights for trapping in the precursor state and for direct dissociative chemisorption, respectively. The fective maximum and minimum values of the barriers are indicated. ε_{prec}, ε_{ion}, and ε_{chem} are the well depths of the precursor, ion-resonance, and sociative chemisorbed states. The dissociation energy, binding energy ε_{chem}, and the electron affinity of molecular oxygen on Rh(111) are taken from the erature (Refs. 23 and 27).

Sticking coefficient → Interaction potential

Electrons et photons

Electrons

Electrons low energy repelled by negatively biaised sheath.

Electrons high not cncerned by reactivity

Main effect →attachment on adsorbed atom/molecule

insulating surfaces : polymères, oxides, ...: a bit brittle

maximum transferred energiy during elastic collision:

$$\Delta E_{max} \approx 4\frac{m_{e^-}}{M}E_{e^-} << E_{e^-}$$

Atom displacement => for having 10eV transferred => E_{e^-}= 100keV

Photons

Substrate coupling

Weak direct effects on adsorbed species

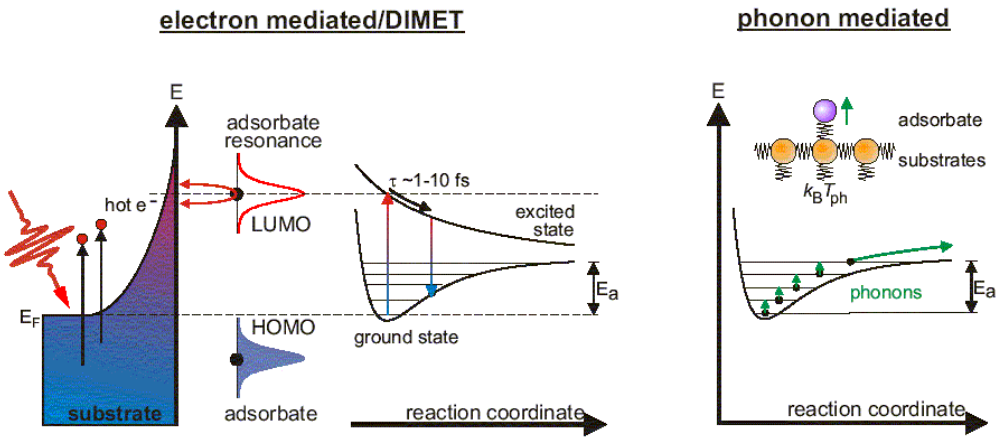

Atom-Surface: initial conditions

Atom sources:

vapor at T_g (gas or evaporation : dist. MB),
molecular beam ($E_c \approx 0.01 – 10$ eV + T_g)
ou sputtered matter
- ion : Thompson distribultion
- laser : ?

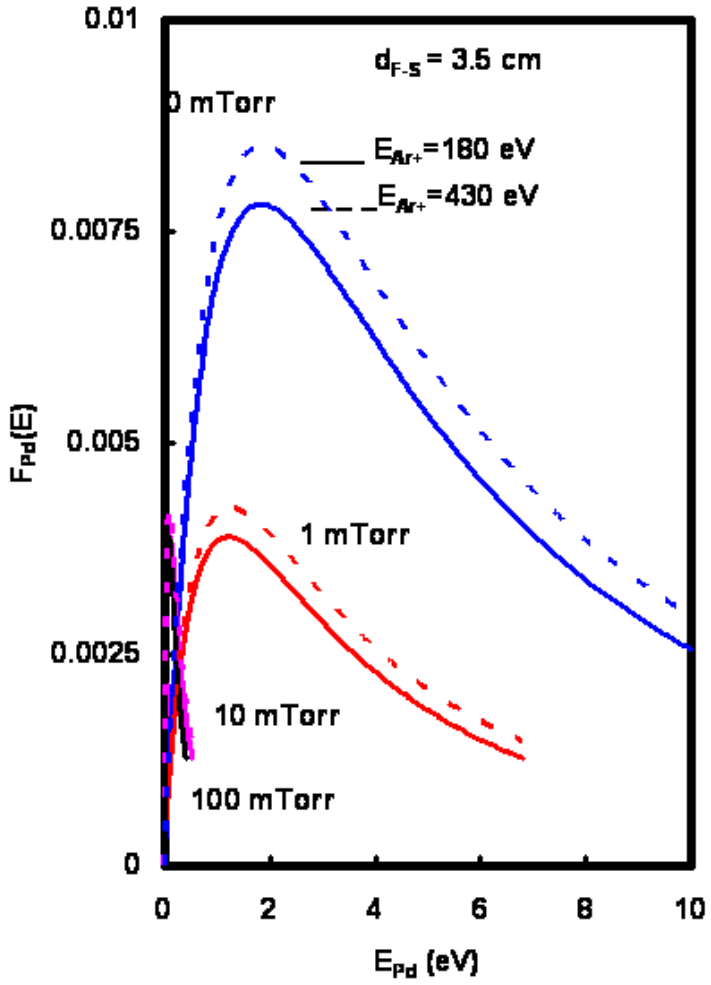

$$f(E) \propto \frac{1 - \left(\frac{E_{coh} + E}{\Lambda E_{Ar^+}} \right)^{\frac{1}{2}}}{E^2 \left(1 + \frac{E_{coh}}{E} \right)^3}$$

Pressure effect on distribution :
P ↗ f(E) → MB, ∀ f(E) et donc <E> ↘

Atom-Surface : Growth

Atom – Surface interactons

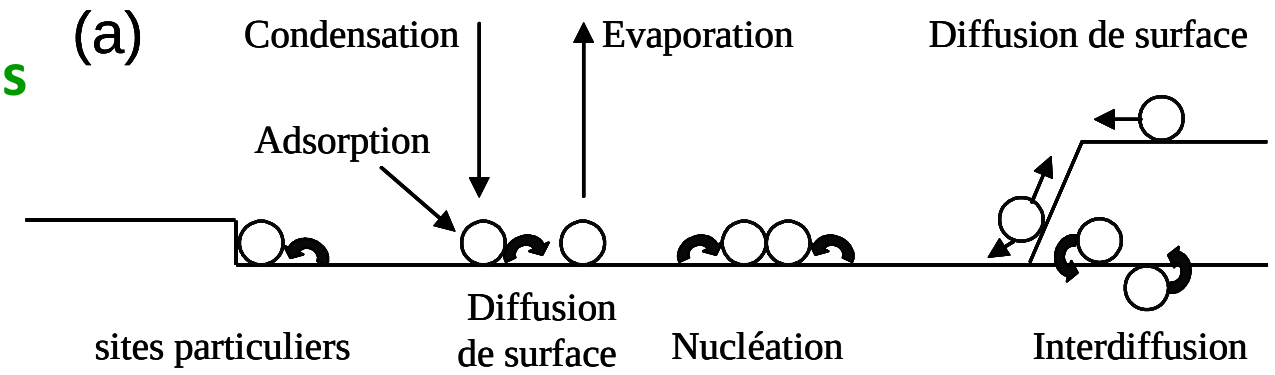

Growth mode

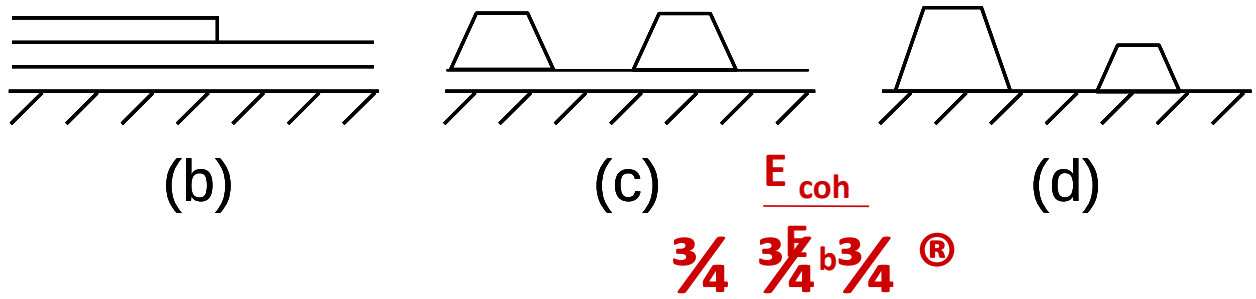

E_{coh}

¾ ¾F¾b¾ ®

(a) Schéma simplifié des processus de nucléation-croissance en surface et des trois modes de croissance principaux

(b) Franck van der Merve (c) Stranski-Krastanov (d) Volmer-Weber

Atom-Surface et growth

M

Ar^+

Ar^*

e^- lent

e^- rapide

hn

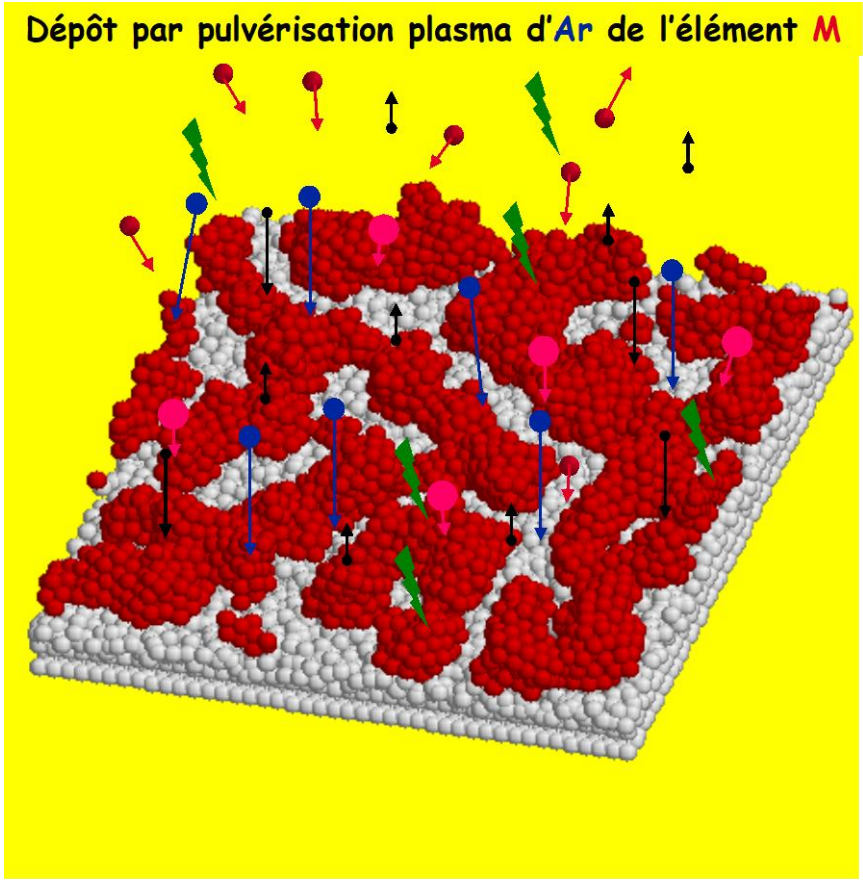

Growth (deposition rate, morphology, structure)

Depends on:

- **Flux et energy of atoms, substrate T° , gas T° ,**
- **Substrate composition, vapor composition (ion, metastable, e^-)**

Molécule – Surface : Réactivité

$E_i, v_i, J_i, Ee_i, \theta_i$

Conversion de l'éthylène en éthylidyne (CCH_3)

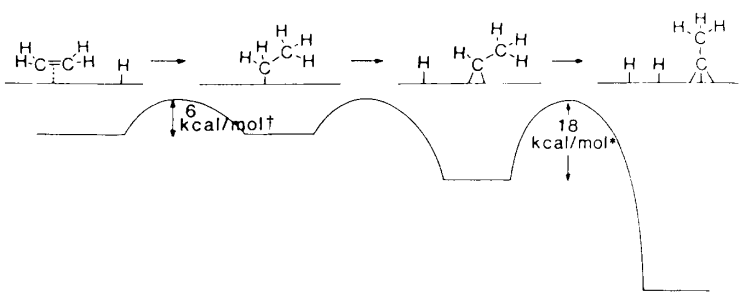

$E^1_f, v^1_f, J^1_f, Ee^1_f, \theta^1_f$

$E^2_f, v^2_f, J^2_f, Ee^2_f, \theta^2_f$

Fragmentation de l'éthylidine
en vinylidène (CCH_2) et acétylure (CCH)

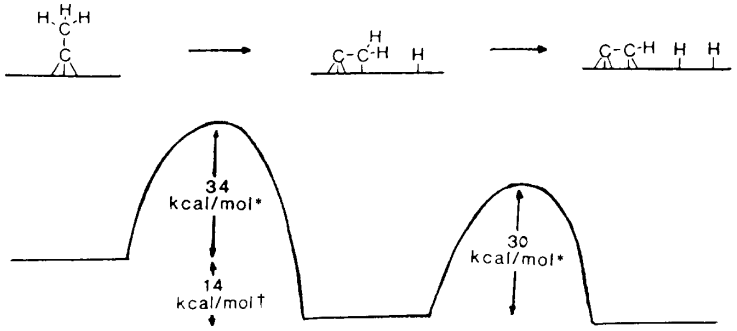

Figure 6.14. (*suite*)

Interactions Faisceau moléculaire - Surface

Approche moléculaire

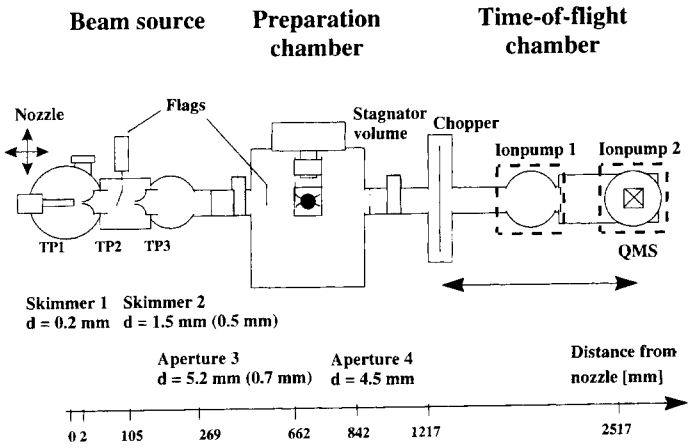

Fig. 6. The beam source and TOF system.

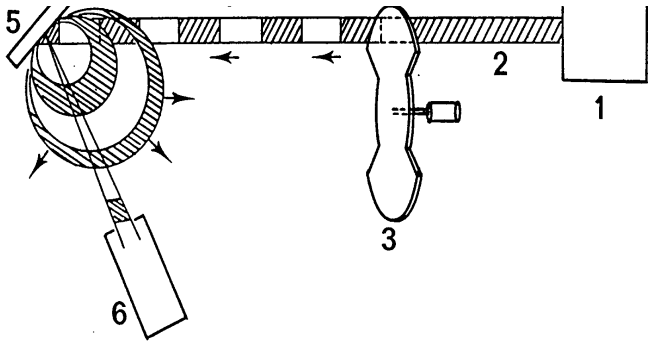

Fig. 5: Schematic drawing of a molecular beam experiment. (1) molecular beam source, (2) molecular beam, (3) modulator, (4) pulsed beam, (5) sample, (6) detector.

Features

E_c, θ, v, J variables

dv/v =1- 15%

⇓

Analysis of the various reaction channels

Interaction potential surface probe

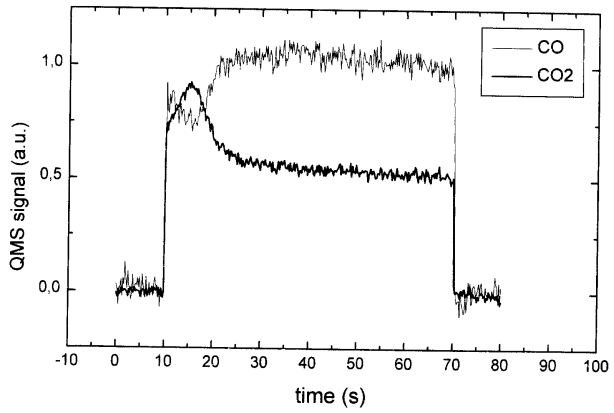

Fig. 42. Molecular beam study of the CO oxidation on a Pd/MgO(1 0 0) model catalyst. A CO_2 product pulse (heavy line) and the associated pulse of unreacted CO (light line) are displayed. $T = 556$ K, $n = 7.2 \times 10^{11}$ cm^{-2} s^{-1}, $D = 5.0$ nm (from L. Piccolo, C.R. Henry, unpublished).

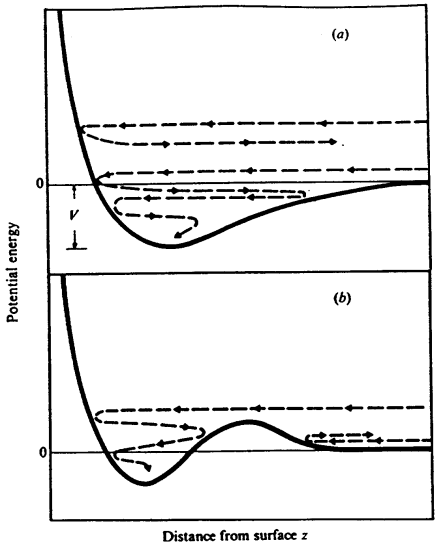

Fig. 4: Schematic representation (after A. Zangwill, 'Physics at surfaces' Cambridge University Press, 1992) of the (1D) interaction potential between a gas molecule and a metal surface as a function of the separation distance (z). Curve (a) corresponds to a molecular adsorption (e.g. CO/Pd) and curve (b) corresponds to a dissociative adsorption (e.g. O_2/Pd).

Measure	Variable	Probe
Dissociation	E_c	- Barrier position(x,y)
	v	- Rotational corrugation
	J	
		- Transition state
	θ	- Surface corrugation
vibrational excitation	E_c v	-Potential surface curvature
rotational excitation	E_c J	- Rotational corrugation
diffraction	E_c	- Surface corrugation
		- Barrier height E_b(x,y)

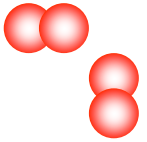

Adsorption/reaction mechanisms

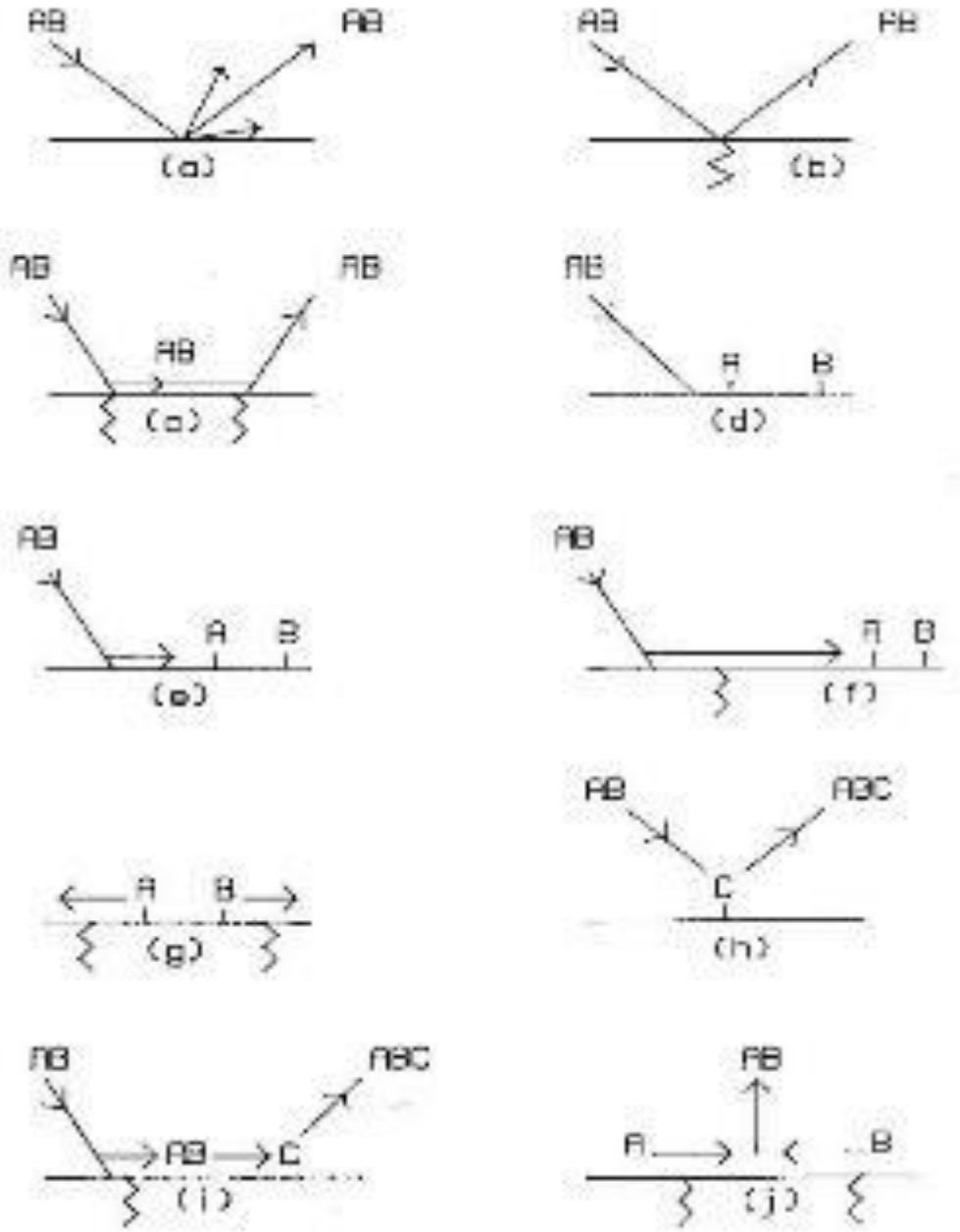

Sticking coefficient evolution

Direct adsorption

$S = S_0(1-\vartheta)$

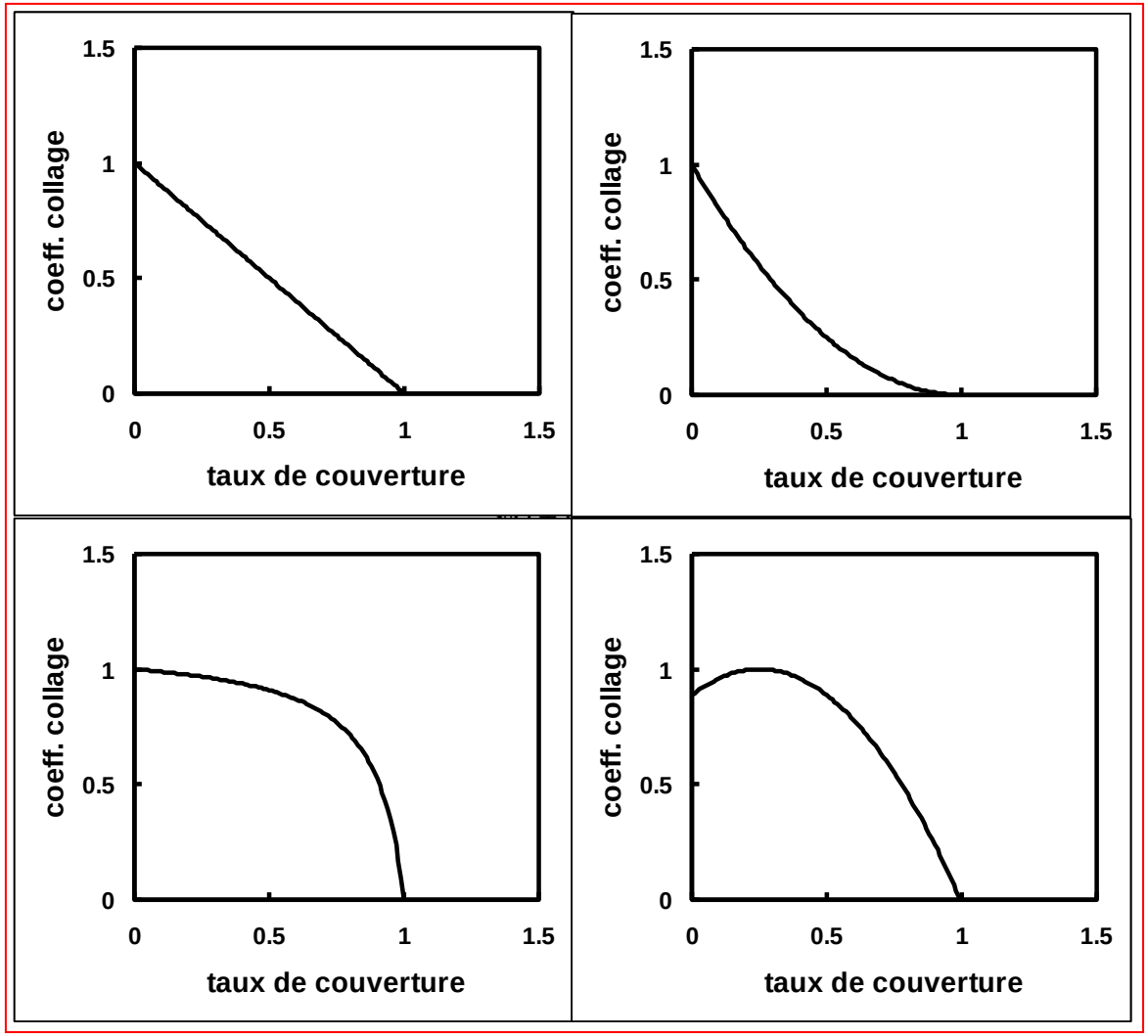

Dissociative adsorption

$S = S_0(1-\vartheta)^2$

Adsorption via precursor

$$S = S_0 \frac{(1+K)(1-\theta)}{1+K(1-\theta)}$$

Adsorption via surface cluster

Video clips

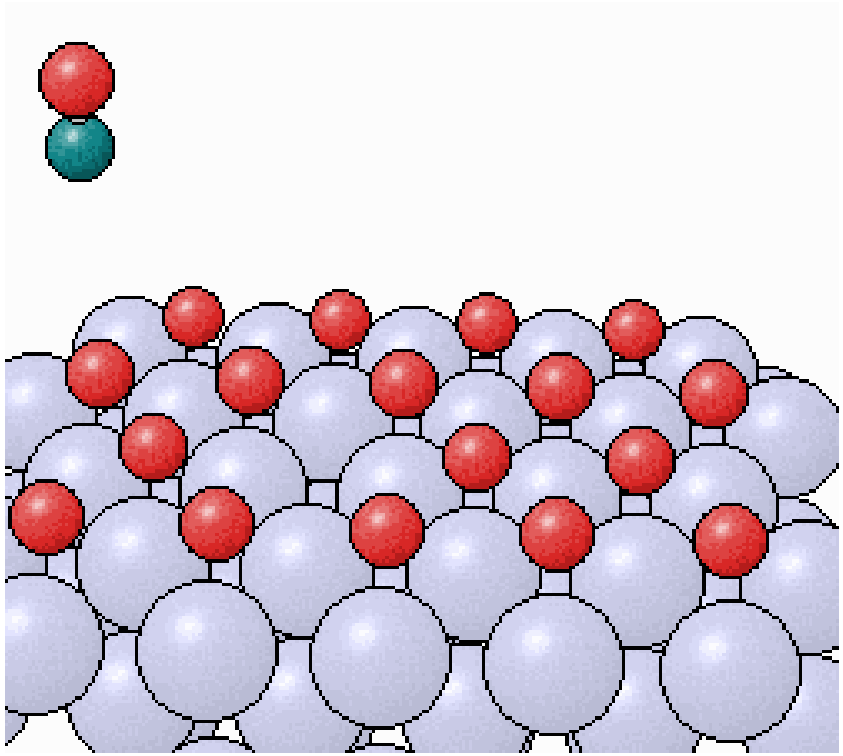

CO oxidation on Ru(111)

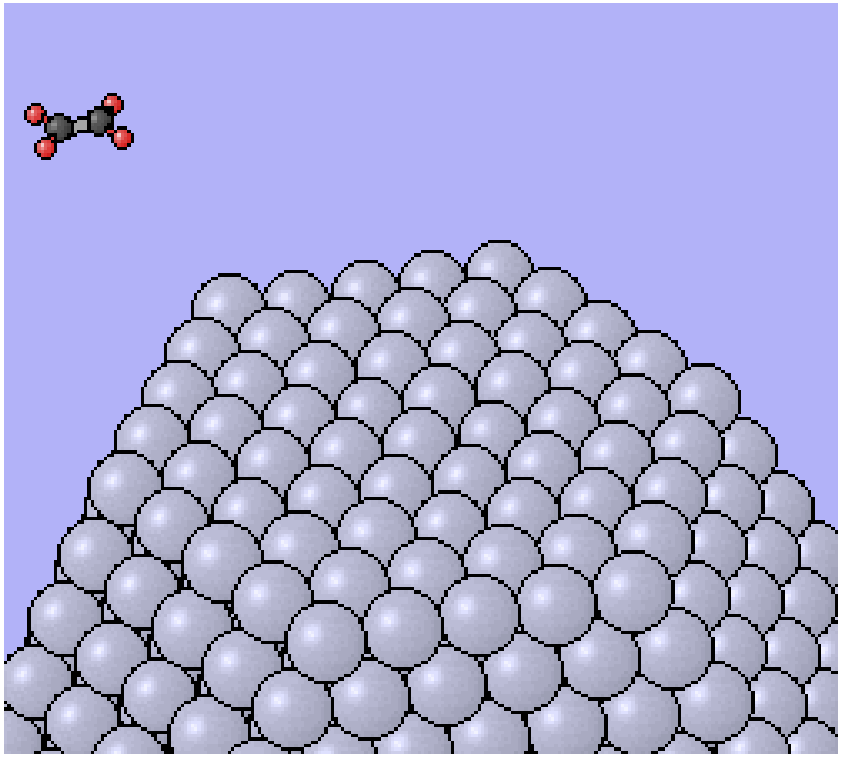

Ethylen dehydrogenation on Ni(111)

High pressure special case

✓ adsorption increases
(more exactly nucleation site density increases)
When incoming flux increase (pressure)

∃ Boundary layer
⇒ Limiting mechanisms
Reaction / transport in BL

Turbulence effect ?

✓ How to observe reactions in HP

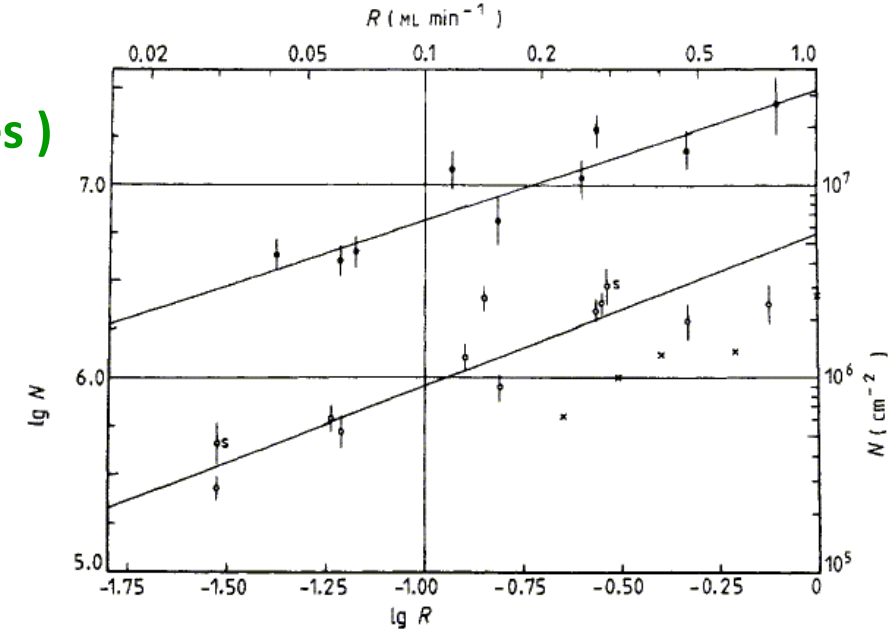

Figure 19. Rate dependence $N_x(R)$ for Ag/W(110) at $T_s = 300$ (●) and 500°C (○) (from Spiller *et al* 1983). Crosses are from Akhter *et al* (1980) nominally at 500°C, but possibly at higher T_s, and points marked s are on noticeably stepped surfaces. (Note N_x in m^{-2}, not cm^{-2}.)

→ Optical methods and close field microscopies (STM/AFM)

HIGH PRESSURE HIGH TEMPERATURE
SFG + STM

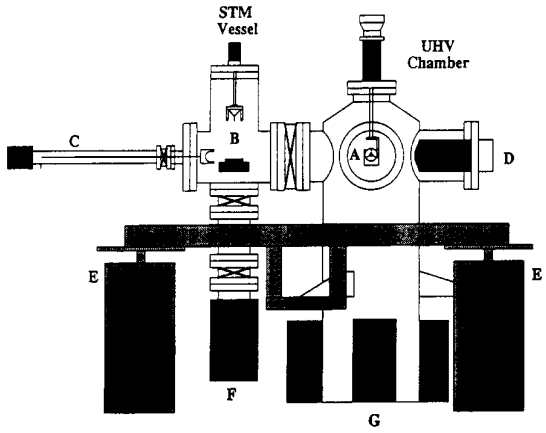

Fig. 1. STM in a high pressure reactor with a UHV surface characterization chamber attached.

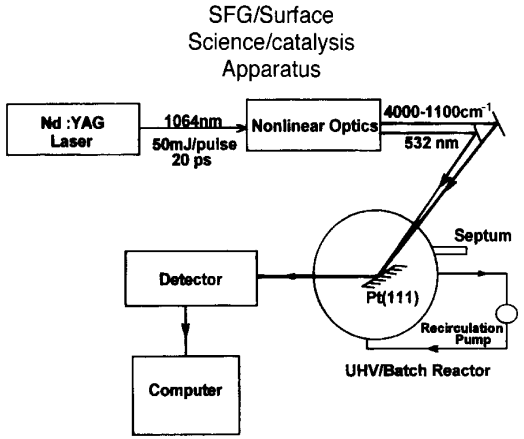

Fig. 2. The UHV/batch reactor apparatus coupled to an Nd:YAG laser for in-situ SFG studies.

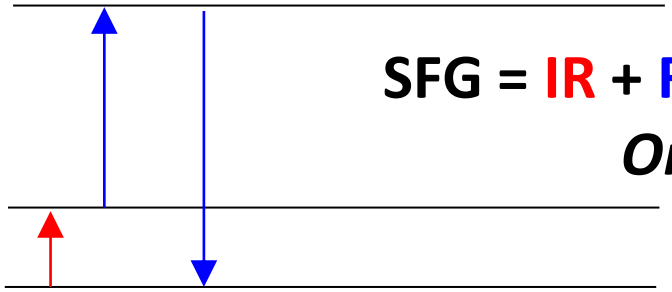

SFG = IR + Raman anti-Stokes (UV-Vis)

Only sensitive to surface

Some pioneering outstanding results

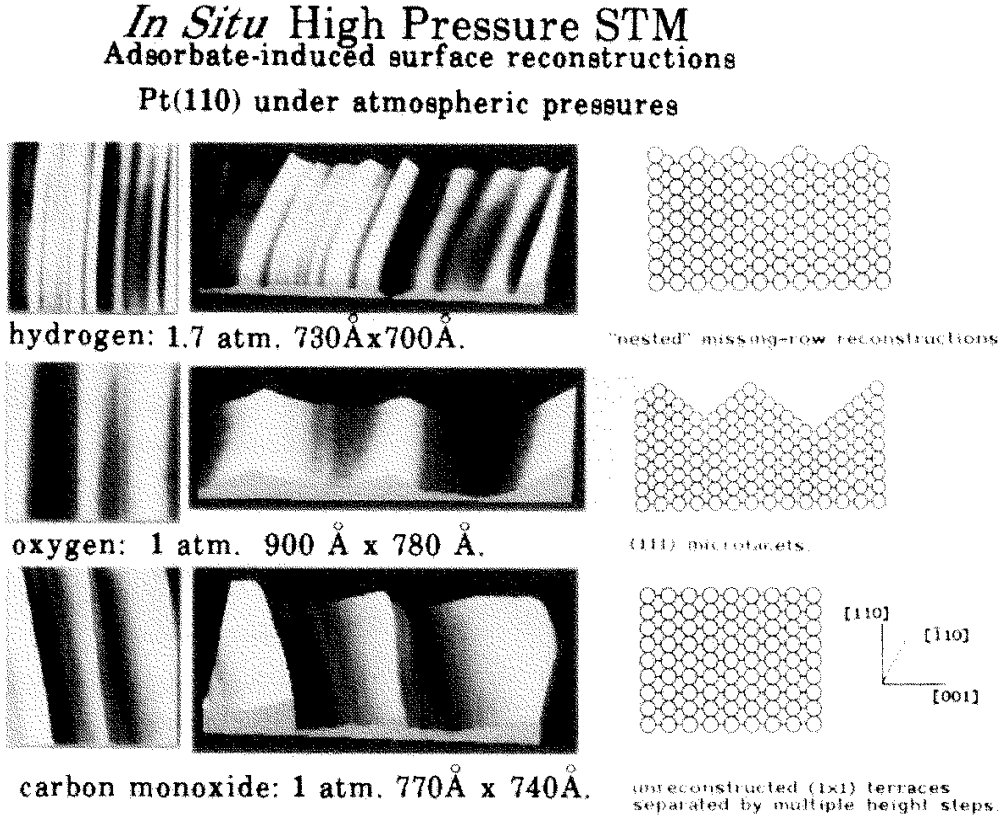

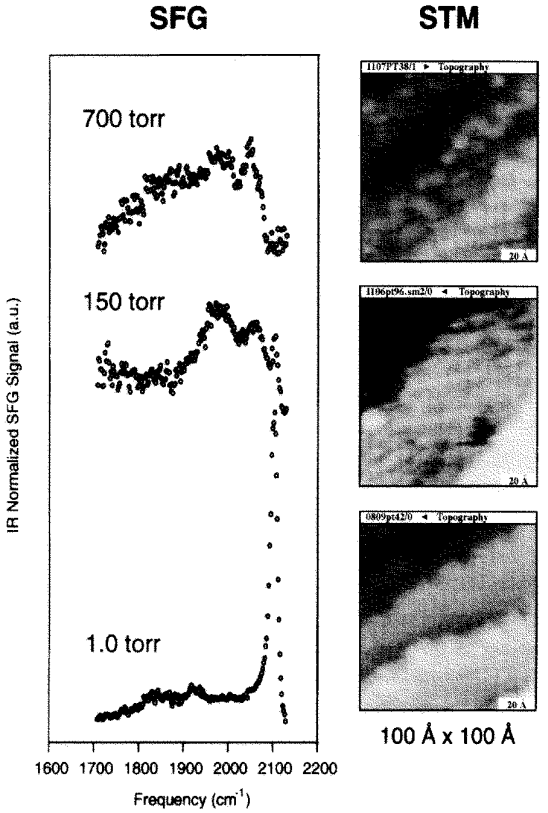

Fig. 7. Scanning tunneling microscope pictures of carbon monoxide over the Pt(111) crystal face at three different pressures: 1.0, 100, and 500 torr.

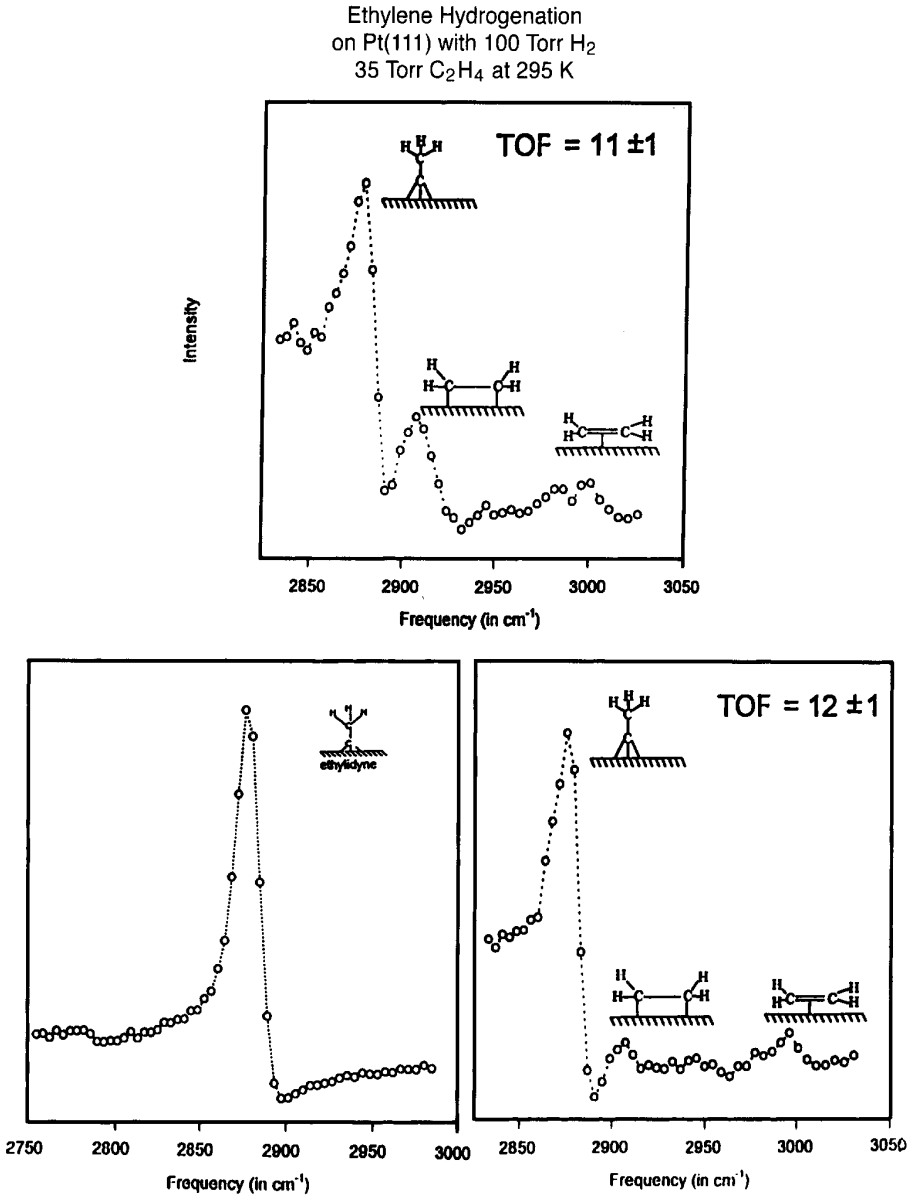

Fig. 8. (a) SFG spectrum of the Pt(111) surface during ethylene hydrogenation with 100 torr H_2, 35 torr C_2H_4, 615 torr He at 295 K. (b) The vibrational spectrum of the same system after the evacuation of the reaction cell. (c) SFG spectrum under the same conditions as (a), but on a surface which was pre-covered in UHV with 0.52 monolayers (ML) of ethylidyne.

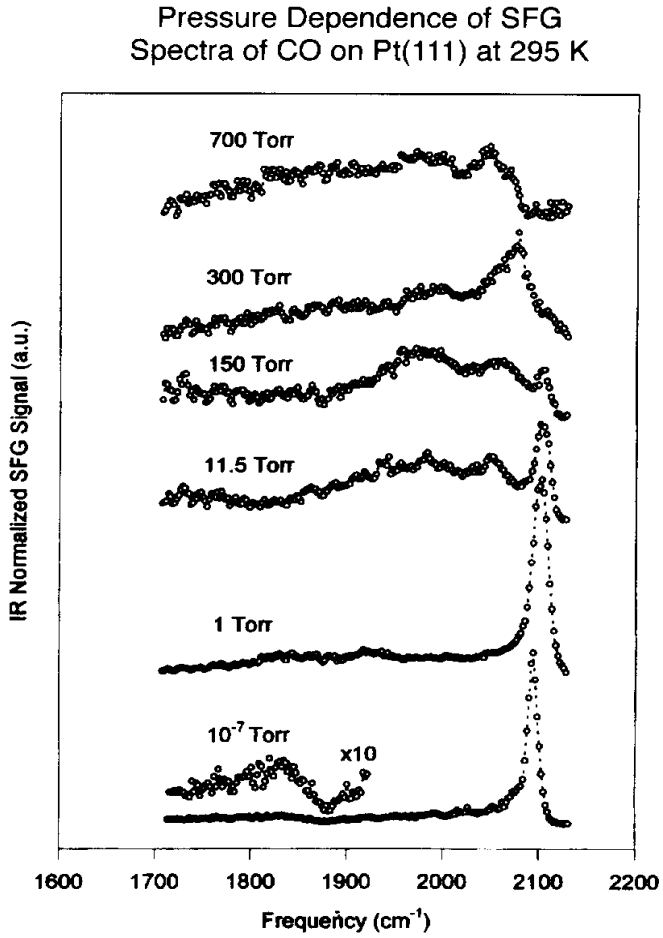

Fig. 6. Pressure dependence of SFG spectra for CO on Pt(111) at 295 K. The spectra change indicates that new surface species appeared at high pressures.

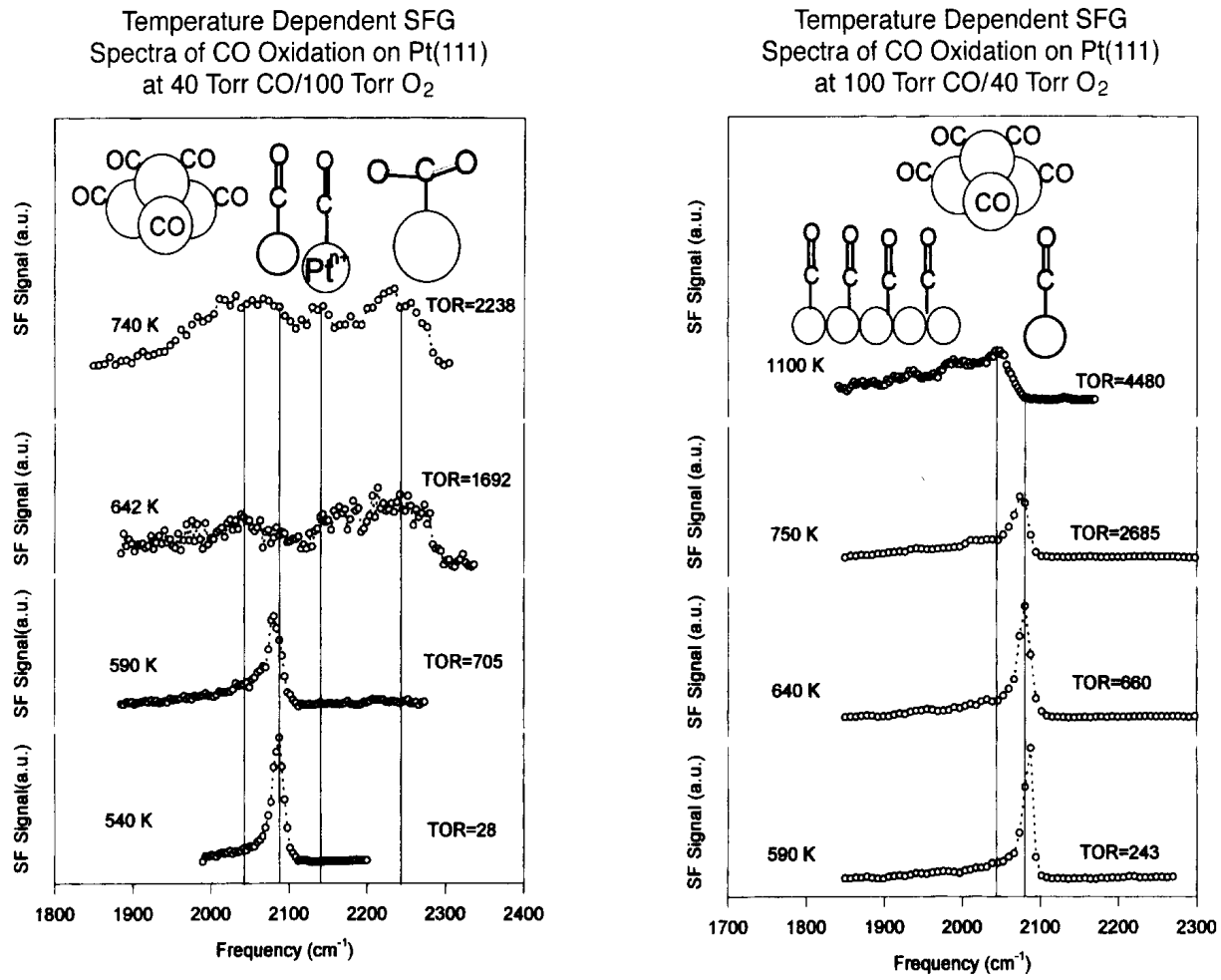

Fig. 11. (a) Temperature dependence of SFG spectra of high pressure CO oxidation over Pt(111) at 100 torr O_2 and 40 torr CO. The temperature and turnover rate are also shown. (b) Temperature dependence of SFG spectra of high pressure CO oxidation over Pt(111) at 100 torr CO and 40 torr O_2. The temperature and turnover rate are also shown.

ABSORPTION X : ...EXAFS

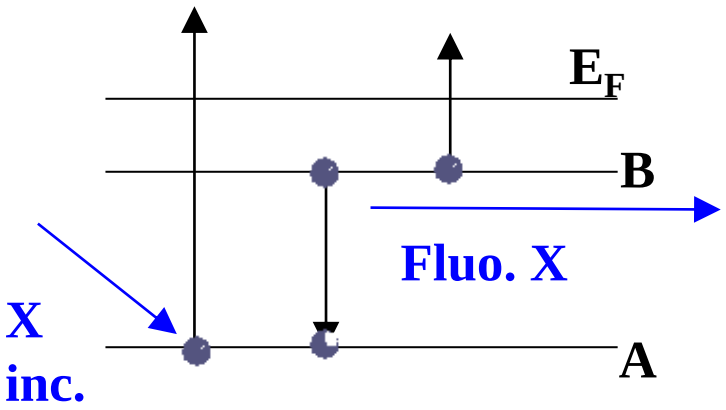

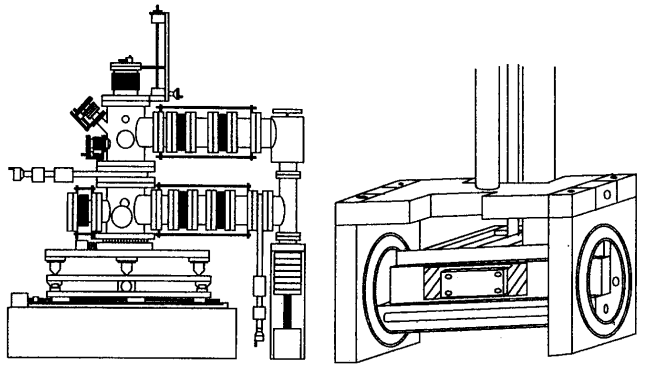

Figure 5. In-situ polarized total-reflection fluorescence XAFS system; (a) the chamber and (b) the sample holder.

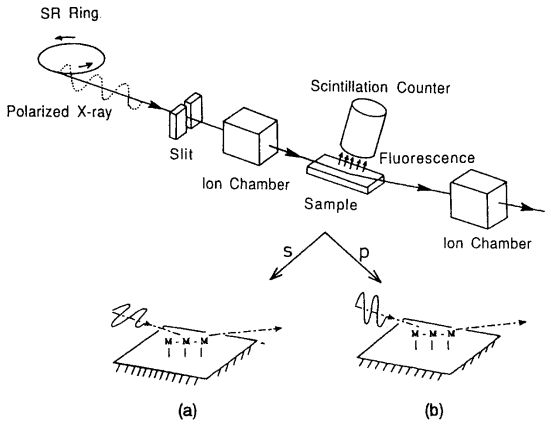

Figure 4. Polarized total-reflection fluorescence XAFS; (a) s-polarization and (b) p-polarization.

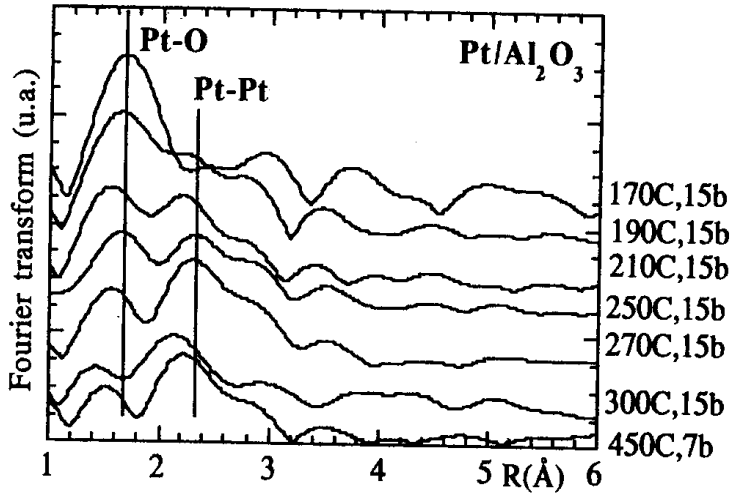

Figure 15 : Evolution of the Fourier transform at the platinum L_{III} edge during the reduction process.

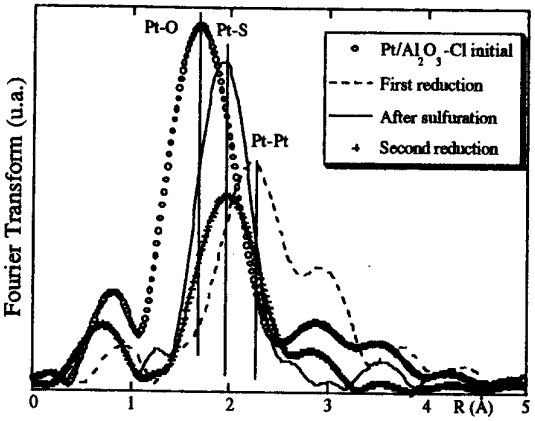

Figure 10 : Moduli of the Fourier transform of the monometallic Pt/alumina.

ion-surface interactions and surface modifications

kinematics :

Binary collision: Energy transfer ΔE (E < few 10 keV)

$$\Delta E_{max} \approx 4 \frac{m_g m_s}{(m_g + m_s)^2} E_g$$

⇒ **atom displacements** E < 10 eV

⇒ **Sputtering** 10 eV < E < 100 keV

- ❑ Sputtering threshold: ≈ 25 - 50 eV
- ❑ Sputtering rate = f(E)

⇒ **implantation** E > 100 keV

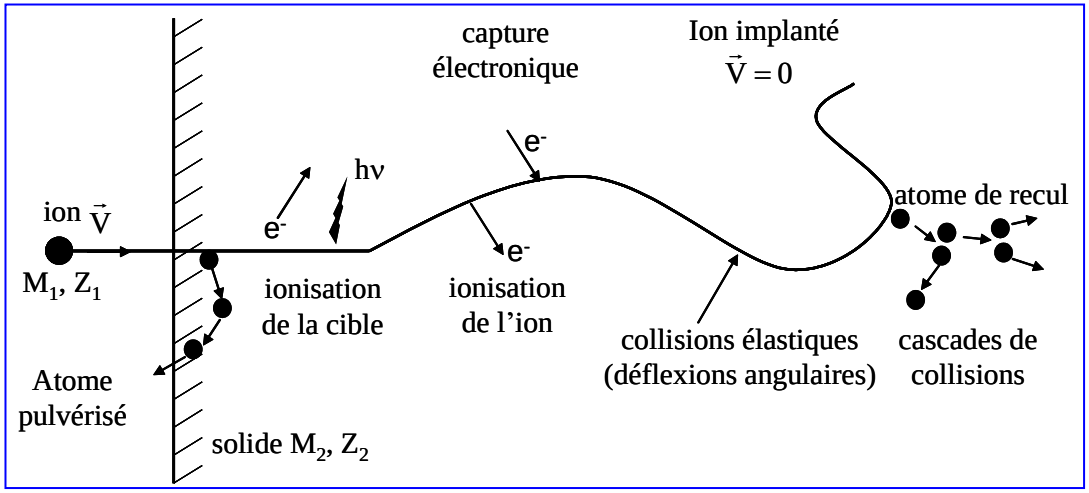

Atom displacement(s)
E < 20 eV

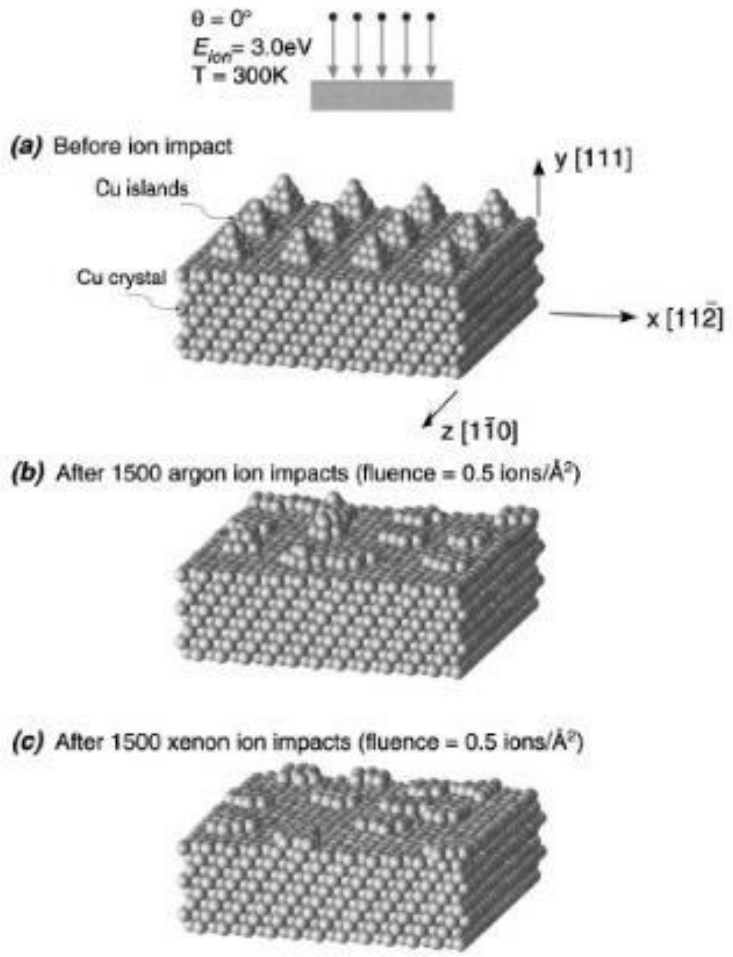

FIG. 1. Evolution of copper islands on copper surface during 3 eV ion impacts.

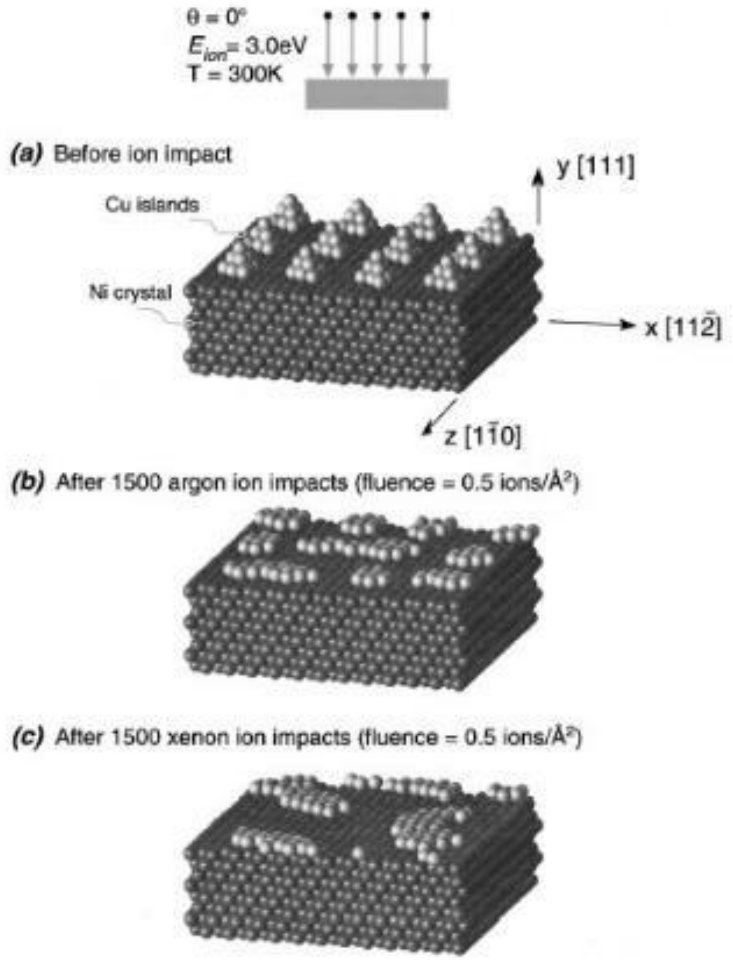

FIG. 2. Evolution of copper islands on nickel surface during 3 eV ion impacts.

Sputtering

Sputtering rate:

$$Y(E) = 0.042\,\frac{Q(Z_2)\alpha^*(M_2/M_1)}{U_s}\,\frac{S_n(E)}{1+\Gamma k_\varepsilon \varepsilon^{0.3}} \times \left[1 - \sqrt{\frac{E_{th}}{E}}\right]^s$$

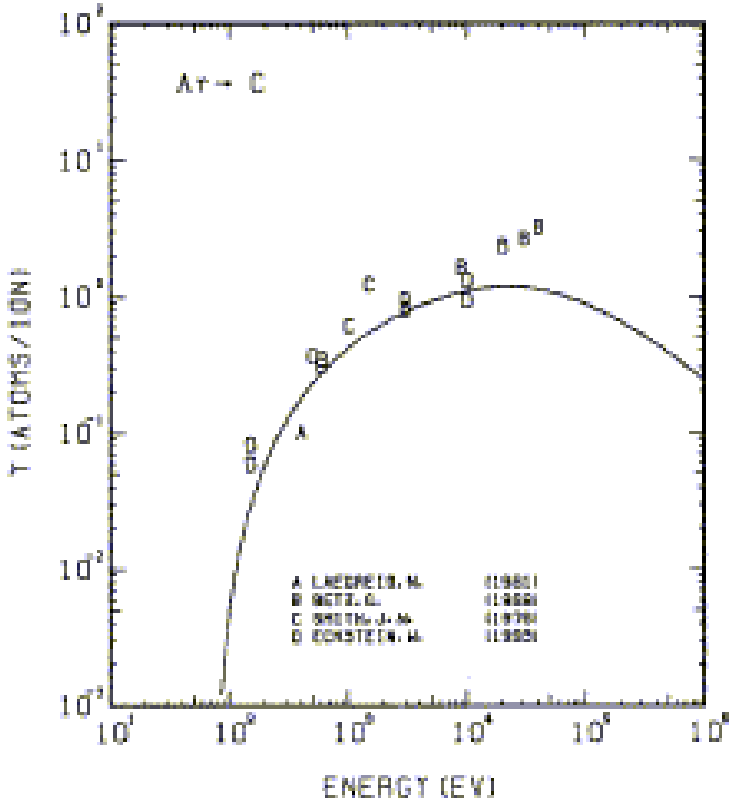

FIG. 21 ENERGY DEPENDENCE OF THE SPUTTERING YIELD OF C WITH AR+. A= 0.30, Q= 1.70, Us= 7.37eV, s= 2.50, W= 0.25Us. EXPERIMENTAL DATA FOR DIFFERENT KINDS OF GRAPHITE ARE INCLUDED.

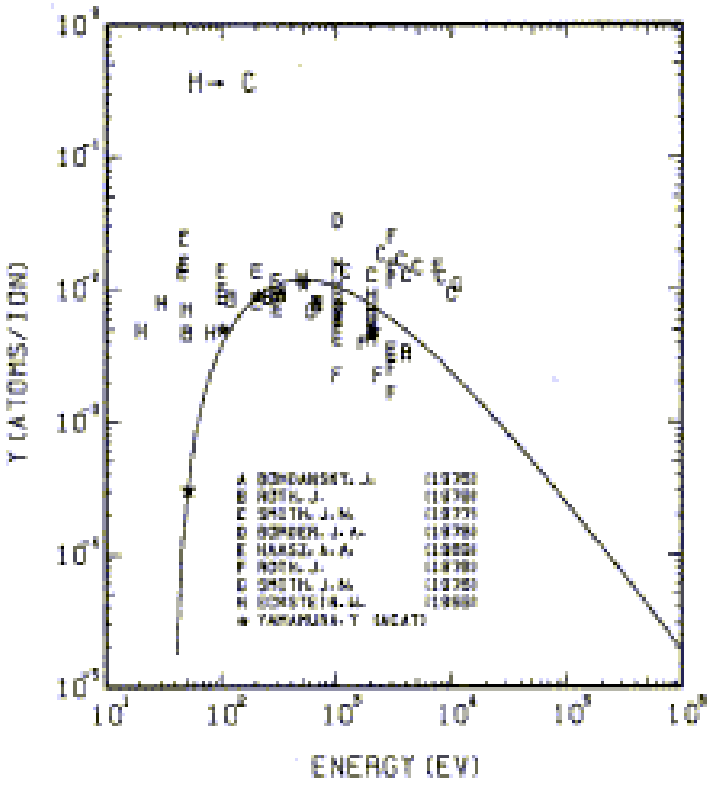

FIG. 15 ENERGY DEPENDENCE OF THE SPUTTERING YIELD OF C WITH H+. A= 11.91, Q= 1.70, Us= 7.37eV, s= 2.50, W= 0.25Us. EXPERIMENTAL DATA FOR DIFFERENT KINDS OF GRAPHITE ARE INCLUDED. THE CHEMICAL EROSION IS FOUND EVEN AT ROOM TEMPERATURE.

Y . Yamamura & H. Tawara, *Atomic and Nuclear Data Tables* 62 (1996) 149 -253

Comparison of different methods for calculating sputtering yields and sputtered atom energy distributions.

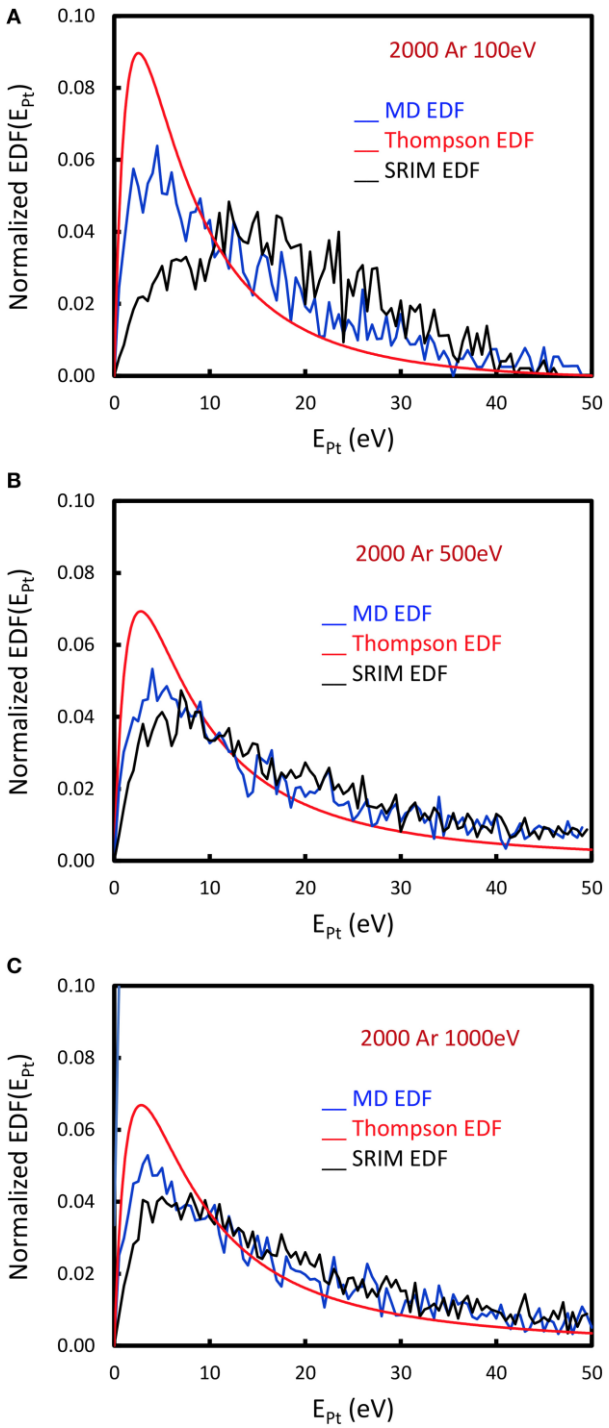

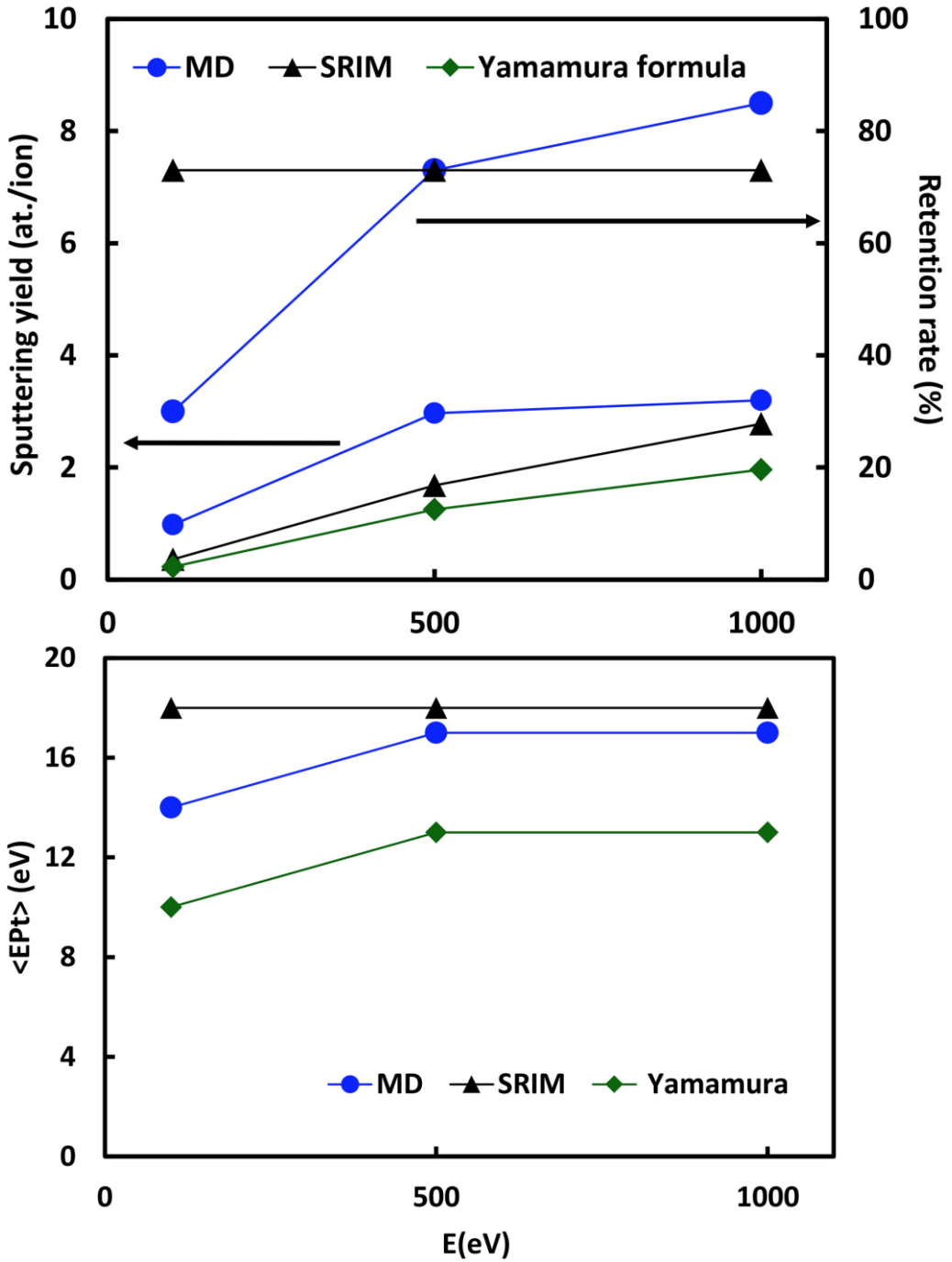

Brault P et al(2016) Molecular Dynamics Simulations of Platinum Plasma Sputtering: A Comparative Case Study. Front. Phys. 4:20. doi: 10.3389/fphy.2016.00020

Structure effects on reactivity

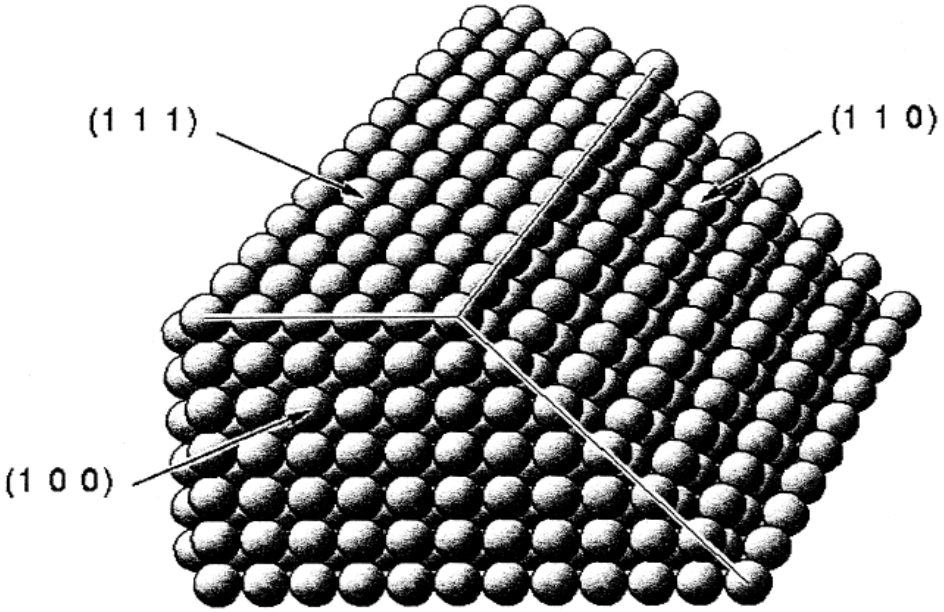

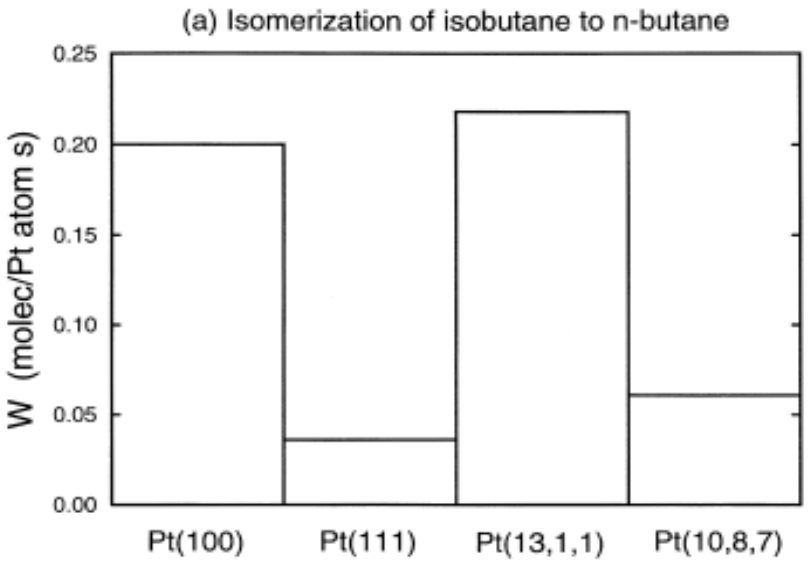

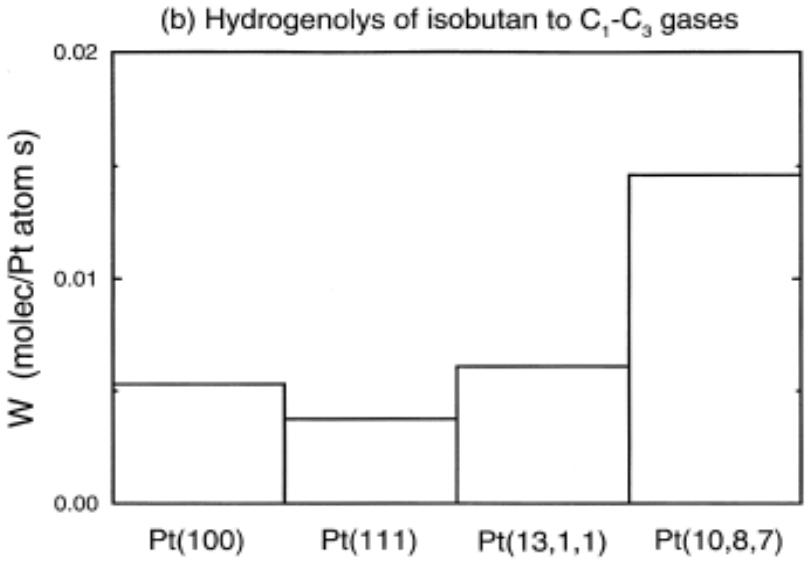

NANO OBJECTS

Morphologies

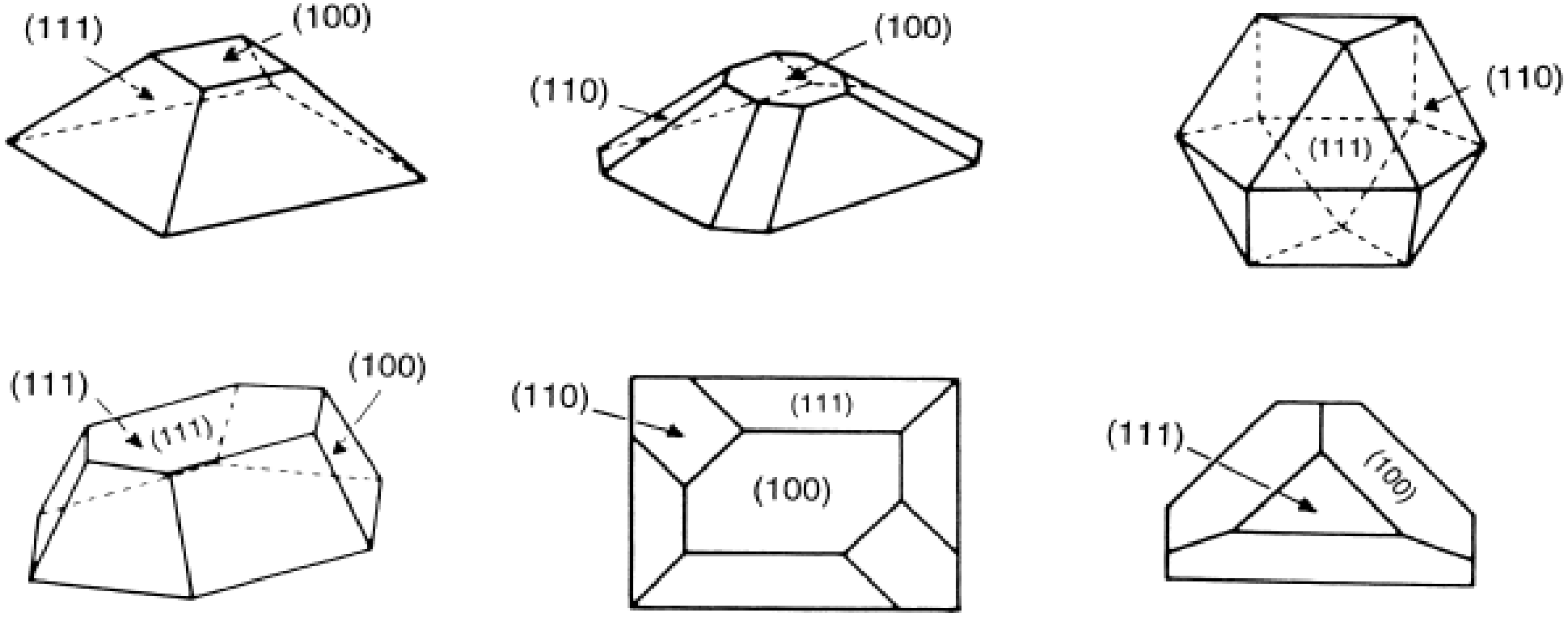

Fig. 18. Typical shapes of supported crystalline 3–20 nm metal particles. (Redrawn from [49].)

➔Many combinations of corner, faces, ridges

Size effects

Recall : dispersion (≡ # surface atoms (N_s) / #total atom (N_t)

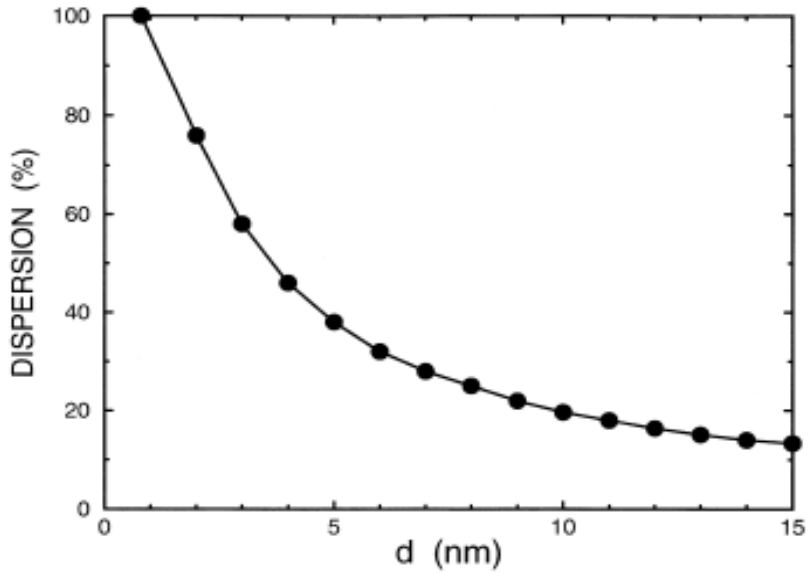

Fig. 1. Dispersion as a function of the Pt particle size. The calculations are based on the sphere and cubo-octahedron models. The size of the data points characterizes the difference of the results for the two models. (Redrawn from [16].)

Example for a sphere with radius r:

$$V = \frac{4}{3}\pi r^3; \quad N_T = \rho_V V = \frac{4\pi}{3}\rho_V r^3$$

$$S = 4\pi r^2; \quad \rho_S = \rho_V^{2/3}; \quad N_S = \rho_S S = 4\pi\rho_V^{2/3} r^2$$

et donc : $$D = \frac{N_S}{N_t} = \frac{3}{\rho_V^{1/3} r}$$

Example

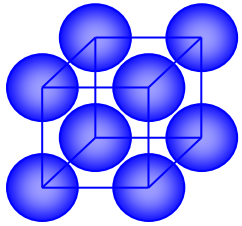

Nano-cube with 8 atoms
All are surface atoms

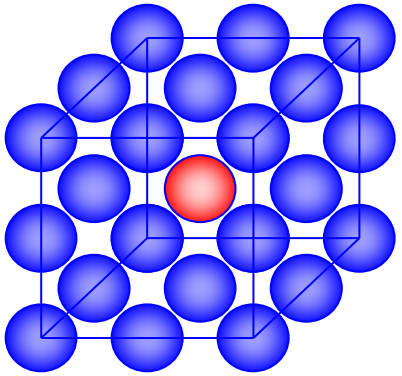

Nano-cube with 27 atoms
26 are surface atoms, only one is bulk atom: red one

Q: for a 4x4x4 = 64 atoms cube, how many surface atoms are there ?

Top + Bottom → 2 x 16 = 32 atoms
Front and rear, it remains → 2 x 8 = 8 atoms
Left and right, it remains → 2 x 4 = 8 atoms

So there are 56 surface atoms in a 4x4x4 cube

reaction rate vs size

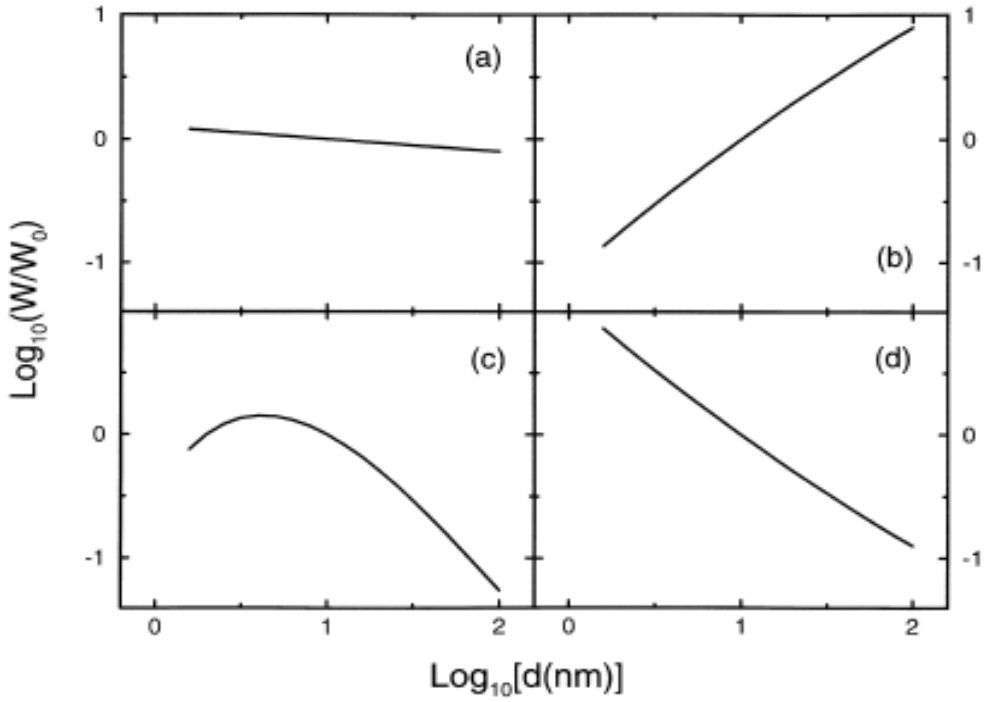

a) Reaction rate is not sensitive to size (rare)

b) Reaction rate is increasing

structure effects (faces, defects).

c) Reaction rate has a maximum

electronic size effects at intermediate sizes 3-4 nm

d) Reaction rate decreases

Small sizes are favored

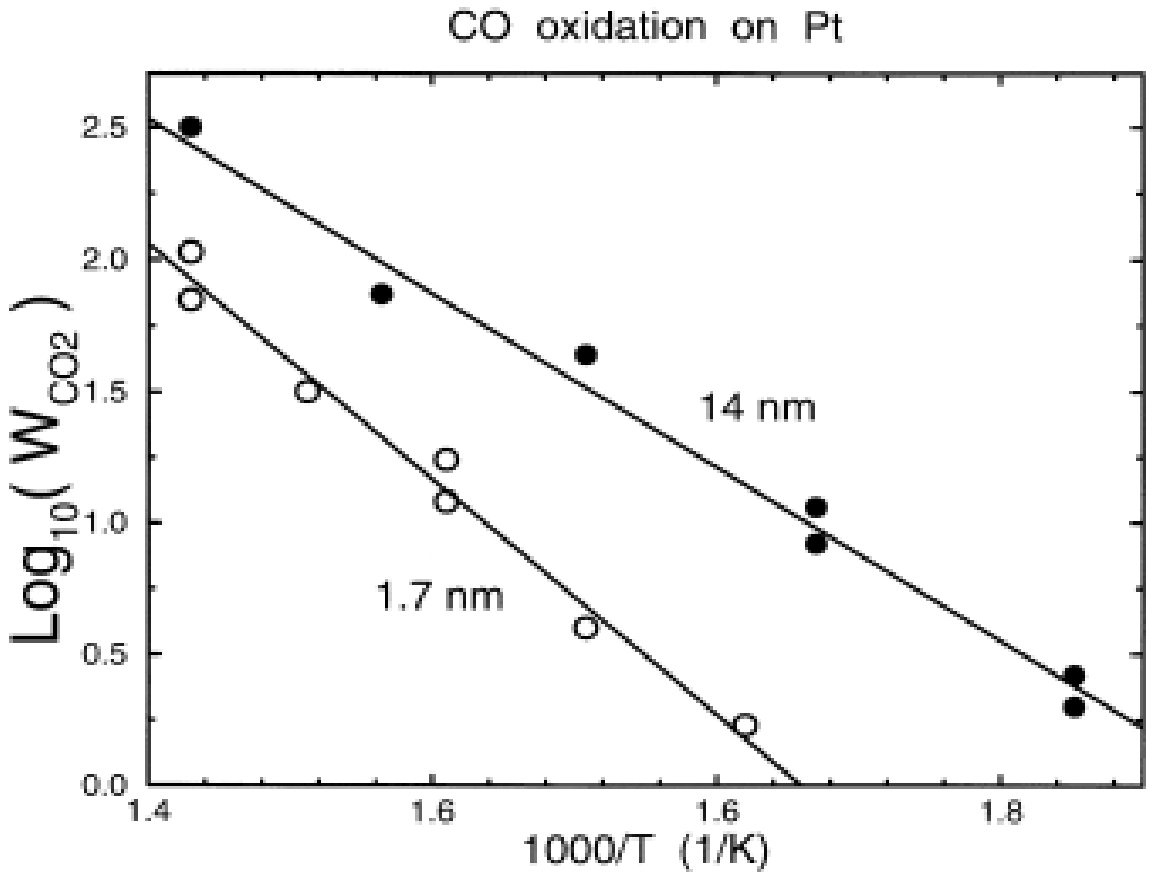

Fig. 3. Rate of CO oxidation, W_{CO_2} (CO_2 molecules/site s), on $Pt/\alpha\text{-}Al_2O_3$ for 14 and 1.7 nm catalyst particles at $P_{CO} = P_{O_2} = 10$ Torr. (Redrawn from [21].)

$W_{1.7\,nm} < W_{14nm}$ car E_{CO} (1.7 nm) > E_{CO} (14nm)

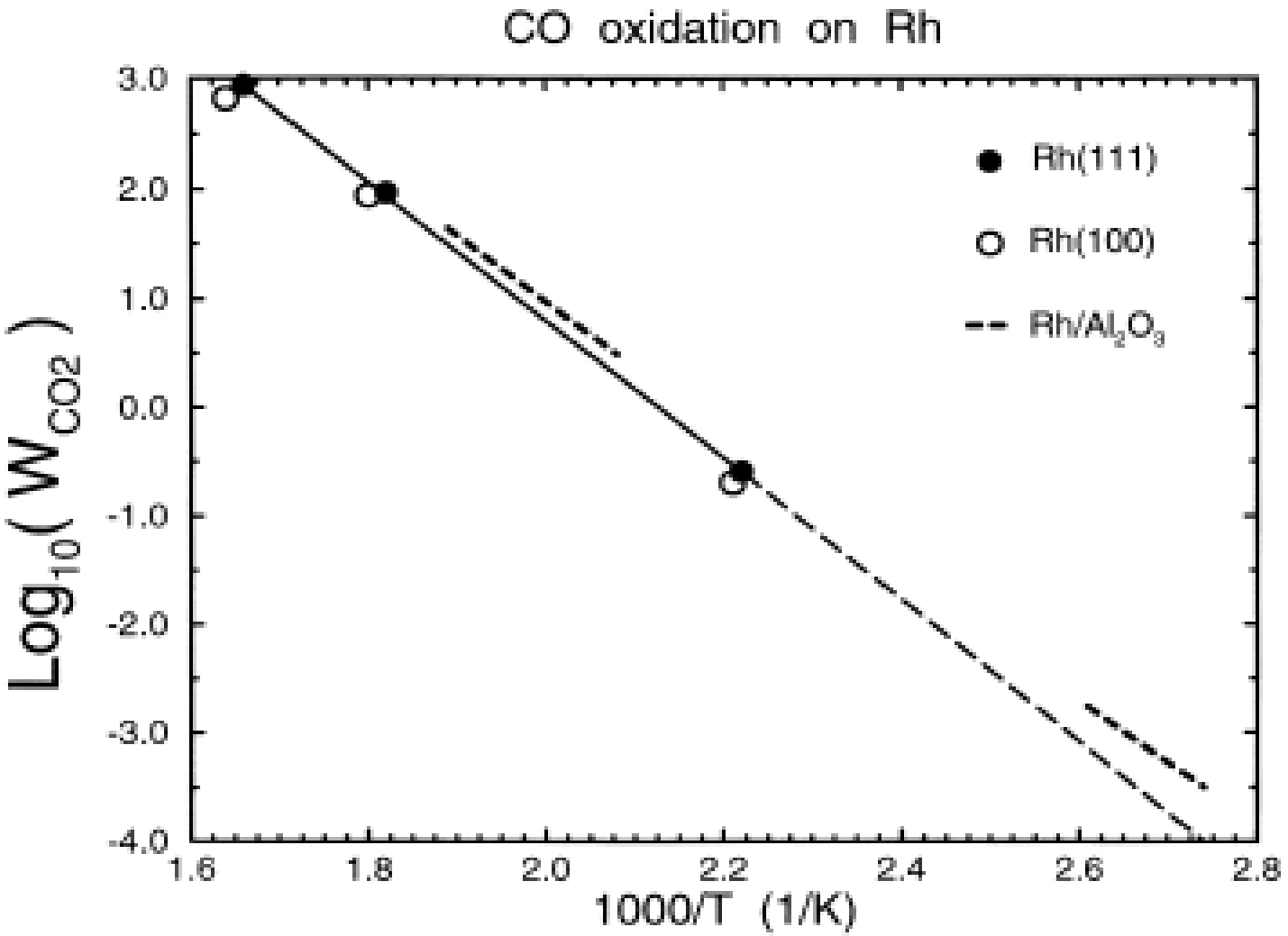

Fig. 4. Rate of CO oxidation, W_{CO_2} (CO_2 molecules/site s), on Rh (1 1 1), Rh (1 0 0), and Rh/Al_2O_3 at $P_{CO} = P_{O_2} = 8$ Torr. The supported Rh catalyst (with dispersion of 12%) was prepared by impregnation of alumina beads. (Redrawn from [22].)

→ Unsensitive to structure/size

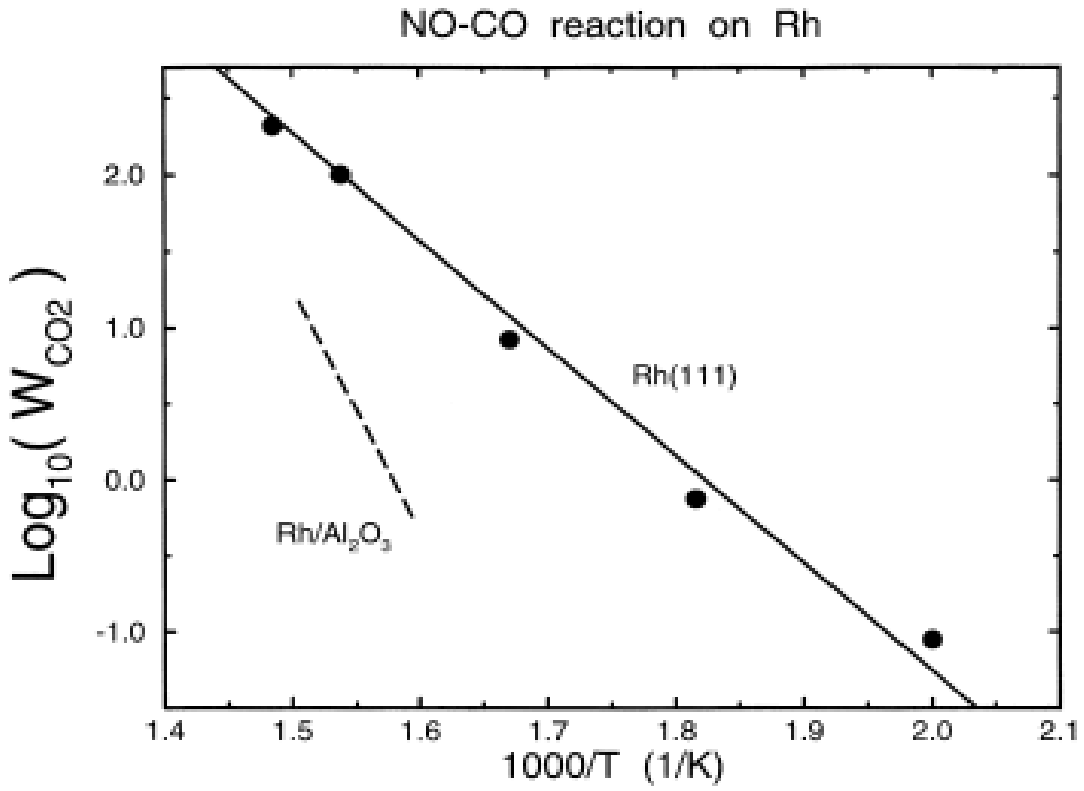

Fig. 5. Rate of CO_2 production, W_{CO_2} (CO_2 molecules/site s), during the NO–CO oxidation on Rh (1 1 1) and Rh/Al_2O_3 at $P_{CO} = P_{O_2} = 8$ Torr. The supported Rh catalyst (with dispersion* of 12%) was prepared by impregnating alumina beads. (Redrawn from [22].)

NO+CO → CO_2 +1/2N_2 on Rh is very sensitive to structure

$$D = 12\% \Rightarrow r = \frac{3}{D\rho_V^{1/3}} = 6nm \ \ pour \ \ Rh; \ \rho_V(Rh) = 7.2310^{22} \, at.cm^{-3}$$

Size effects and temperature

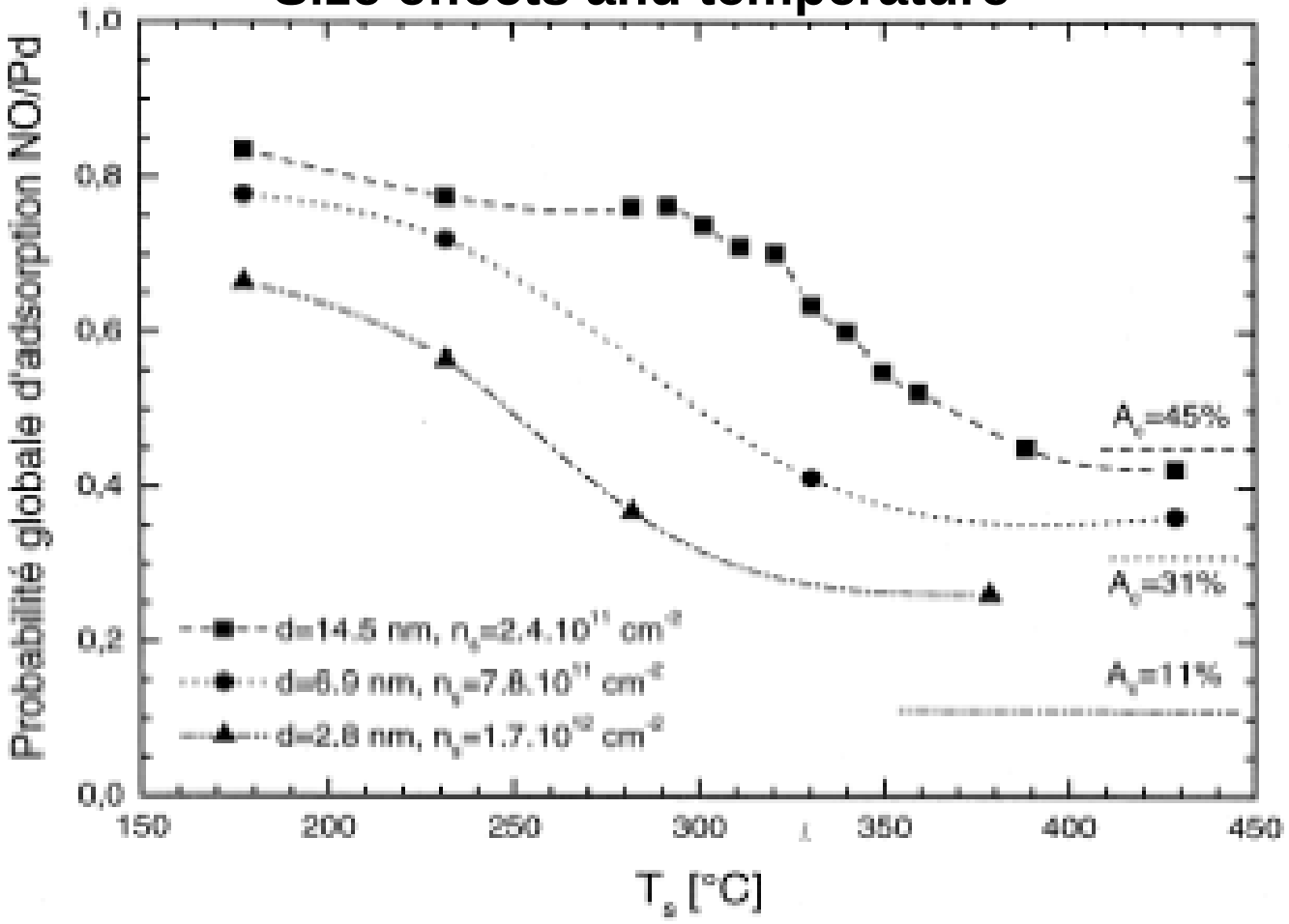

figure 2.12 : Probabilité globale d'adsorption α_g de NO sur Pd en fonction de la température pour trois types de catalyseurs. Pour chaque type, les points expérimentaux sont reliés par une fonction spline et la valeur A_v de la fraction d'aire couverte par le Pd est représentée par un trait de style (tirets, pointillés ou tirets-pointillés) identique au style de la fonction spline. L'erreur sur les valeurs absolues de α_g est estimée à 10% du fait de l'approximation (1.19) conduisant à l'expression (1.20) du paragraphe 1.3.2.1, utilisée dans le calcul de α_g.

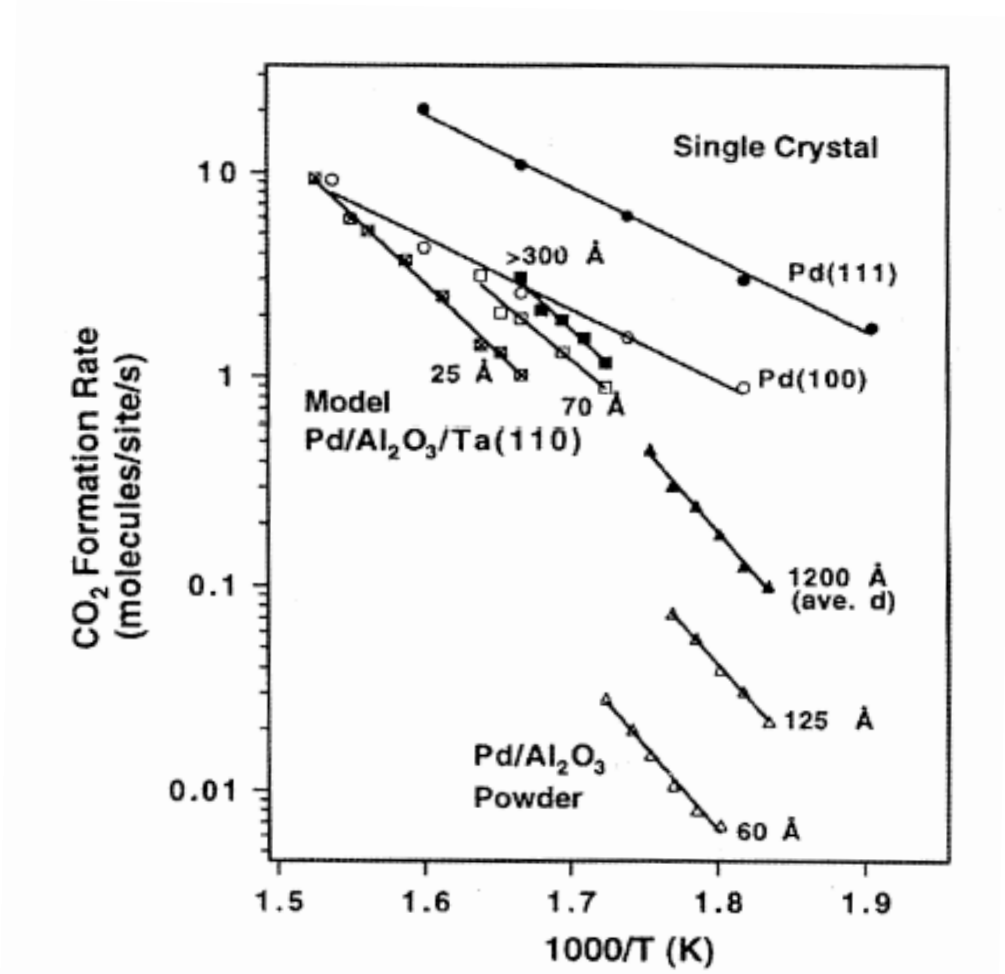

figure 3.1 : *Turnover number* de production de CO_2 en fonction de l'inverse de la température (diagramme d'Arrhénius) pour différents types de catalyseurs (réf. [34] p.237).

$W(CO_2)$ increases on single crystals with increasing size

NO sur agrégats de Pd déposés sur MgO

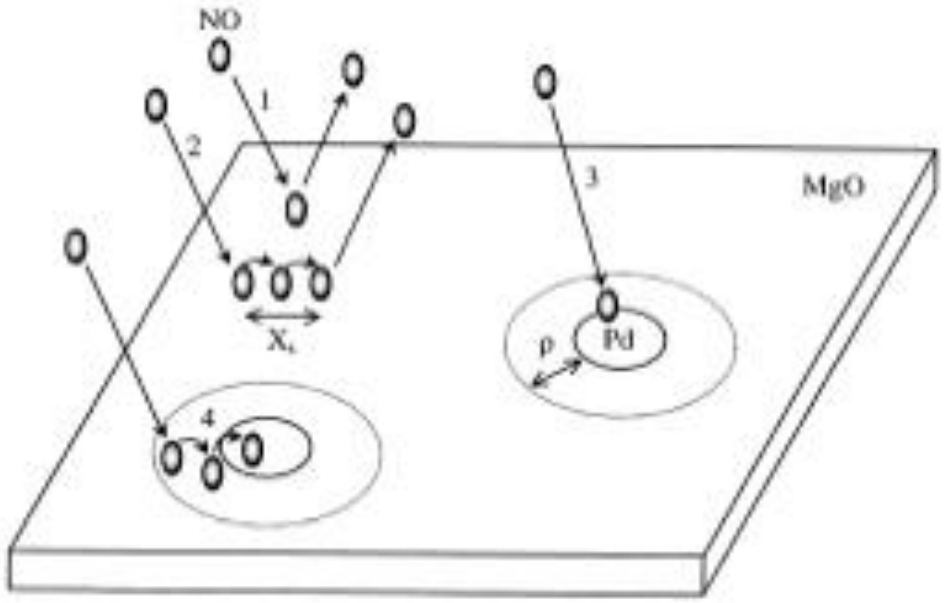

figure 2.13 : Représentation schématique des étapes élémentaires de l'interaction NO/Pd/MgO précédant la chimisorption: (1) réflexion (spéculaire ou diffuse), (2) adsorption et diffusion sur le support (libre parcours moyen X_s), (3) adsorption sur les agrégats par impact direct, (4) adsorption sur les agrégats par capture de molécules diffusant sur le support, à l'intérieur d'une zone de capture de largeur ρ. *NB :* Bien sûr, la réflexion peut aussi survenir à l'intérieur d'une zone de capture.

Square lattice of Pd half-spheres with radius R, surrounded by a fictitious capture area (width ρ =mfp of NO on MgO). When NO is landing on the capture area, it belongs to the cluster

$P = P_{direct}(cluster) + P_{NO/MgO} n_s [\pi(R+\rho)^2 - \pi R^2)$

Steps of the interaction of NO on Pd/MgO

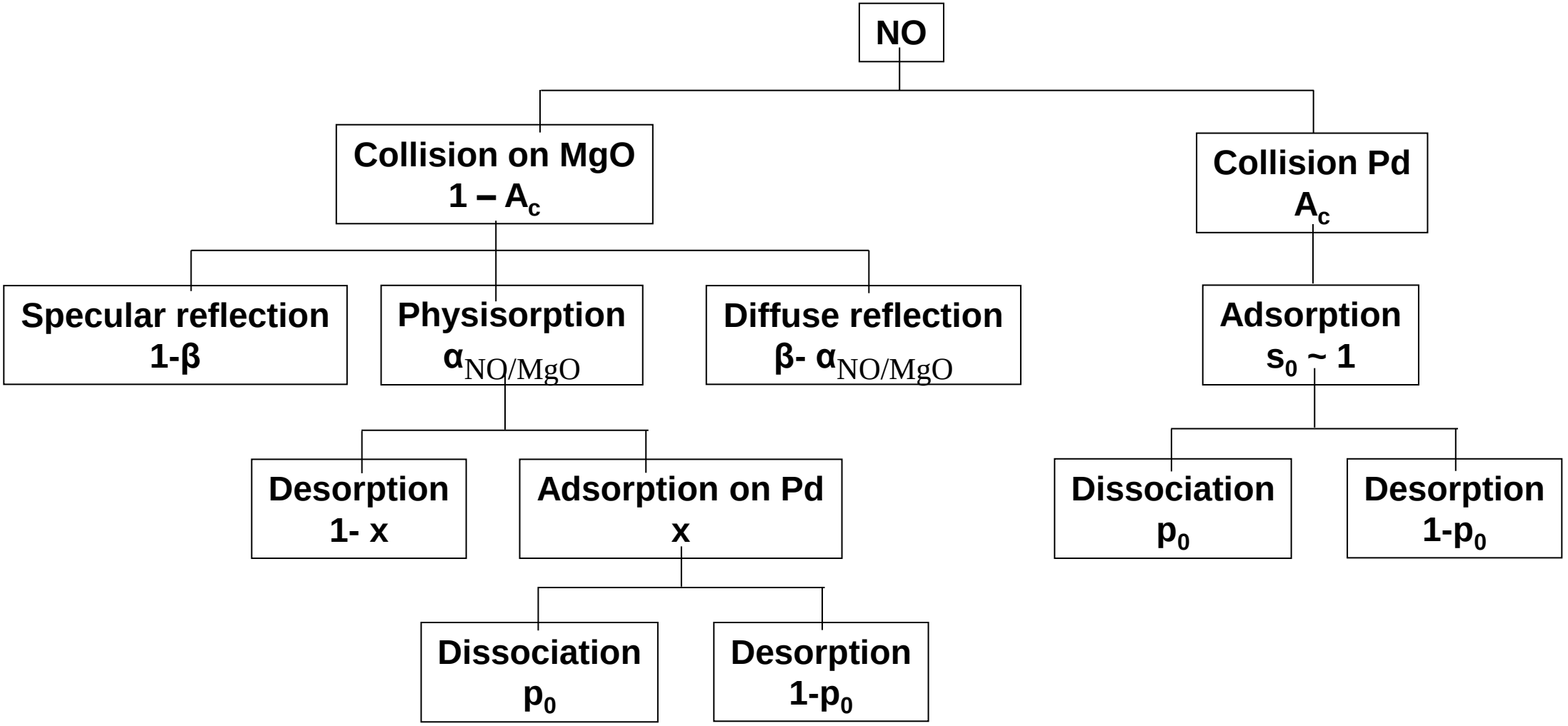

$\Rightarrow$ NO on Pd total probability of adsorption $P = A_c + (1-A_c)\alpha_{NO/MgO}x$

Morphology effects

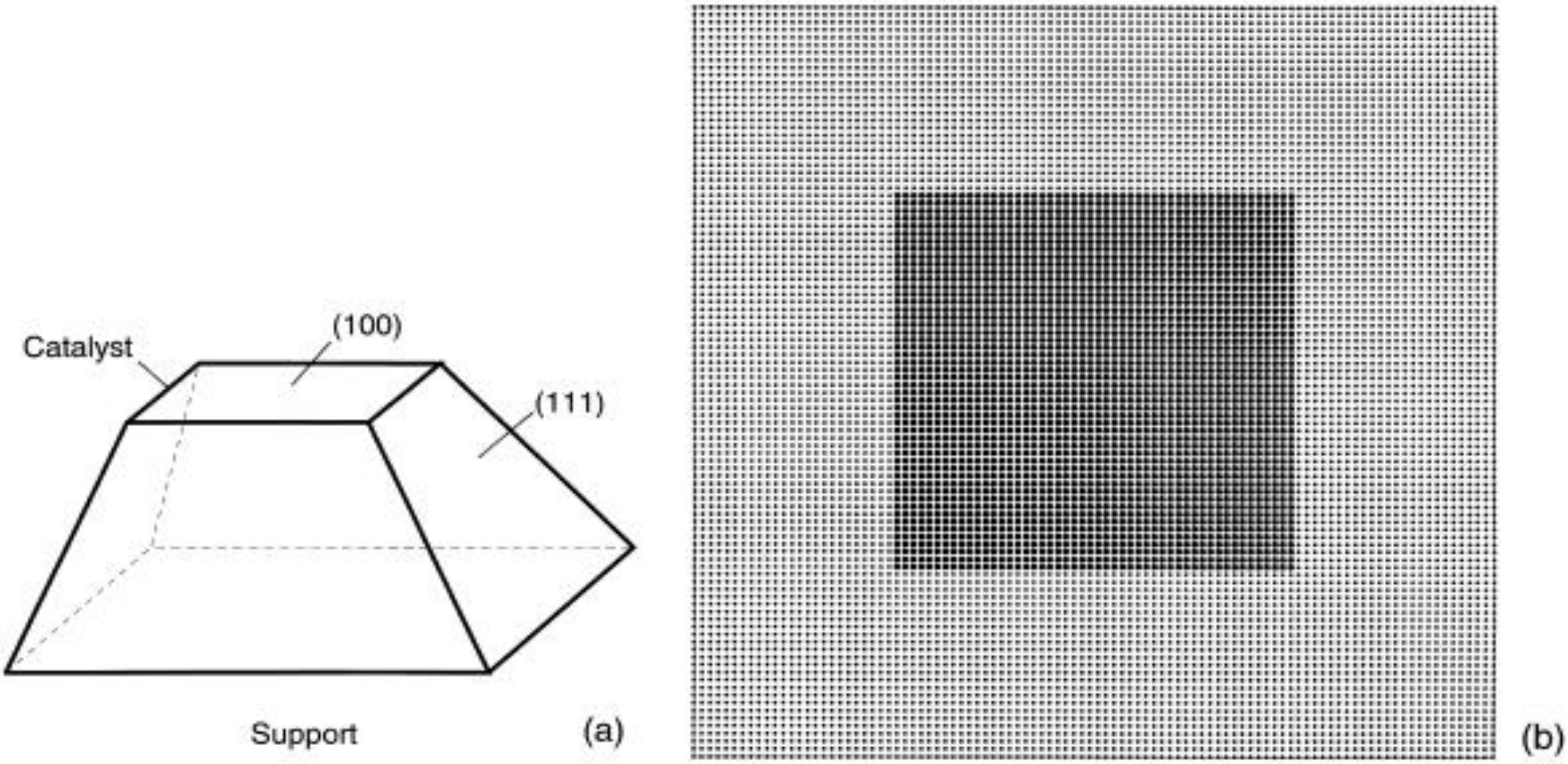

Fig. 23. (a) Typical shape of a supported metal particle. (b) 2D 100 × 100 lattice mimicking a particle shown on panel (a). The central 50 × 50 part of the lattice (large filled circles) represents the top (0 0 1) facet. The periphery (small circles) models the side (1 1 1) facets. (From [77].)

V. P. Zhdanov, B. Kasemo, *simulations of the reaction kinetics on nanometer supported catalyst particles.* Surf. Sci. Rep. 39 (2000) 25 - 104

Algorithm

Step 1: The arriving molecule is chosen to be A with the probability p and B_2 with the probability $1 - p$.

Step 2: If the arriving molecule is B_2, two adjacent sites are selected at random. If either site is occupied, the trial ends [corresponding to direct second-order adsorption (no precursor states)]. Otherwise, B_2 dissociates and adsorbs on the chosen sites with unit probability, if both sites belong to the central part of the lattice, or with the probability $s^{p}_{B_2}$ if at least one of the sites is located on the periphery of the lattice.

Step 3: If the arriving molecule is A, a site (site 1) on the lattice is selected at random. If that site is occupied, the trial ends (no precursor states). Otherwise, A adsorbs. The subsequent reaction of A does not occur with a B particle adjacent to site 1, but somewhere else on the lattice. The reason is that A diffusion is even more rapid than the reaction step. We also need to take into account that the A-binding energies and the LH*-reaction rate constants for the central part and the periphery of the lattice might be different. For these reasons, the A consumption is executed via a few substeps.

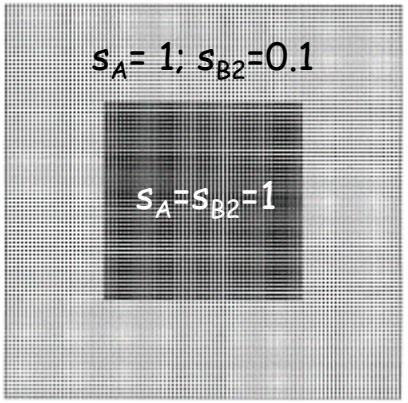

Algorithm (Cont'd)

Step 3.1: Taking into account that diffusion of an A particle is very rapid, we realize the canonical distribution for this particle on all the available sites (i.e., on the sites which are free of B particles). In our case, this distribution depends the binding-energy difference, ΔE ($\Delta E > 0$), between the central and peripheral sites. Practically, the canonical distribution is imitated by choosing at random another site, i.e., site 2 (after site 1 was chosen and provided site 1 was empty). If this site 2 is vacant, the A particle originally landing on site 1 is placed on site 2 with the probability q_p if site 2 is located on the periphery, and with the probability q_c if it belongs to the central part of the lattice [the parameters q_c and q_p are chosen so that one of them is equal to unity and the other is lower than or equal to unity; thus, the lower value of q, i.e., $q_{min} = \min(q_c, q_p)$, and ΔE are interconnected as $q_{min} = \exp(-\Delta E/T)$].

If an attempt of replacement from site 1 to site 2 is not successful [i.e., site 2 is occupied or a generated random number (from 0 to 1) is higher than q_c or q_p, respectively], a new site (site 3) is chosen for another attempt of replacement, etc., until a successful replacement occurs.

Step 3.2: After successful replacement, the A particle tries to react. An adjacent site to, where A was placed in (step 3.1) is randomly selected, and if this site is occupied by a B particle this A–B pair is removed from the lattice (i.e., AB leaves the surface) with the probability r_p, if either reactant is located on the periphery, and with the probability r_c, if both reactants are adsorbed on the central part of the lattice (the parameters r_c and r_p are chosen so that one of them is equal to unity and the other is lower than or equal to unity). If the reaction trial is realized, we return to (step 1) above. Otherwise, steps 3.1 and then 3.2 are repeated again until a successful reaction event occurs.

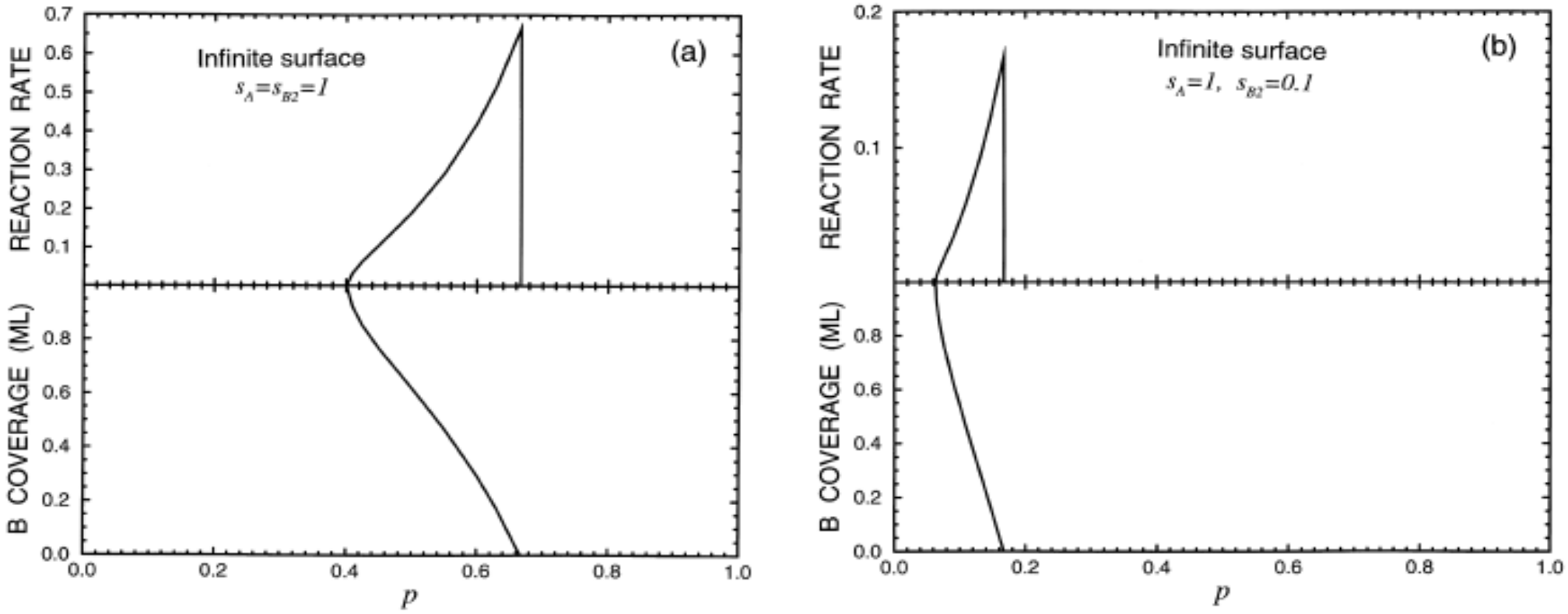

Fig. 24. Reaction rate (A molecule/site MCS) and B coverage for rapid $2A + B_2 \rightarrow 2AB$ reaction with irreversible A and B_2 adsorption, rapidly-diffusing A particles and immobile B particles. The catalyst surface is infinite. (a) Results for the case when the A and B_2 sticking coefficients are equal, $s_A = s_{B_2} = 1$. (b) As (a) but for $s_A = 1$ and $s_{B_2} = 0.1$. (From [77].)

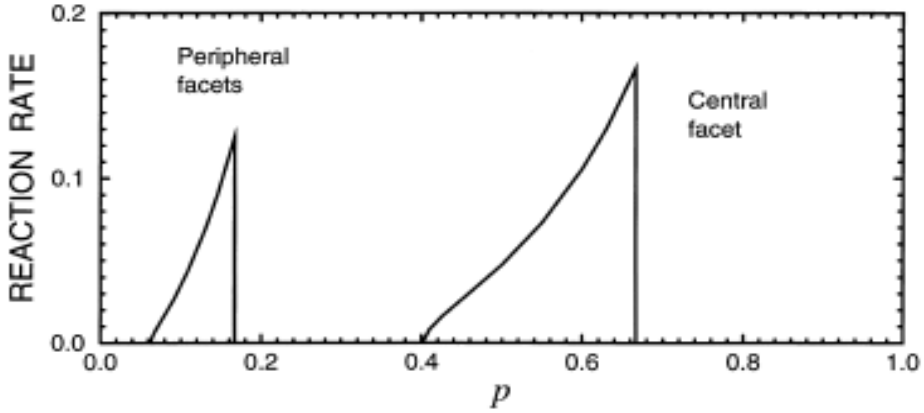

Fig. 25. Superposition of the reaction rates shown in Figs. 24a and b. (From [77].)

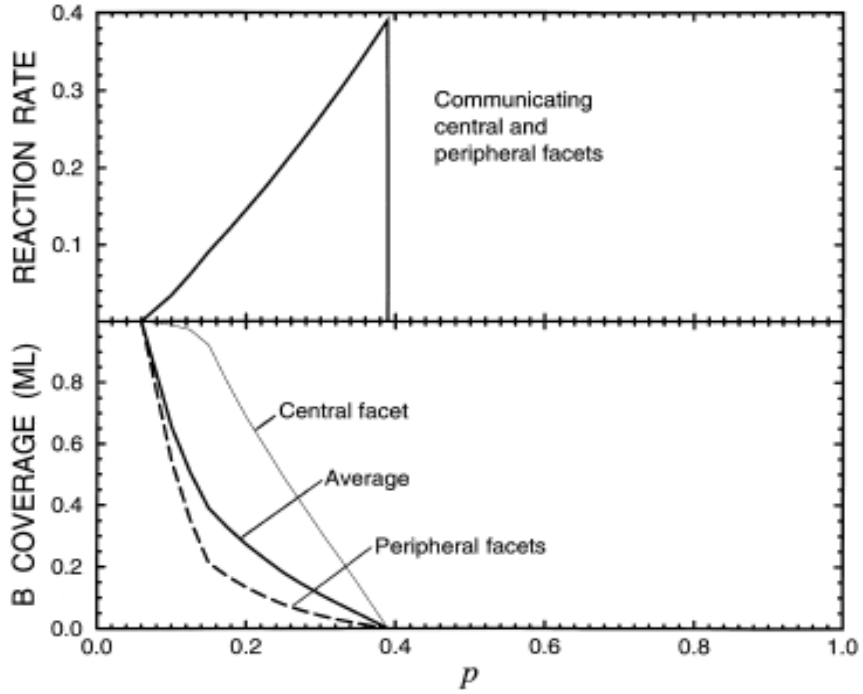

Fig. 26. Reaction rate (A molecule/site MCS) and B coverages for rapid $2A + B_2 \rightarrow 2AB$ reaction occurring on the finite lattice (Fig. 23b) mimicking a supported catalyst. The thick solid line (on panel (b)) shows the average coverage, the thin solid line corresponds to the coverage of the central facet of the nanoparticle, and the dashed line exhibits the coverage of sites on the peripheral facets. The parameters employed are as follows: $s_A = 1$, $s^c_{B_2} = 1$, $s^p_{B_2} = 0.1$, $q_c = q_p = 1$, and $r_c = r_p = 1$.

Example of kinetics

$2A + B_2 \rightarrow 2AB$ reaction $\theta_{A,B}$ = coverage rate of A, B

$$\frac{d\theta_A}{dt} = k_A^a P_A(1 - \theta_A - \theta_B) - k_A^d \theta_A - k_r \theta_A \theta_B,$$

$$\frac{d\theta_B}{dt} = k_{B_2}^a P_{B_2}(1 - \theta_A - \theta_B)^2 - k_r \theta_A \theta_B,$$

Case (1) $\theta_B \gg \theta_A$ and $\theta \simeq \theta_B$, where $\theta = \theta_A + \theta_B$),

$$\frac{d\theta}{dt} = k_{B_2}^a P_{B_2}(1 - \theta)^2 - k_A^a P_A(1 - \theta).$$

Case (2) P_A/P_{B_2} is sufficiently large and $\theta \simeq \theta_A$

$$\frac{d\theta}{dt} = k_A^a P_A(1 - \theta) - k_A^d \theta - k_{B_2}^a P_{B_2}(1 - \theta)^2.$$

Alloy effects

Mixing

Segregation

	$e_{mix} > 0$ alloy formation	$e_{mix} < 0$ phase separation
$e_{segr} < 0$ adsorbate atoms stay at the surface	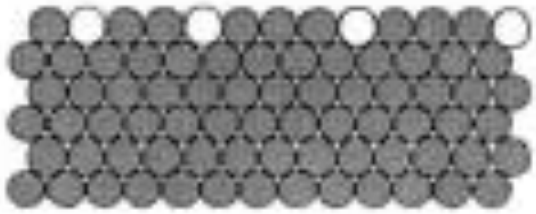	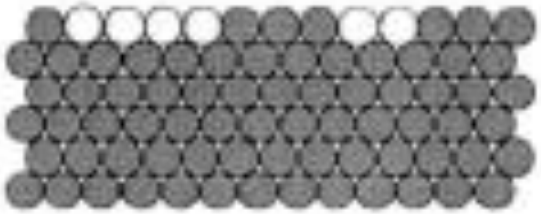
$e_{segr} > 0$ adsorbate atoms migrate into the bulk	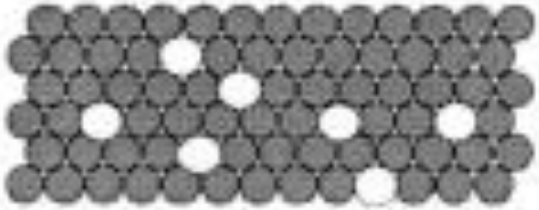	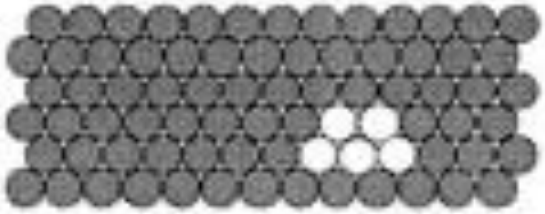

Alloy effects

Segregation \ Mixing	$e_{mix} > 0$ alloy formation	$e_{mix} < 0$ phase separation
$e_{segr} < 0$ adsorbate atoms stay at the surface	Co*, Ru, Rh, Pd, Ag, Pt, Au / Fe Rh, Pd, Ag, Pt, Au / Co Cu*, Rh, Pd, Ag, Pt, Au / Ni Pd, Ag, (Pt), Au / Cu Fe*, Co*, Ni*, Pt, Au / Ru (Fe*), Ni*, Pt, [Au] / Rh Au / Pd	Ni, Cu / Fe ([Fe]), [Ni], Cu / Co Cu*, Rh, Pd, Ag / Ru Cu, Pd, Ag / Rh Ag* / Pd Ag*, Au / Pt
$e_{segr} > 0$ adsorbate atoms migrate into the bulk	Ru / Co Fe*, [Co*], Ru / Ni Ni* / Cu (Co*) / Rh Fe*, Co*, Ni*, (Cu*) / Pd Co*, Ni*, Cu*, Rh*, Pd*, Pt*, (Au) / Ag Fe*, Co*, Ni*, Cu*, Ru*, Rh*, ([Pd*]) / Pt Fe*, Co*, Ni*, Cu*, Rh*, Pd*, (Ag*), Pt* / Au	Fe*, Co*, Ru, [Rh] / Cu Ru* / Rh Ru, Rh*, [Pt*] / Pd Fe*, Ru* / Ag Ru* / Au

Alloys effects

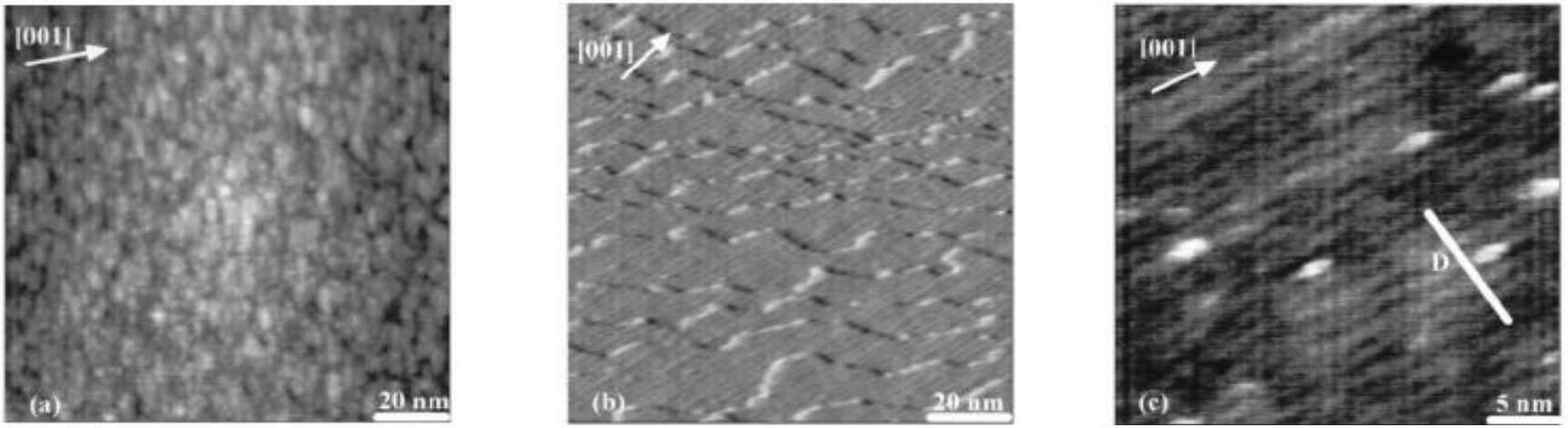

3 ML Pd/Ni(110) : (a) as deposited (b, c) after annealing at 250° C
Nanostructuration issu de la relaxation des contraintes.

Catalytic activity for the 1,3-butadiene hydrogenation reaction[a] of pure Ni(110), pure Pd(110) and Pd/Ni(110) [as-deposited at room temperature (RT) and after further heating at ≈200–250°C] deposits [4]

	Catalyst									
	Ni(110)	0.25 ML RT	0.25 ML heated	0.5 ML RT	0.5 ML heated	1 ML RT	1 ML heated	4 ML RT	4 ML heated	Pd(110)
Activity ($\times 10^{15}$ cm^2 s^{-1})	0.35	1.1	2.2	7.4	69	8.4	46	42	142	4.3

[a] Results are given for a hydrogen pressure of 20 Torr and a hydrogen/butadiene ratio of 5.

CO adsorbed on Co/Cu(111)
STM picture

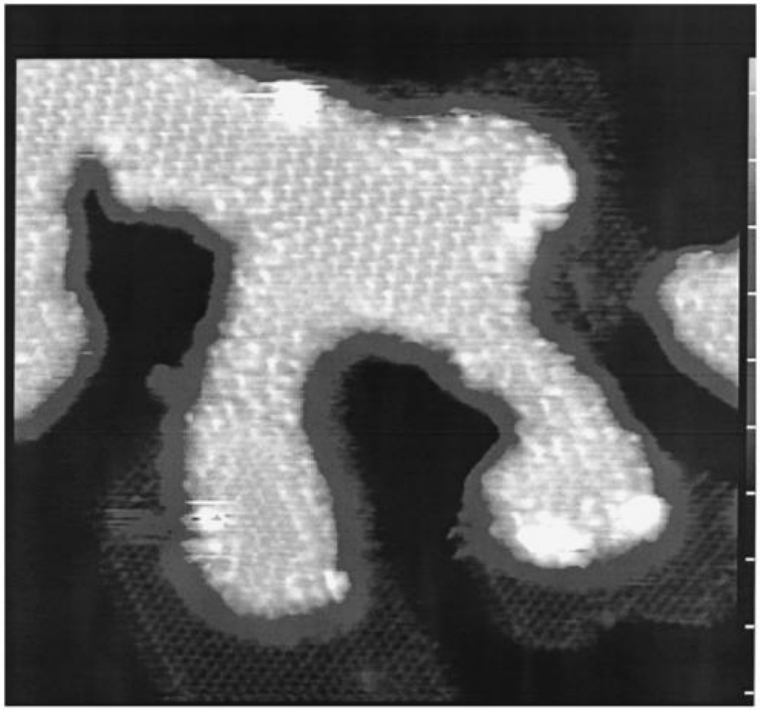

Fig. 42. STM picture of CO adsorbed on Co/Cu(111). The Co was deposited at 150 K and then CO was dosed. The scanning took place at room temperature so that CO only was bonded to Co sites. The image, covering 140 Å×160 Å, is from Ref. [177].

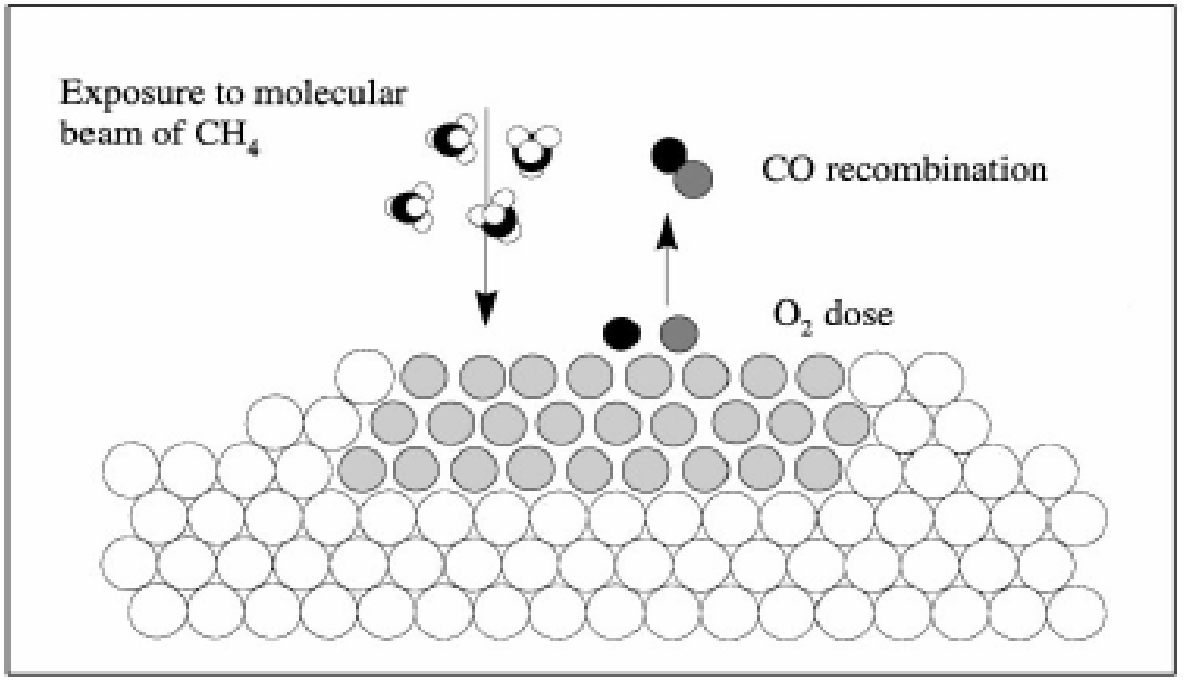

Adsorbed CO on Co/Cu(111)

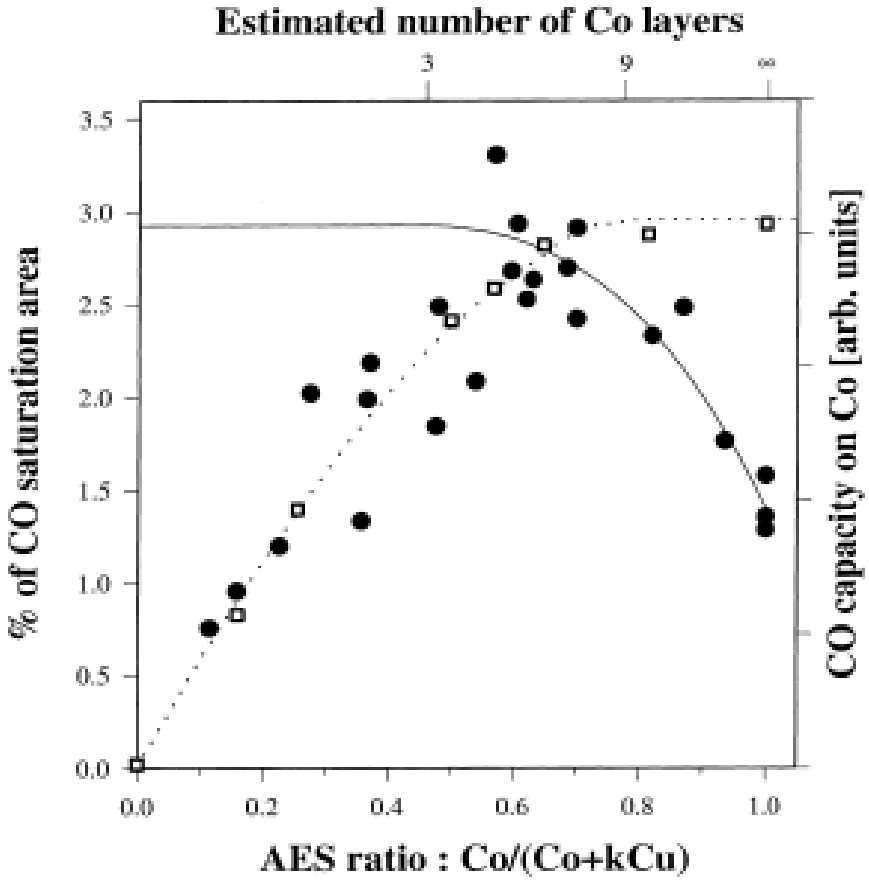

Fig. 41. Measurement of the dissociation probability of CH_4 on Co/Cu(111). The dissociation probability (solid circle) is shown as the area of the recombination peak of carbon and oxygen in percent of CO saturation as a function of the Co amount. The value of the Co amount is the ratio of Auger line heights for Co divided by a weighted sum of Co and Cu. A value of 1.0 corresponds to an infinite number of Co layers. Also shown in this figure with open squares and the dotted line is the CO TPD area from Co indicating the number of Co sites available on the surface. Finally, the solid line indicates the reactivity per surface Co atom towards CH_4. The behavior of this line is further discussed in the text. From Auger measurements, the number of Co layers corresponding to the AES ratio has been indicated for 3, 9 and an infinite number of Co layers.

Alloys effects

$$2H^+ + 1/2O_2 + 2e^- \rightarrow OOH \rightarrow O + OH \rightarrow H_2O$$

At fuel cell cathode

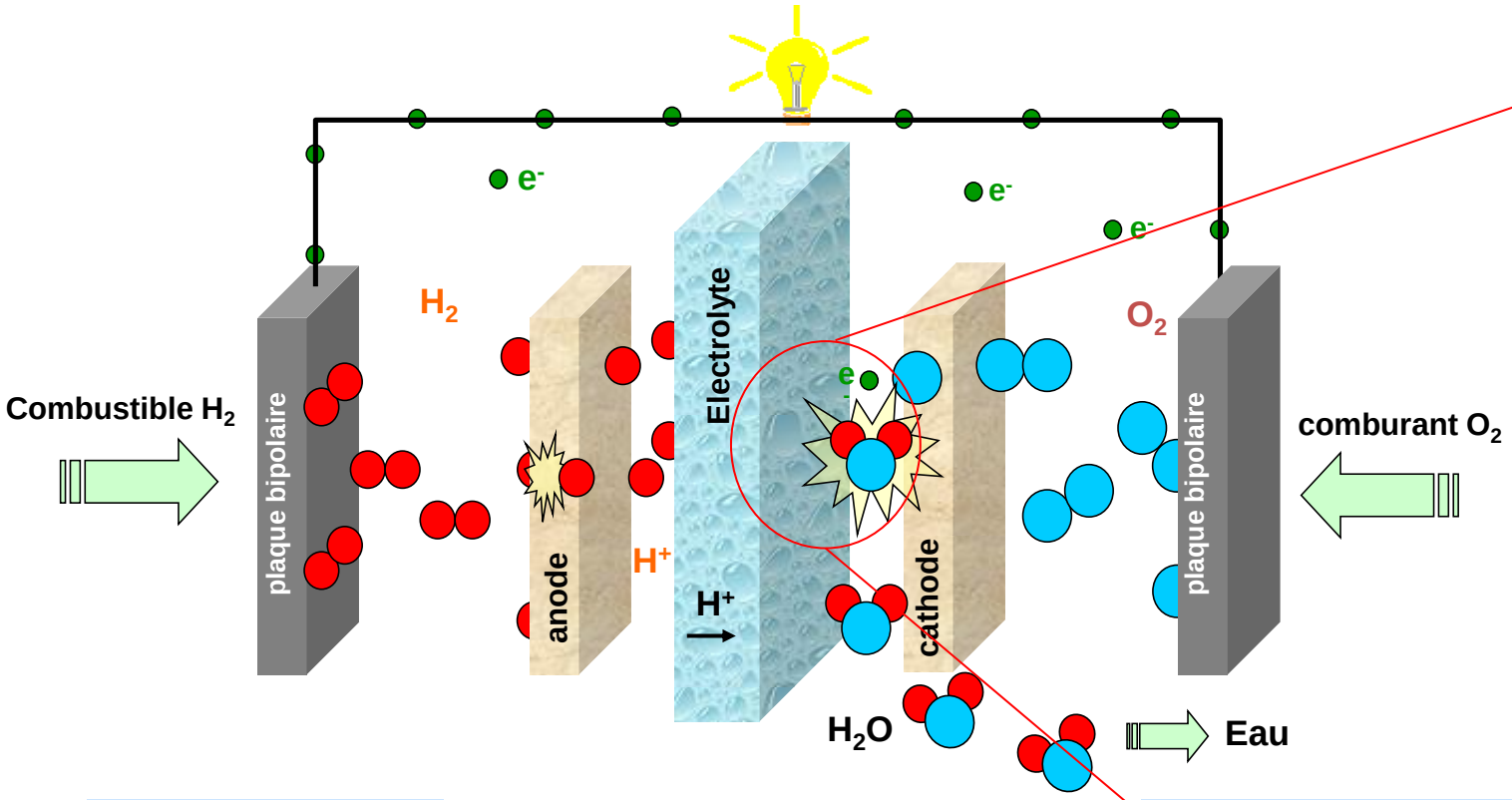

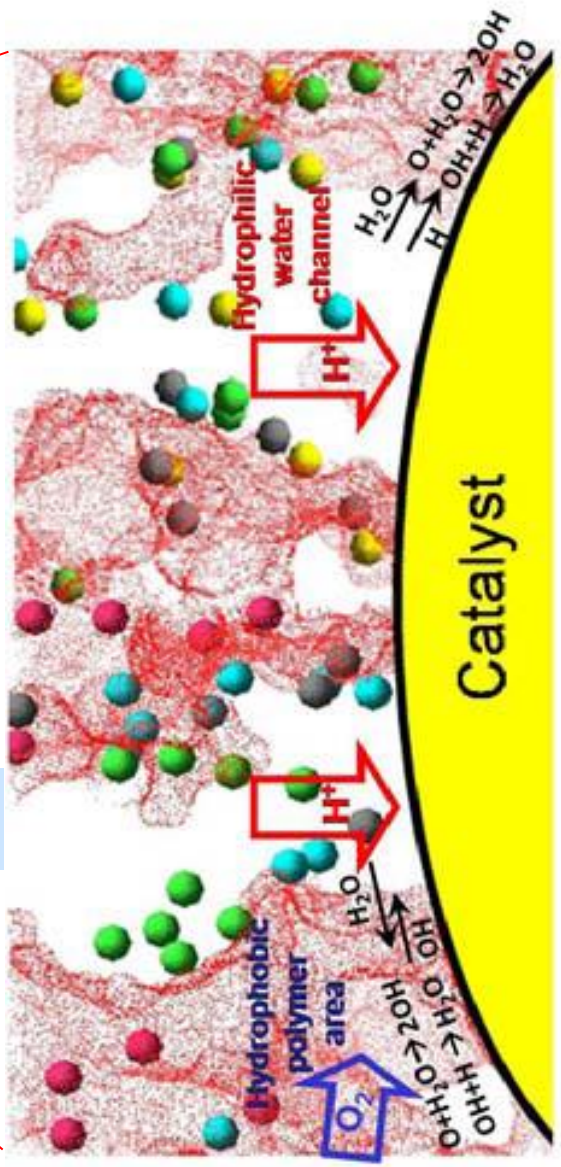

Réaction anodique
$H_2 \leftrightarrows 2\ H^+ + 2\ e^-$

Réaction cathodique
$O_2 + 4\ H^+ + 4\ e^- \leftrightarrows 2\ H_2O$

Réaction totale:

$$2\ H_2 + O_2 \rightarrow 2\ H_2O + E_{elec}$$

+ 40-50% de l'énergie est produite sous forme de chaleur

Alloy effects

$$2H^+ + 1/2O_2 + 2e^- \rightarrow OOH \rightarrow O + OH \rightarrow H_2O$$

Fuel cell cathode Pt_3Ni

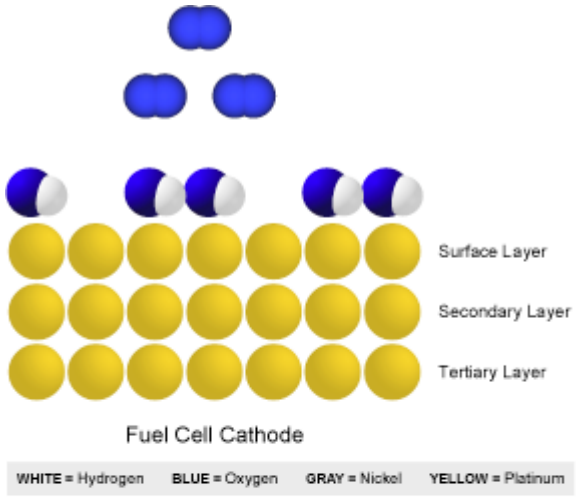

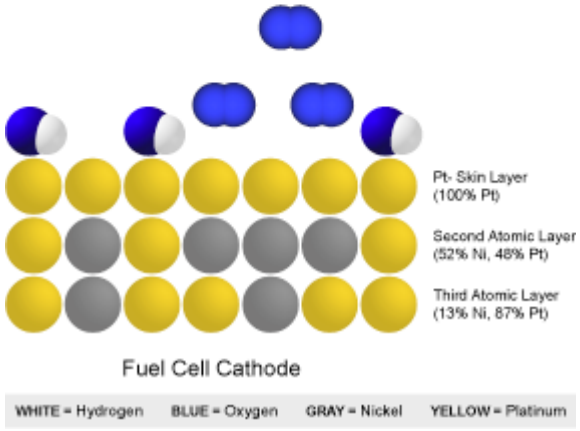

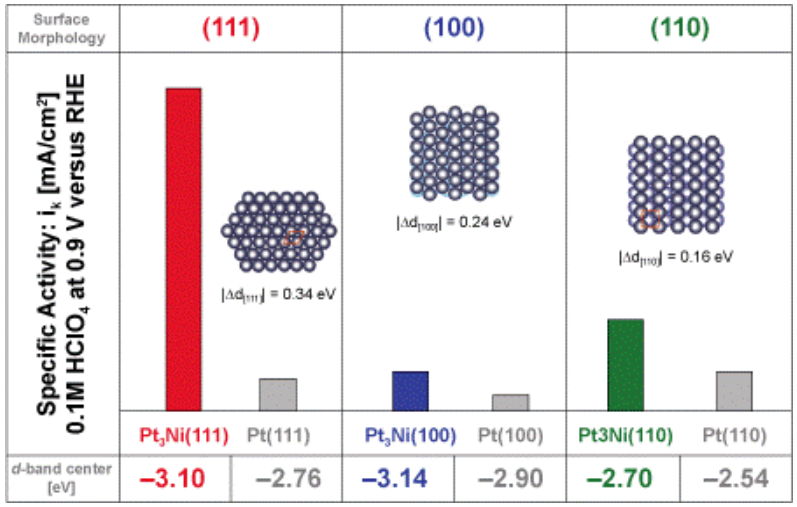

TOP. Pt(111). OH^- bonds tightly to platinum surface atoms, leaving less room for O_2 to adsorb onto Pt active sites. Since hydroxyde blocking species do not have an active role in reduction of oxygen molecules, their presence substantially hinders the rate of cathodic reaction.

BOTTOM. $Pt_3Ni(111)$. With Ni in the subsurface layers, the topmost Pt atoms (Pt-skin) have a modified electronic structure, which alters different adsorption properties of Pt. Consequently, interaction between OH^- ions and Pt-skin is weaker compared to the pure Pt catalysts, and surface is less covered by blocking species, leaving more Pt sites active for adsorption of O_2. The overall effect generates an increase in specific activity for cathodic reaction: 10 times more active than the Pt(111) surface and 90 times more active than state-of-the-art Pt/C catalysts currently used in fuel cells.

Alloys effects

$$2H^+ + 1/2O_2 + 2e^- \rightarrow OOH \rightarrow O + OH \rightarrow H_2O$$

Fuel cell cathode Pt_3Ni - Mo

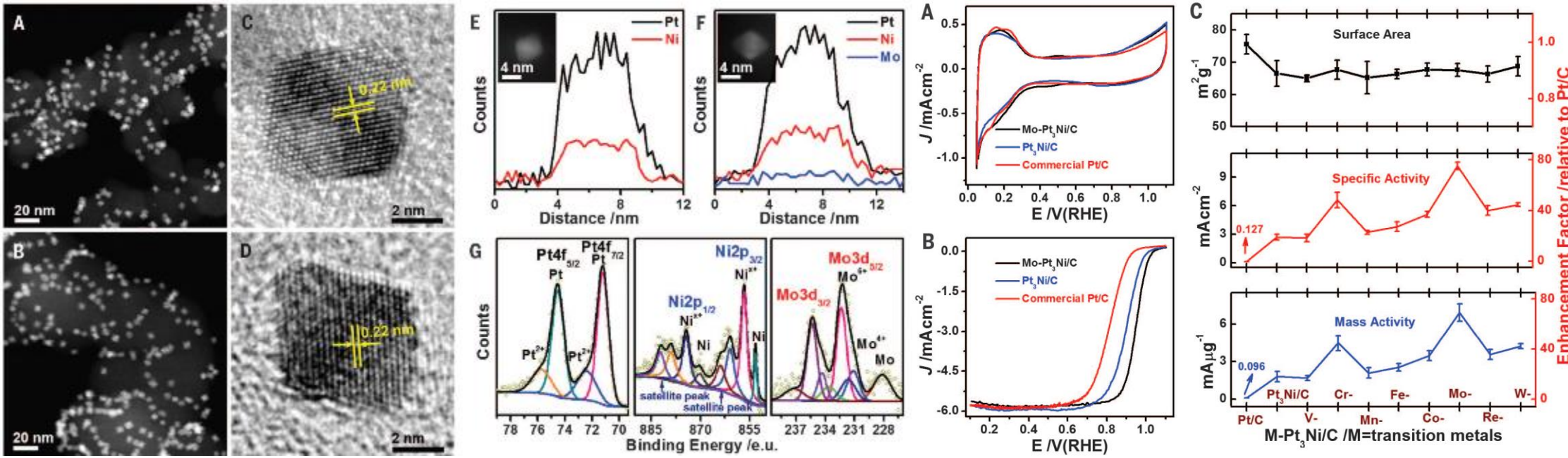

Practical Molecular Dynamics simulation

- ✓ Calculate all trajectories of a set of atoms, molecules, ...
  via the Newton equation of motion
  → Suitable for processes at nanoscale (up to 10^9 atoms)

$$\vec{F}_i = m_i \vec{a}_i = m_i \frac{d\vec{v}_i}{dt} = m_i \frac{d^2\vec{r}_i}{dt^2}$$

and

$$\vec{F}_i = -\vec{\nabla}_{ri} U\left(\vec{r}_1, \vec{r}_2, \vec{r}_3, \cdots, \vec{r}_N\right)$$

- ✓ A rigourous approach requires the use of robust interaction potentials
  If necessary running DFT, i.e. electronic calculations → *ab-initio* or *first-principles* MD and/or Machine Learning methods

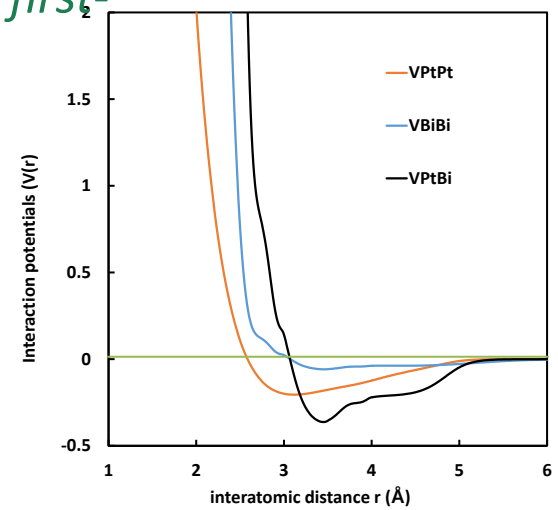

- ✓ and initial conditions (positions, velocities) preferably matching experimental conditions
  → appropriate velocity distribution functions can be derived from experimental conditions.

- ✓ Proper energy dissipation:
  - Energy release during deposition, bond formation/breaking
  - Annealing

  → via friction term(s), thermostat(s)

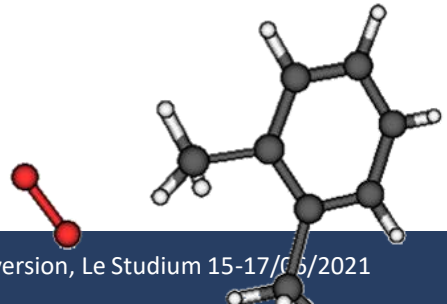

Practical Molecular Dynamics simulation

Relevance/significance of MD Simulations

Flux :

Exp. 1 10^{15}cm^{-2} s^{-1} = 10 species / nm^2 / s - MD 1 specie /10x10 nm^2 / 2 ps

Prohibit long time diffusion, except if including specific strategies (fbMC, CVHD, hyperdynamics, …)

Pressure/simulation box size

Solid density : Pt 65 nm^{-3} Liquid density: water 33 nm^{-3}

If box size is in the range 10 x 10 x 10 nm^3 → 65 000 Pt atoms or 33 000 water molecules

→ Statistical quantities (diffusion coeff, reaction rates, etc) can be directly calculated

Gas density : 1 atm = 2.4 10^{-2} nm^{-3}

-> Not enough species in box of size d at pressure P

→ Chemistry and reactivity in the gas phase require scaling law between simulation box and reactor sizes

Solution: relevant parameter = Collision number $\propto$ P.d → ↑P ↓d should work.

Practical Molecular Dynamics simulation

1/ recovering/scaling experimental conditions

Hypothesis : Collision number are the same in experiments and simulations so, $P_{exp}d_{exp} = P_{sim}d_{sim}$ thus $N_{sim} = \frac{P_{exp}}{k_B T_g} \cdot S_{sim} \cdot d_{exp}$ and if r_{cut} is the largest cutoff radius : $d_{sim} > \frac{N_{sim}}{S_{sim}} \cdot {r_{cut}}^3$

Or equivalently $\rho_{sim} = \frac{N_{sim}}{V_{sim}} < \frac{1}{r_{cut}^3}$

(S_{sim}, V_{sim} are the chosen smallest area, volume of the simulation box)

2/ Experimental time recovery

→ Velocities are same in experiments and simulations

$$v = \frac{d_{exp}}{t_{exp}} = \frac{d_{sim}}{t_{sim}}, when\ d_{exp}, d_{sim} > 2\rho$$

$$then, t_{exp} = \frac{d_{exp}}{d_{sim}} . t_{sim}, when\ d_{exp}, d_{sim} > 2\rho$$

$$or, t_{exp} = t_{sim}, when\ d_{exp}, d_{sim} \leq 2\rho$$

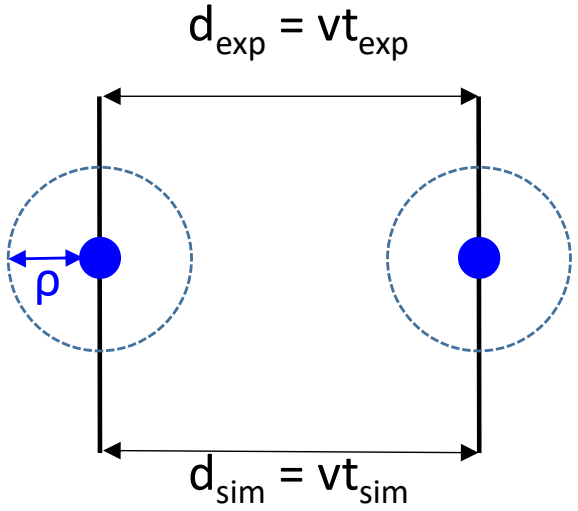

P. Brault, *Multiscale Molecular Dynamics Simulation of Plasma Processing: Application to Plasma Sputtering*, Front. Phys. 6 (2018) 59

Practical Molecular Dynamics simulation

Thermal relaxation

- Choose a relevant specie release time: i.e. greater than thermalisation time
- Choose a relevant thermostat (region i.e. which should be thermostated) within this relevant time
- For interactions with surface, one can guess that only the substrate should be thermostated

Practical Molecular Dynamics simulation
Interaction potentials

New reactive and including electron interaction potentials (force fields) allow targeting multiscale MD simulations

2/ combine improved force fields

Plasma factor	Possible?	Example
electric field	yes	CNT growth
atoms and hyperthermal species	yes	Si-NW oxidation
radicals	yes	a-C:H growth
ions	yes	sputtering
electronically excited states	yes	etching
vibrationally excited states	yes / no (reaxFF)	/
photons	implicit	(polymer degradation)
electrons	Yes (eFF, e-reaxFF)	/

E. Neyts, P. Brault (Review article), *Molecular dynamics simulations for plasma surface interactions*, Plasma Processes and Polymers 14 (2017) 1600145

Practical Molecular Dynamics simulation: Interactions potentials

Metals : Embedded Atom Method (EAM) (well suited for metal catalysts)

⇒ energy of a solid is a unique functional of the electron density.

⇒ uses the concept of electron (charge) density to describe metallic bonding:

⇒ each atom contributes through a spherical, exponentially-decaying field of electron charge, centered at its nucleus, to the overall charge density of the system.

⇒ Binding of atoms is modelled as embedding these atoms in this "pool" of charge, where the energy gained by embedding an atom at location r is some function of the local density.

⇒ The total energy thus writes:

$$E_{pot} = \sum_{i=1}^{N} E_i = \frac{1}{2}\sum_{i=1}^{N}\sum_{i,j,i\neq j}^{N}\phi_{ij}\left(r_{ij}\right) + \sum_{i=1}^{N} F_i\left(\rho_i\right) \qquad \rho = \sum_{j,j\neq 1}^{N} f_i\left(r_{ij}\right) \qquad f(r) = \frac{f_e \exp\left[-\beta\left(\frac{r}{r_e}-1\right)\right]}{1+\left(\frac{r}{r_e}-\lambda\right)^{20}}$$

With pairwise function:

$$\phi(r) = \frac{A\exp\left[-\alpha\left(\frac{r}{r_e}-1\right)\right]}{1+\left(\frac{r}{r_e}-\kappa\right)^{20}} - \frac{B\exp\left[-\beta\left(\frac{r}{r_e}-1\right)\right]}{1+\left(\frac{r}{r_e}-\lambda\right)^{20}}$$

and mixing rule:

$$\phi^{ab}(r) = \frac{1}{2}\left[\frac{f^b(r)}{f^a(r)}\phi^{aa}(r) + \frac{f^a(r)}{f^b(r)}\phi^{bb}(r)\right]$$

S.M. Foiles, M.I. Baskes Contributions of the embedded-atom method to materials science and engineering, MRS Bulletin, 37 (2012) 485-491.
X. W. Zhou et al, Misfit-energy-increasing dislocations in vapor-deposited CoFe/NiFe multilayers, Phys. Rev. B 69 (2004) 144113

Practical Molecular Dynamics simulation: Interactions potentials

ReaxFF allows for computationally efficient simulation of materials under realistic conditions, *i.e.* bond breaking and formation with accurate chemical energies. It also includes variable partial charges.

Due to the chemistry, ReaxFF has a complicated potential energy function: $E_{system} = E_{bond} + E_{over} + E_{angle} + E_{tors} + E_{vdWaals} + E_{Coulomb} + E_{Specific}$

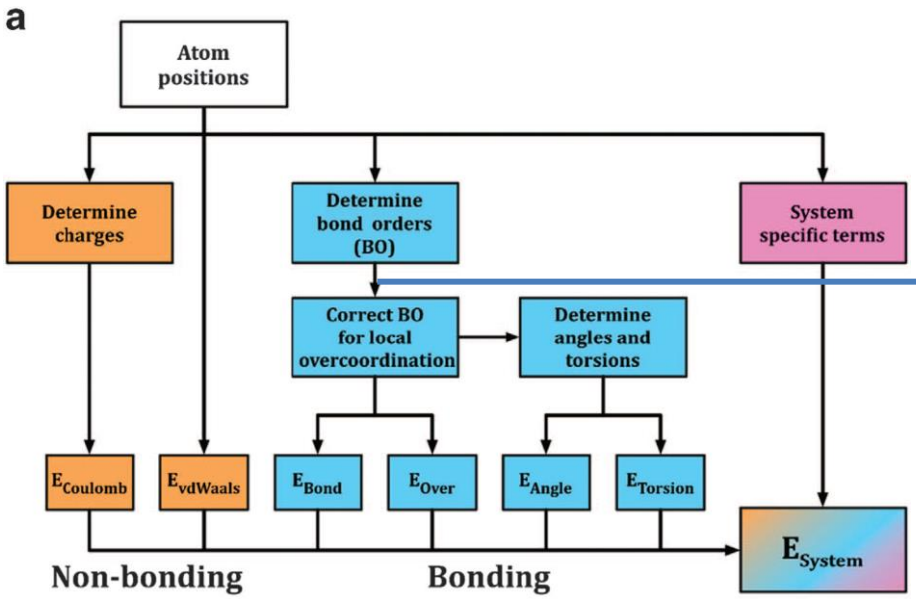

Overview of the ReaxFF total energy components

$$BO_{ij} = BO_{ij}^{\sigma} + BO_{ij}^{\pi} + BO_{ij}^{\pi\pi}$$
$$= \exp\left[p_{bo1}\left(\frac{r_{ij}}{r_o^{\sigma}}\right)^{p_{bo2}}\right] + \exp\left[p_{bo3}\left(\frac{r_{ij}}{r_o^{\pi}}\right)^{p_{bo4}}\right]$$
$$+ \exp\left[p_{bo5}\left(\frac{r_{ij}}{r_o^{\pi\pi}}\right)^{p_{bo6}}\right]$$

Correct Bond Order ⇒ Correct description of reaction energy barriers

Parametrization using experimenatal known data and DFT calculations

TP Senftle et al, *The ReaxFF reactive force-field: development, applications and future directions*, npj Computational Materials 2, (2016) 15011

Molecular Dynamics of plasma assisted nanocatalyst growth: Supported Pt_2PdAu nanocatalyst growth on porous carbon

Potentials used in the system:

Pt-Pd-Au: EAM potentials

C – C: Tersoff potential -> thermostat

Metal – C: LJ potential (Steele)

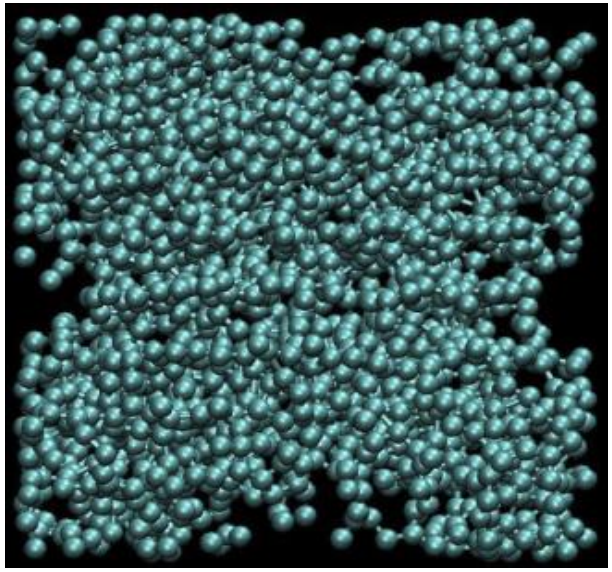

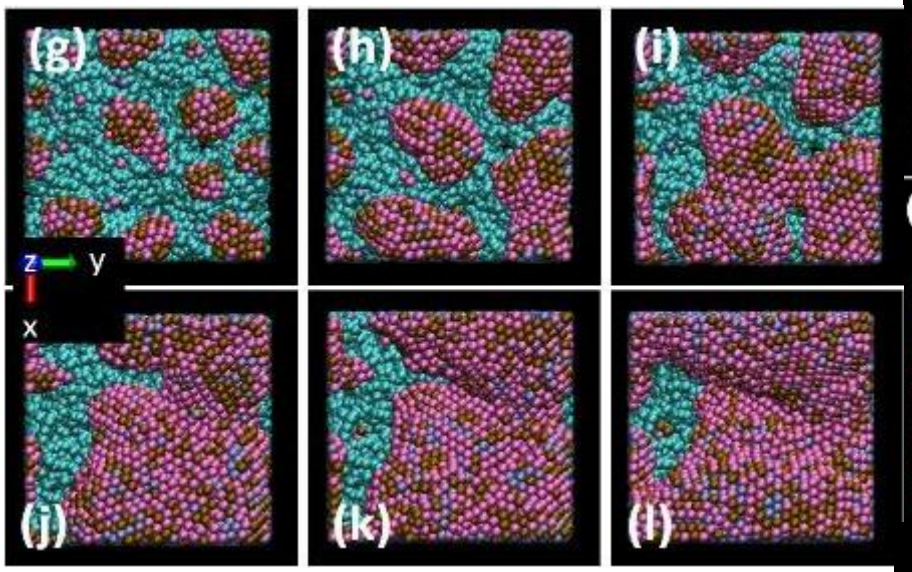

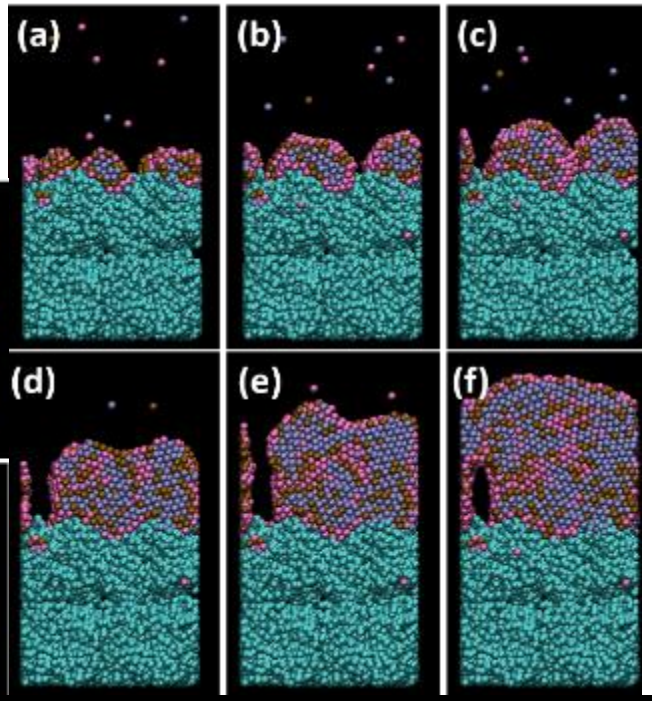

• Pt; • Pd; • Au

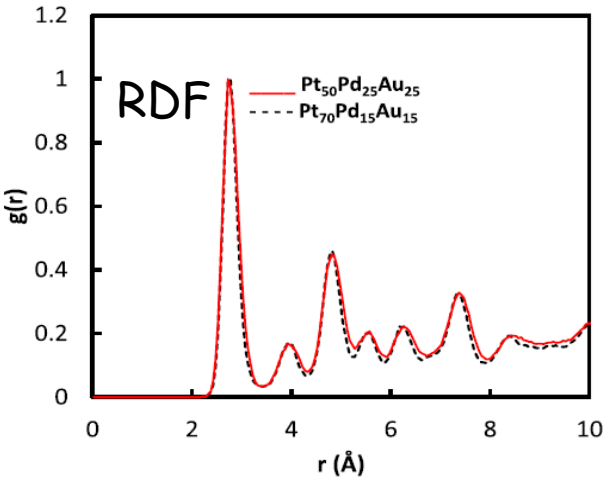

Table 1 – EAM and average experimental surface energies of the low index faces of Pt, Pd, Au in Jm^{-2} [40].

	Pt	Pd	Au
(111)	1.44	1.22	0.79
(100)	1.65	1.37	0.92
(110)	1.75	1.49	0.98
Experimental, face averaged	2.49	2.00	1.5

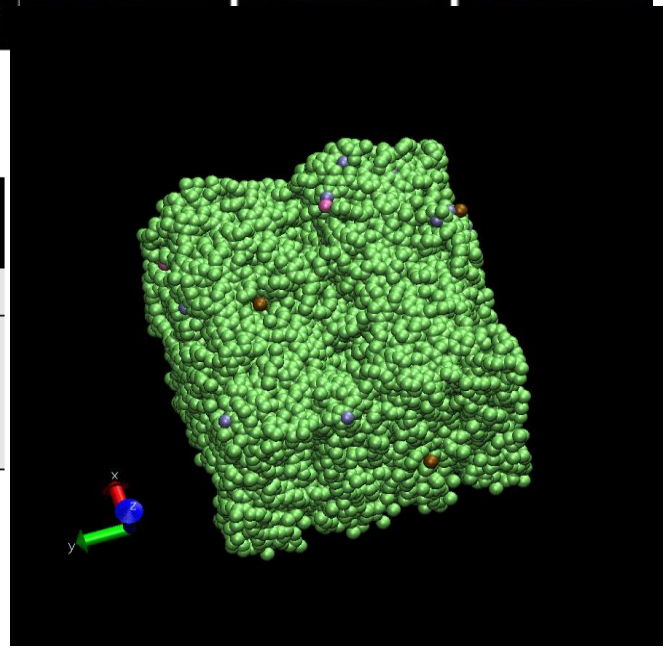

Molecular Dynamics of plasma assisted nanocatalyst growth: Supported PdAu@Pt_2 core@shell nanocatalyst growth on porous carbon

• Pt; • Pd; • Au

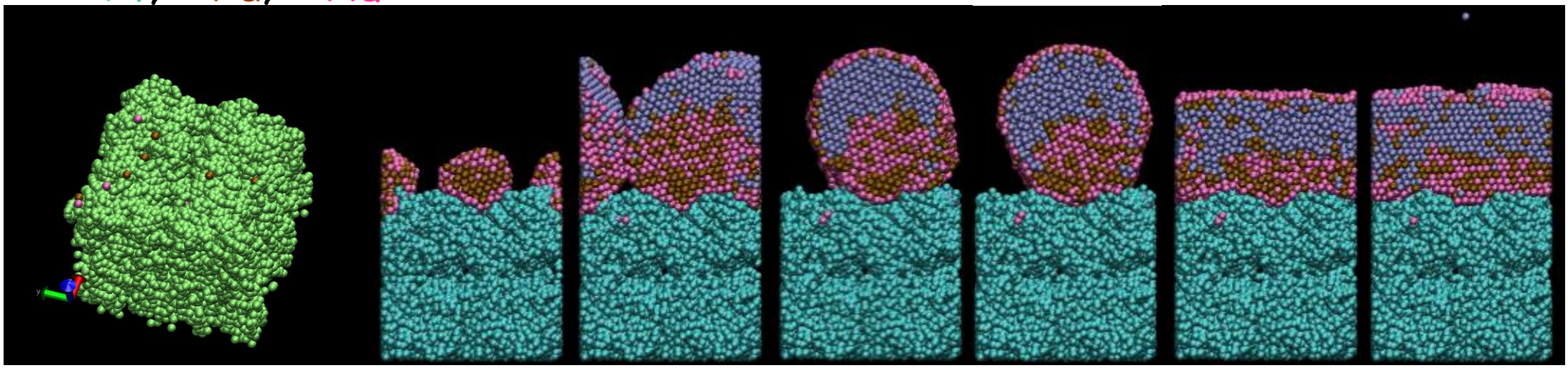

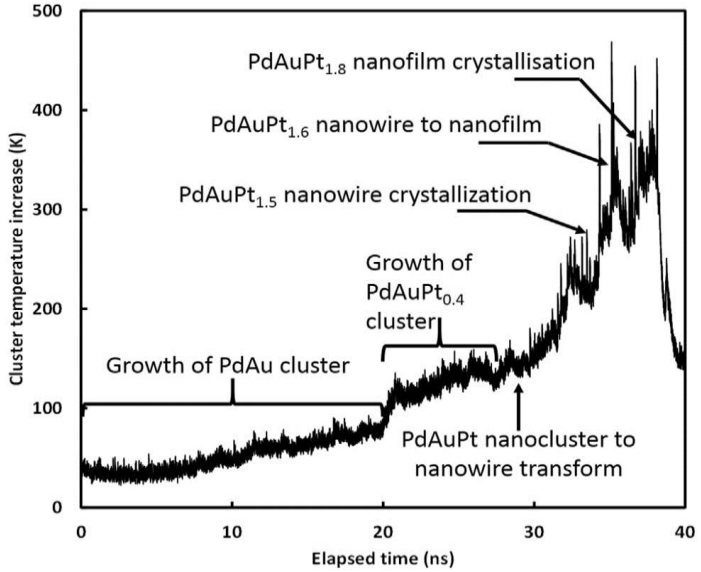

Correlations between cluster temperature evolution and morphology transform in the course of deposition of core-shell PdAu@Pt_2 nanocatalyst

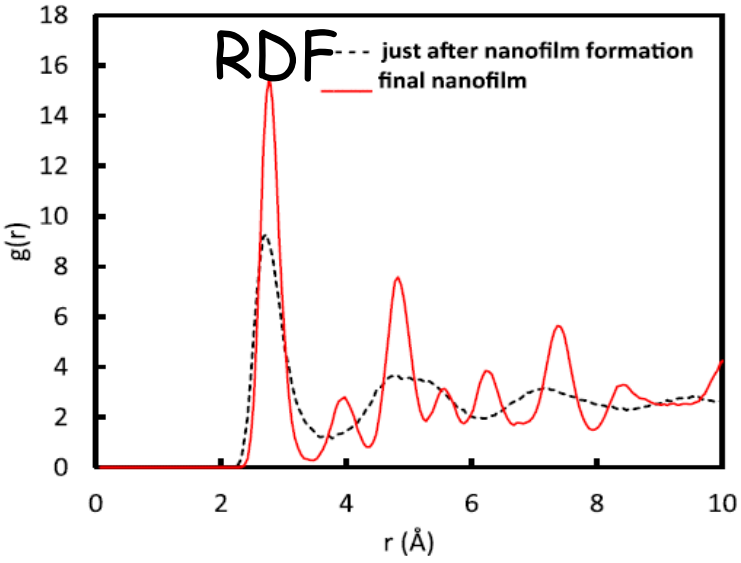

- L. Xie, P. Brault, C. Coutanceau, A. Caillard, J. Berndt, E. Neyts Appl. Cat. B, 62 (2015) 21 – 26
- P. Brault, C. Coutanceau, P. C. Jennings, T. Vegge, J. Berndt, A. Caillard, S. Baranton, S. Lankiang, International Journal of Hydrogen Energy 41 (2016) 22589-22597
- E. Neyts, P. Brault, Plasma Processes and Polymers 14 (2017) 1600145 (Review article)

- FP7 FCH-JU SMARTCat project #325327

Molecular Dynamics of plasma assisted nanocatalyst growth: Supported Pt_3NiAu nanocatalyst growth on porous carbon

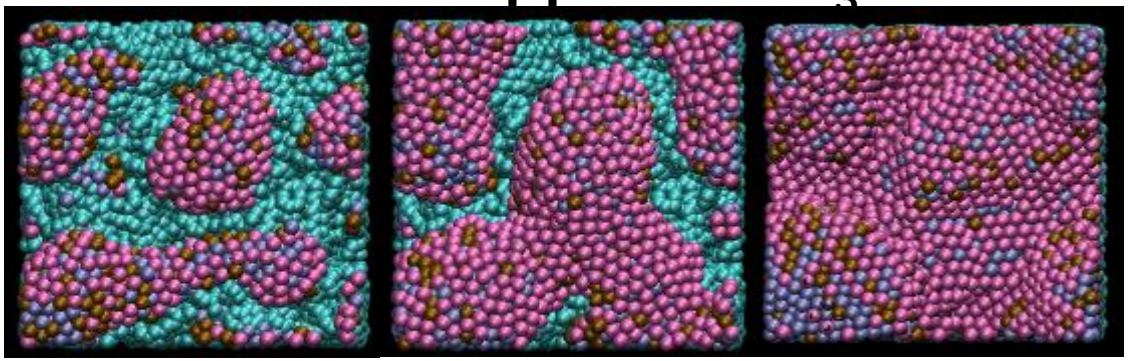

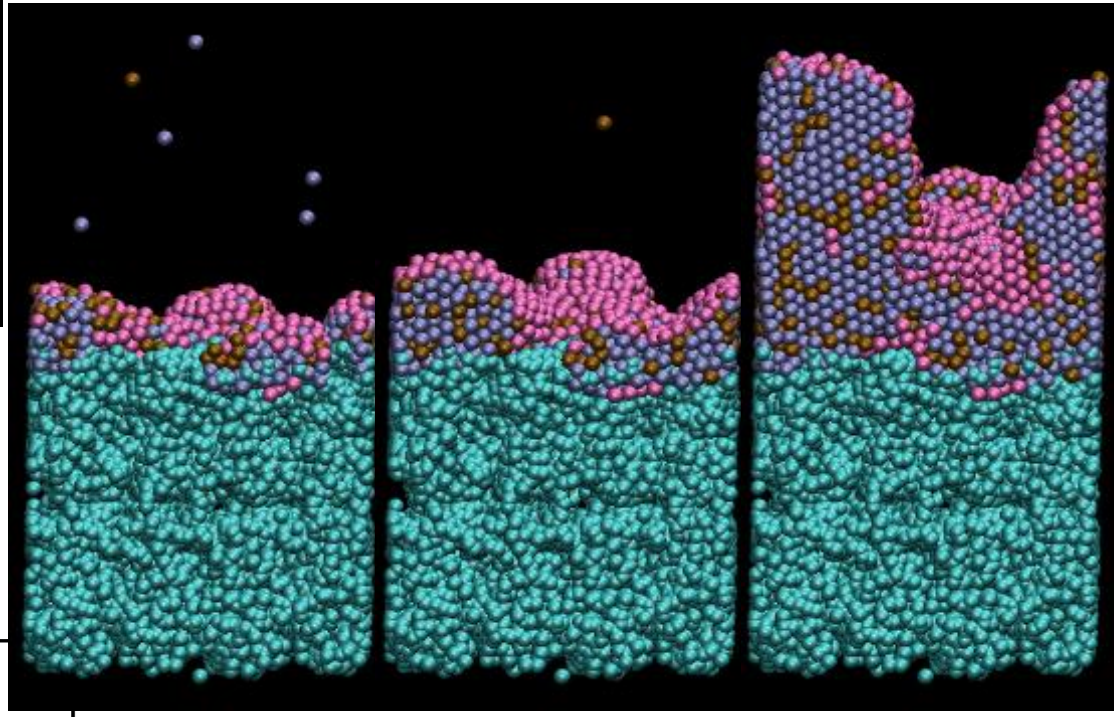

• Pt; • Ni; • Au

→ $Pt_3Ni@Au$

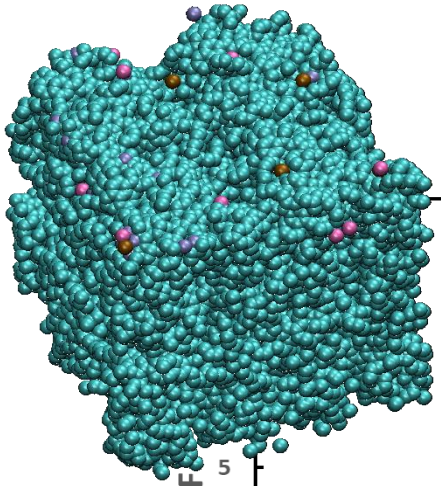

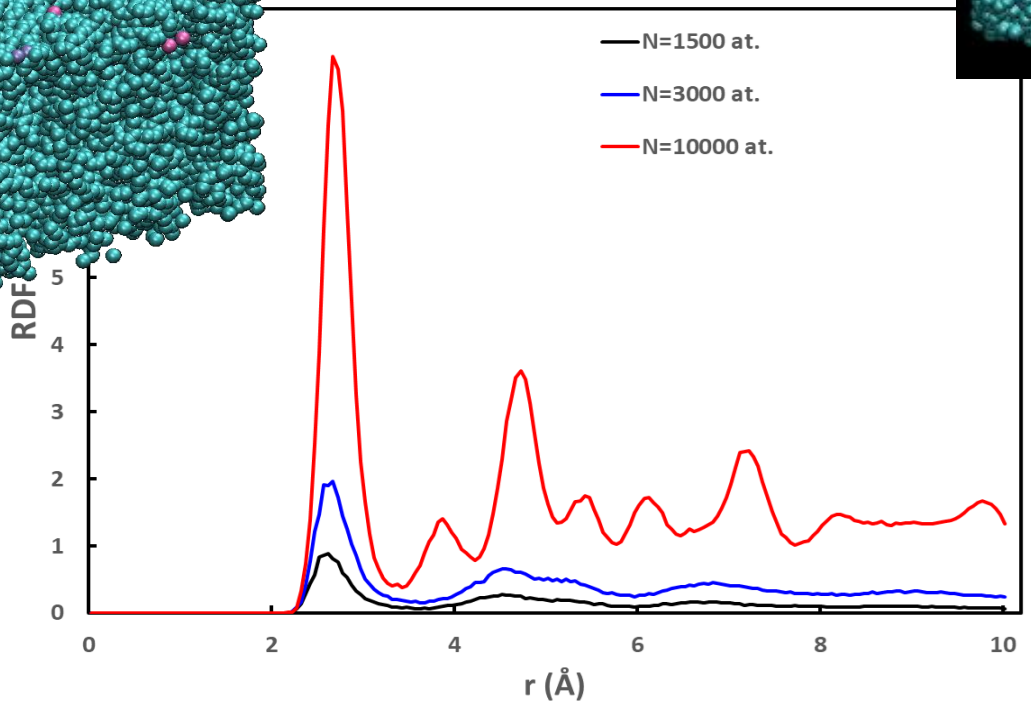

10000 at.

1st NN : d = < a(3Pt, 1Ni)/√2> (fcc

2nd NN : a_0 = <a(3Pt, 1Ni)>

CN = 12 (3000 et 10000 at.)

Molecular Dynamics of plasma assisted nanocatalyst growth: Free Pt_3NiAu nanocatalyst growth in an Ar plasma

Gas condensation nanocluster source

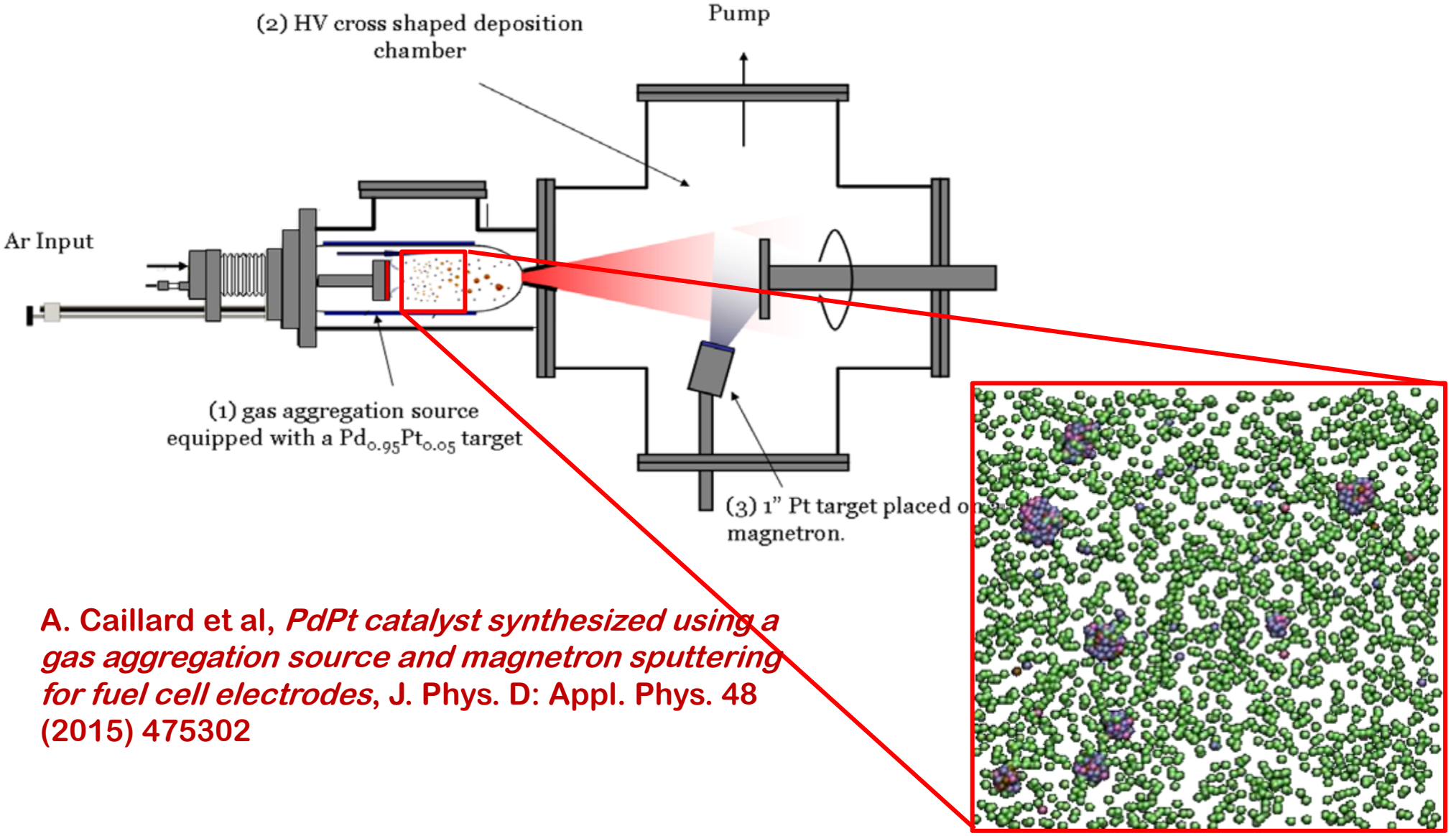

A. Caillard et al, *PdPt catalyst synthesized using a gas aggregation source and magnetron sputtering for fuel cell electrodes*, J. Phys. D: Appl. Phys. 48 (2015) 475302

Molecular Dynamics of plasma assisted nanocatalyst growth: Free Pt_3NiAu nanocatalyst growthin an Ar plasma

• Ar; • Pt; • Ni; • Au

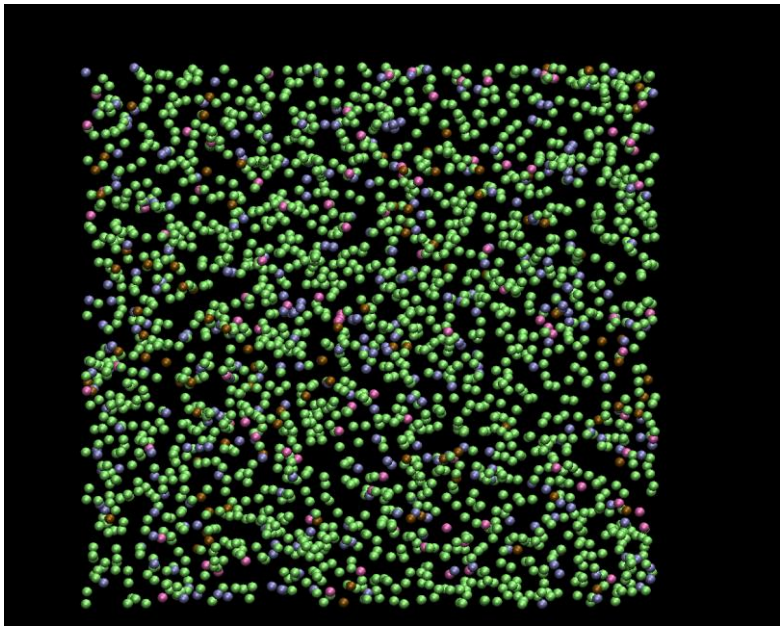

Temperature evolution of the vapor and of the metal vapor and then clusters display the cluster growth and coalescence : breaks in the plot (green vertical sticks)

Tricks :

NVE ensemble for Ar, Pt, Ni and Au

Ar surrounding gas is the thermostat

Ratio of N_{Ar} to N_{metal} estimated from experiments : depends from discharge current, Ar pressure, …

=4 here: N_{Ar}=2000; N_{Pt}=300; N_{Ni}=100; N_{Au}=100

Significance : Collision number identical in experiments and in simulation

i.e. $P_{exp}.d_{exp} = P_{sim}.d_{sim}$

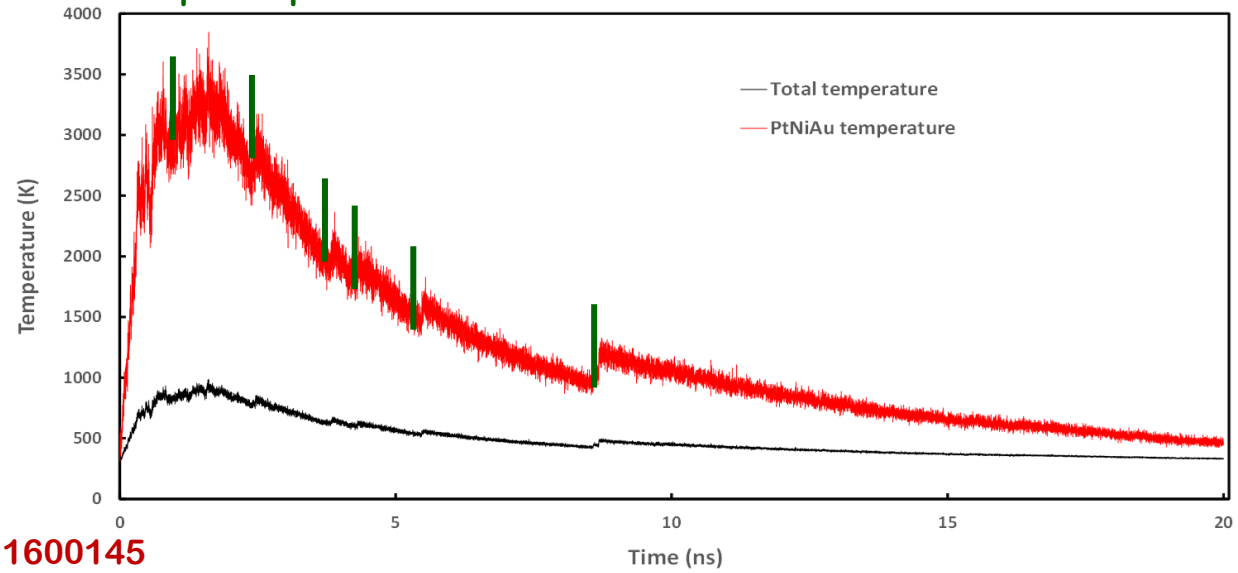

E. Neyts, P Brault, Plasma Process Polym 14 (2017) 1600145
P. Brault, Front. Phys. 6 (2018) 59

Free $Pt_3Me(Au)$ (Me = Ni, Cu) nanocatalyst growth

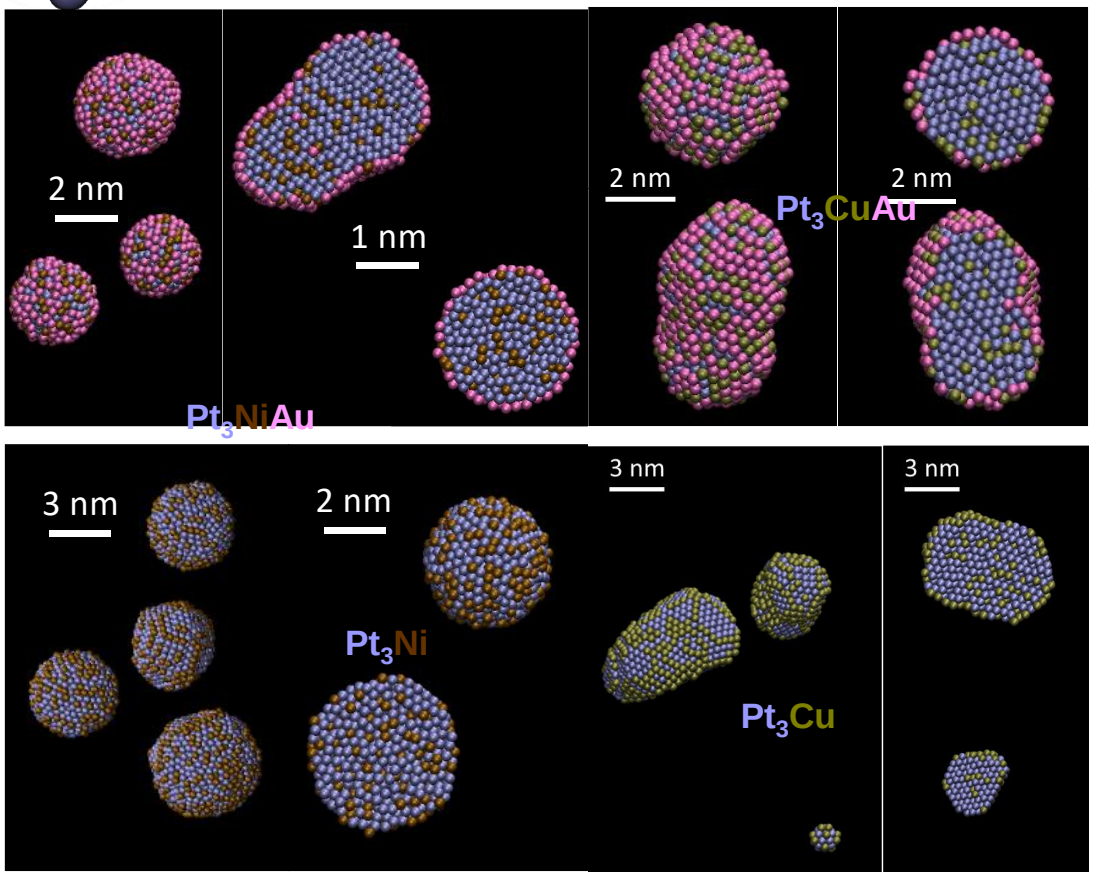

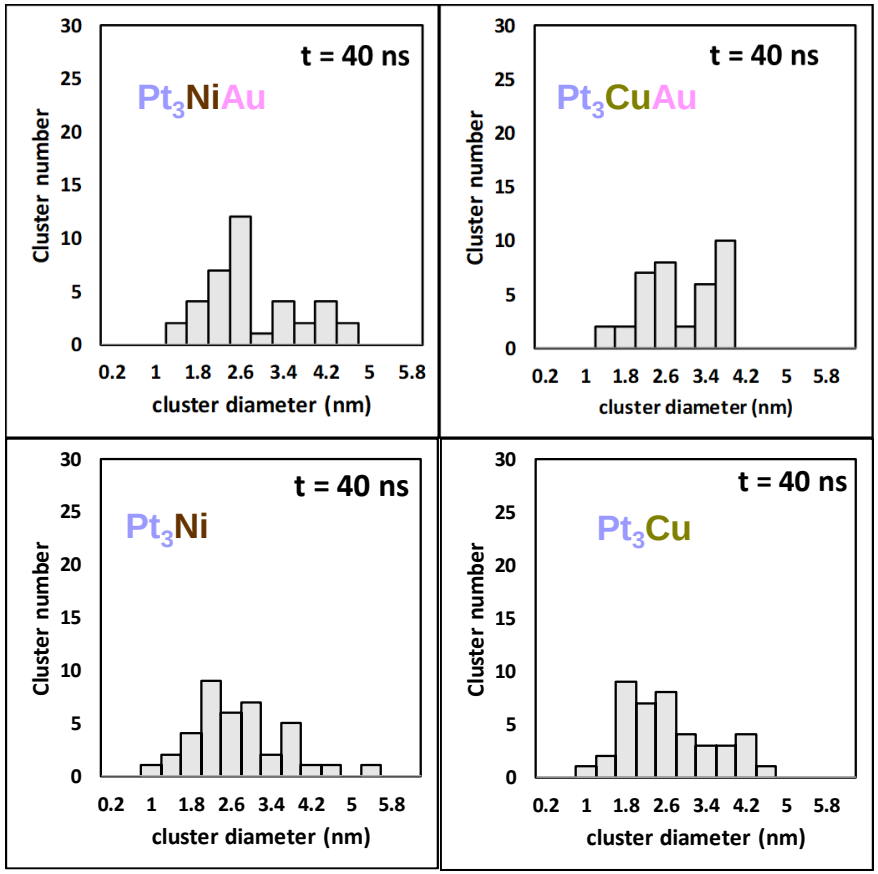

- Au segregation towards cluster surface
- CuAu surface alloy for Pt_3CuAu → better efficiency for Oxygen Reduction Reaction
- $Pt_3Cu(Au)$ more well crystallized

P. Brault, et al, Pt_3MeAu (Me = Ni, Cu) fuel cell nanocatalyst growth, shapes and efficiency: A molecular dynamics simulation approach, J. Phys. Chem. C 123 (2019) 29656 − 29664

Molecular Dynamics of plasma assisted nanocatalyst growth: Free Pt_3NiAu nanocatalyst growthin an Ar plasma

• Pt; • Ni; • Au

Cluster 1 (318 at.) : cuboctahedron ?
$Pt_{189}Ni_{62}Au_{67} \approx Pt_3NiAu$

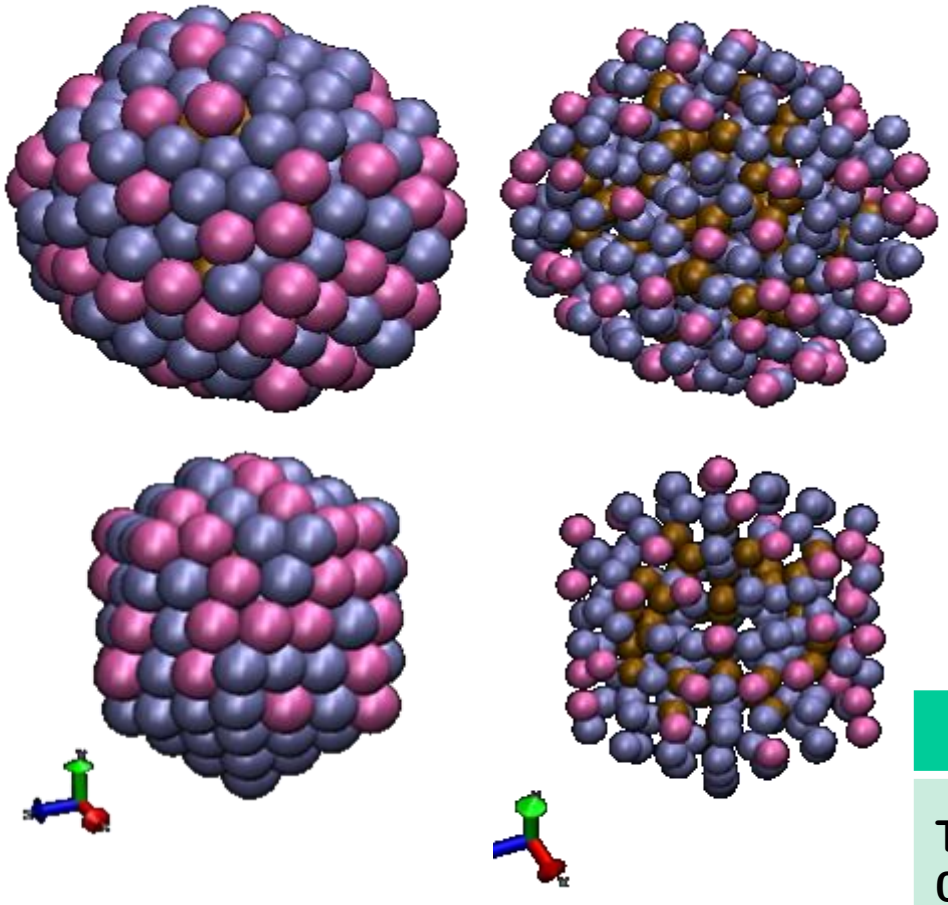

Cluster 2 (182 at.) : icosahedron ?
$Pt_{111}Ni_{38}Au_{33}$

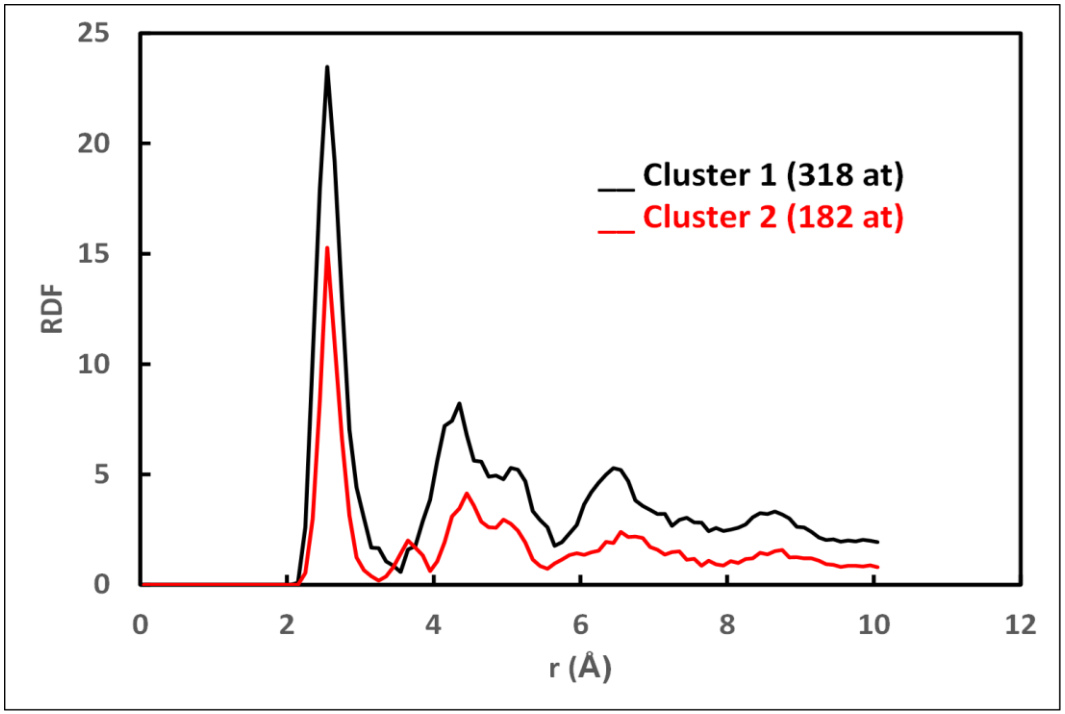

	1st NN	2nd NN	3rd NN
Theoretical (fcc) 0.6Pt+0.2Ni+0.2Au	2.738 Å	3.872 Å	4.74 Å
Cluster 1	2.55 Å	(3.75 Å)	4.35 Å
Cluster 2	2.55 Å	3.65 Å	4.45 Å

Pt_xBi_y nanocatalyst growth

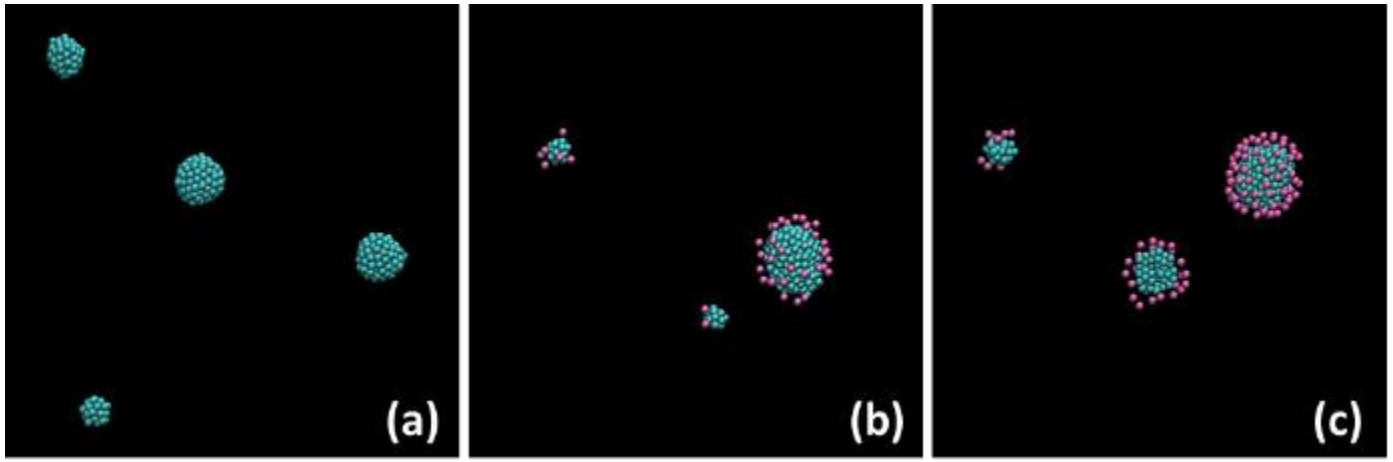

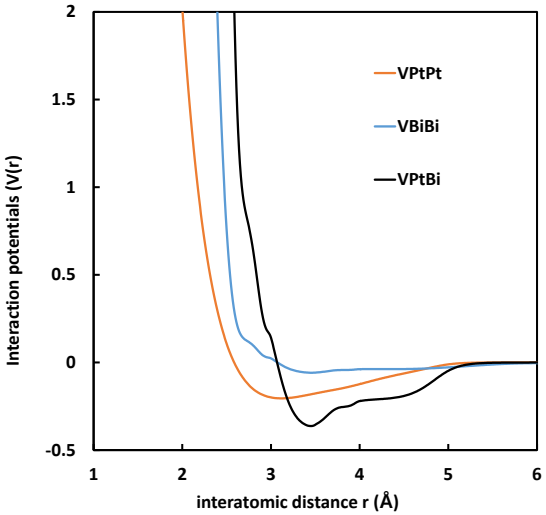

Snapshot of the final clusters at 20 ns. Argon atoms (4000) are not represented for clarity. $n_{Pt} + n_{Bi} = 500$. (a) Pt alone (b) Pt_9Bi_1 (c) Pt_8Bi_2. Box size 16x16x16 nm^3

Plots of the pair part of the EAM interaction potentials: $V_{PtPt}(r)$, $V_{BiBi}(r)$, $V_{PtBi}(r)$.

- Cluster atomic arrangements are typical of a crystalline structure of the Pt cores, with numbers of 1st nearest neighbors between 10 and 12 (i.e. consistent with fcc arrangement)
- Bi composition < 20% leads to cluster surfaces with both Pt and Bi, allowing catalytic activity enhancement.
- Pt/Bi atomic composition is not only globally preserved, but is also verified for each cluster

B.S.R. Kouamé et al, Insights on the unique electro-catalytic behavior of PtBi/C materials, Electrochimica Acta 329 (2020) 135161

Molecular dynamics simulation of sputtering plasma catalysts growth: Reactive PdO nanocatalyst growth

ReaxFF reactive variable charge potentials for Pd sputtering in Ar-O_2 gas mixture

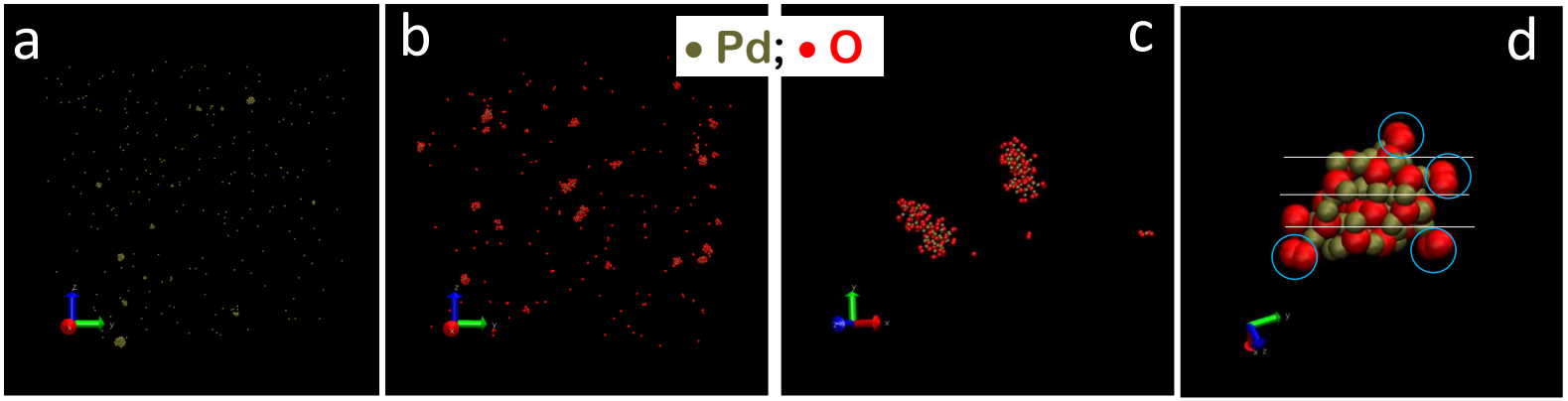

Snapshot of (a-b) the overall Pd and PdO clusters at 25 ns simulation time (b-c) of the detailed PdO clusters.

First results: O addition -> no more free Pd, more PdO than Pd clusters

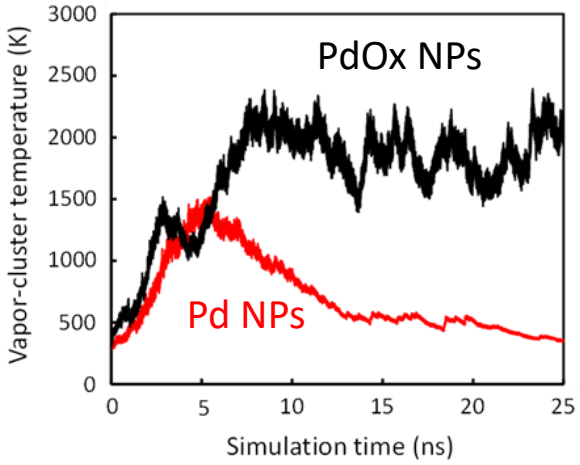

Ratio of N_{Ar} to N_{metal} estimated from experiments = 40 here;

N_{Ar} = 20000; N_{Pd} = 500; N_O = 1000; Box size : 40 x 40 x 40 nm^3

Integration time 0.25 fs → 1. 10^8 iterations

Potential ReaxFF : T. Senftle et al, J. Chem Phys 139 (2013) 044109

P. Brault et al, Molecular Dynamics simulations of initial Pd and PdO nanocluster growths in a magnetron gas aggregation source, Frontiers in Chemical Science and Engineering (2018) accepted.

Hydrocarbon plasma and nanoparticles

µwave plasma H_2/10% CH_4
Initial conditions for MD simulations
from 0D model (*)

	1450 K	1650 K	1950K
H_2 (*)	1000	1000	1000
H	7	30	100
CH_4	200	100	100
$\bullet CH_3$	2	5	7
C_2H_4	50	20	3
C_2H_2	400	500	600

(*) au lieu de 10000
Suffisant pour thermostat

→ Reactions can freely occur

→ Bond formation energy is transported to walls by H_2 buffer gas, as in experiment (96% of molecules are H_2). H atoms from H_2 are thermostated.

S. Prasanna, A. Michau, C. Rond, K.Hassouni, A Gicquel, Plasma Sources Sci. Technol. 26 (2017) 097001

P Brault, C Rond, unpublished

Hydrocarbon plasma and and nanoparticles

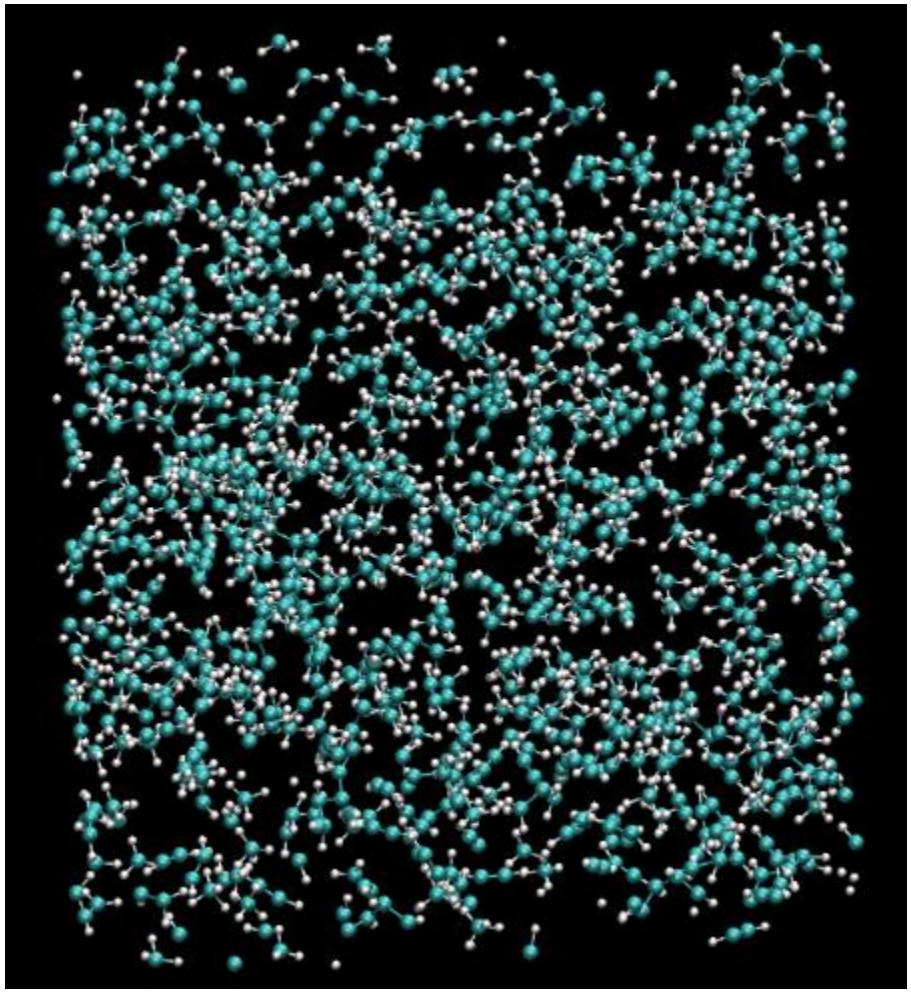

1450 K

- ReaxFF potential
- NVT for H_2 → thermostat
- NVE for other species
- 4 x 4 x 4 nm^3
- dt = 0.25 fs; 10^7 timesteps
- 300h on 8 core Intel Xeon

Hydrocarbon plasma and nanoparticles

1450 K

- Negatively charged ions

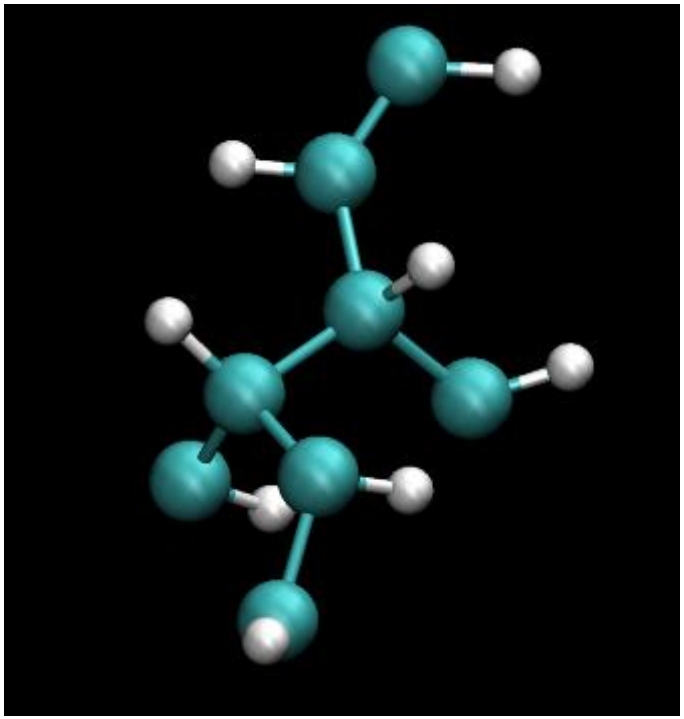

#2603
q = -0.45

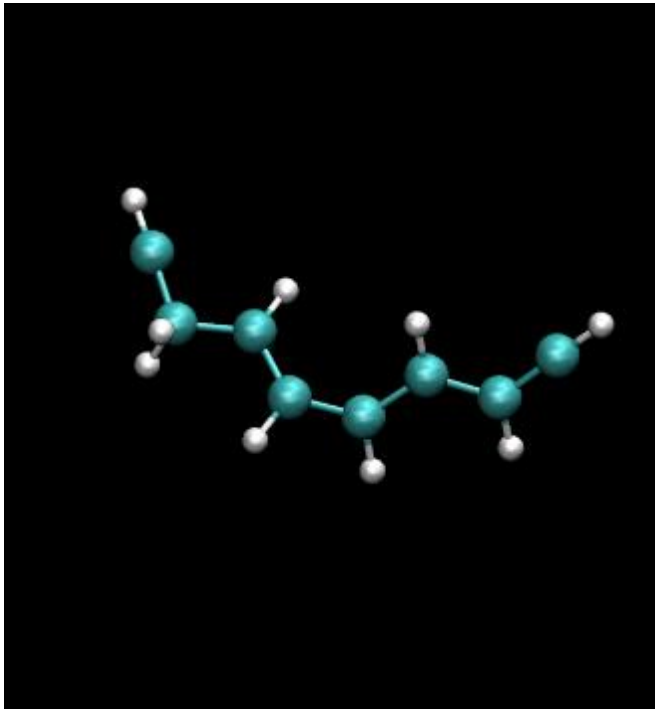

#2004
q = -0.2

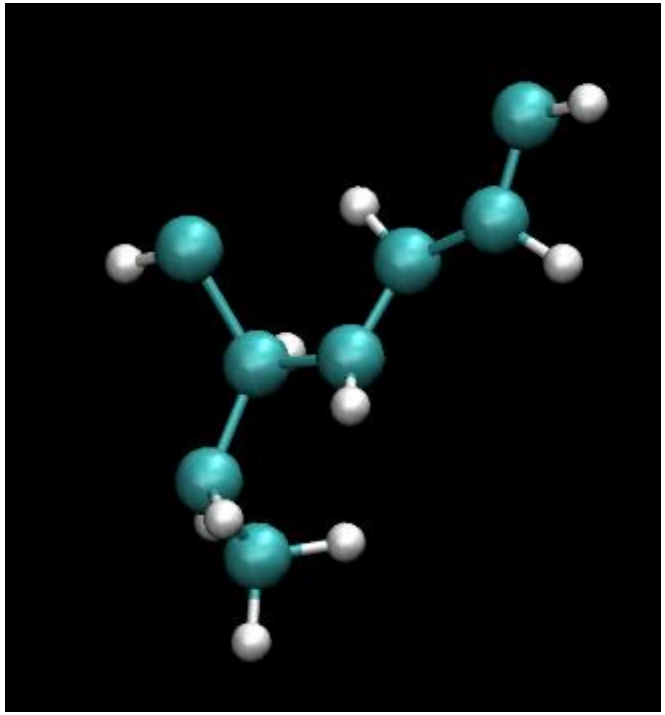

#3088
q = -0.25